NOVEL TECHNIQUES FOR PULSED FIELD GRADIENT NMR MEASUREMENTS

By

WILLIAM W. BREY

A DISSERTATION PRESENTED TO THE GRADUATE SCHOOL
OF THE UNIVERSITY OF FLORIDA IN PARTIAL FULFILLMENT
OF THE REQUIREMENTS FOR THE DEGREE OF
DOCTOR OF PHILOSOPHY

UNIVERSITY OF FLORIDA

1994

ACKNOWLEDGMENTS

I would like to thank Janel LeBelle, Igor Friedman, and Don Sanford for construction of the gradient coil prototypes, and Jerry Dougherty for performing the simulations of the coils they all helped to construct. Stanislav Sagnovski, Eugene Sczezniak, Doug Wilken, and Randy Duensing participated in many helpful discussions concerning gradient coils. Debra Neill-Mareci provided the excellent illustration of a gradient coil in Figure 22. For their part in the microscopy project, thanks go to Barbara Beck, Michael Cockman, and Dawei Zhou. Ed Wirth and Louis Guillette provided the samples. For help measuring eddy current fields I am grateful to Wenhua Xu, and to Steve Patt for help with the software. Thanks go to my parents, Mary Louise and Wallace Brey, and my brother, Paul Brey, for encouragement and help with red tape. Paige Brey has my special thanks for her extensive help preparing the thesis. Katherine Scott, Richard Briggs, Jeff Fitzsimmons, and Neil Sullivan enriched my graduate experience with their wide knowledge and diverse interests. Thanks go to them for their enthusiasm and for reading this thesis. Raymond Andrew served as supervisory committee chairman. Thanks go to Thomas Mareci for directing the research, for providing

financial and moral support, and for encouraging me to pursue this work to its conclusion.

TABLE OF CONTENTS

Abstract of Dissertation Presented to the Graduate School of the University of Florida in Partial Fulfillment of the Requirements for the Degree of Doctor of Philosophy

NOVEL TECHNIQUES FOR PULSED FIELD GRADIENT NMR MEASUREMENTS

By

William W. Brey

December, 1994

Chairman: E. Raymond Andrew
Major Department: Physics

Pulsed field gradient (PFG) techniques now find application in multiple quantum filtering and diffusion experiments as well as in magnetic resonance imaging and spatially selective spectroscopy. Conventionally, the gradient fields are produced by azimuthal and longitudinal currents on the surfaces of one or two cylinders. Using a series of planar units consisting of azimuthal and radial current elements spaced along the longitudinal axis, we have designed gradient coils having linear regions that extend axially nearly to the ends of the coil and to more than 80% of the inner radius. These designs locate the current return paths on a concentric cylinder, so the coils are called Concentric Return Path (CRP) coils. Coils having extended linear regions can be made smaller for a given sample size. Among the advantages that can accrue from using smaller coils are improved gradient strength and

switching time, reduced eddy currents in the absence of shielding, and improved use of bore space.

We used an approximation technique to predict the remaining eddy currents and a time-domain model of coil performance to simulate the electrical performance of the CRP coil and several reduced volume coils of more conventional design. One of the conventional coils was designed based on the time-domain performance model.

A single-point acquisition technique was developed to measure the remaining eddy currents of the reduced volume coils. Adaptive sampling increases the dynamic range of the measurement. Measuring only the center of the stimulated echo removes chemical shift and B_0 inhomogeneity effects. The technique was also used to design an inverse filter to remove the eddy current effects in a larger coil set.

We added pulsed field gradient and imaging capability to a 7 T commercial spectrometer to perform neuroscience and embryology research and used it in preliminary studies of binary liquid mixtures separating near a critical point.

These techniques and coil designs will find application in research areas ranging from functional imaging to NMR microscopy.

GENERAL INTRODUCTION

As pulsed field gradient technology for NMR matures, new and diverse applications develop. Pulsed Gradient Spin Echo techniques allow the measurement not only of the bulk diffusion tensor, but of the structure factor of the sample.[1] Editing techniques use pulsed field gradients to simplify the complex spectra of biomolecules.[2] Local gradient coils allow functional imaging in the human head.[3] NMR microscopy can require field gradients much larger and switched more rapidly than conventional imaging experiments.[4] Localized spectroscopy allows chemical shift information to be collected from specific voxels in a living animal.[5] This paper will address some approaches for producing and evaluating pulsed field gradients.

A technique was developed to measure the eddy current field that persists after a field gradient is switched off and, based on the measurement, a filter to correct for the eddy current field was designed. The technique, which employs a series of experiments based on the stimulated echo, was then used to evaluate the performance of the

---

[1] D. G. Cory and A. N. Garroway, Magn. Reson. Med. 14, 435, 1990.
[2] D. Brühwiler and G. Wagner, J. Magn. Reson. 69, 546, 1986.
[3] K. K. Kwong et al., Proc. Natl. Acad. Sci. 89, 5675, 1992.
[4] Z. H. Cho et al., Med. Phys. 15, 815, 1988.
[5] H. R. Brooker et al., Magn. Reson. Med. 5, 417, 1987.

filter. If an eddy current field persists during the period when the NMR signal is detected, distortions in the spectrum or image will result. The distortions are particularly severe when chemical shift information is obtained in the same experiment as spatial localization by encoding spatial information in the phase of the NMR signal. It is important to be able to measure the residual gradient field, which is usually due to eddy currents in the metal structures of the magnet, so that it can be corrected by changing the drive to the gradient amplifier, or by whatever other technique is available, and to evaluate the remaining uncorrected field to estimate the distortion that will result in a desired experiment.

One way to avoid eddy currents for experiments such as spatially selective spectroscopy is to employ actively shielded gradient coils. Another, much simpler, approach is to reduce the size of the gradient coil so that it is widely separated from the eddy-current-producing structures in the magnet. This approach is only possible when the clear bore of the magnet is much larger than the volume of interest, which is often the case. To make possible experiments, such as spatially selective spectroscopy, that require rapidly switched high intensity field gradients, I developed pulsed field gradient systems based on reduced volume gradient coils for a 2 T, 31 cm bore magnet used for small animal studies. This magnet was replaced with a 4.7 T, 33 cm bore magnet, and the gradient systems were adapted accordingly.

These pulsed field gradient systems offer much better performance than the large and unshielded gradient system supplied with the magnet, given their limitation on sample size. I also developed a pulsed field gradient coil for a 7 T, 51 mm bore magnet used for NMR microscopy and spectroscopy.

Another experiment which requires gradient coils to perform exceptionally well is functional imaging of the human brain. The head is much smaller than the whole-body magnets in general use. A smaller coil can allow faster switching to higher gradient fields, as well as reduce eddy current fields. In order to get a gradient coil that is matched to the size of the head, some provision must be made to allow for the shoulders. Conventional designs, even existing designs with a large linear volume, have current return paths arrayed on both sides of the linear volume. A coil matched to the size of the head would not fit over the shoulders. A coil that trades radial linear region for increased axial linear region is more appropriate. A design utilizing concentric return paths was developed that significantly improved the axial region of linearity. A prototype was constructed and tested.

In order to perform NMR microscopy and pulsed field gradient experiments, we adapted an NMR spectrometer and probe for a 7 T, 51 mm bore magnet. The instrument included a simple amplitude modulator to carry out slice selection. A probe that allowed sample loading from above was

constructed. Artifacts were eliminated from the images. A software interface that allows the user to set up an experiment by entering values in a spreadsheet was developed. Useful contrast was obtained on fixed biological samples. Preliminary imaging experiments on both biological and nonbiological systems were carried out.

MEASUREMENT OF EDDY CURRENT FIELDS

Introduction

It is well known that, when a current pulse is passed through a field gradient coil in a superconducting magnet, eddy currents are produced in the conducting structures of the magnet. Experiments such as diffusion-weighted imaging[6] and multiple-quantum spectroscopy[7] require that the eddy current field be a much smaller fraction of the applied field than do conventional spin-echo magnetic-resonance imaging experiments. Strategies to reduce the eddy current field consequently become increasingly important. The two effective strategies are signal processing of the gradient demand, known as preemphasis, and self-shielding of gradient coils, which greatly reduces the interaction of the coil with the metal structures of the magnet. Often, the two techniques are used together. When the sample or subject is substantially smaller than the magnet, another approach is to minimize the size of the gradient coil. In order to evaluate and improve the effectiveness of these three strategies, it is desirable to have a technique to measure eddy current fields. To implement the preemphasis, it is necessary to measure the eddy current field in order to

---

[6] D. G. Cory and A. N. Garroway, Magn. Reson. Med. 14, 435, 1990.
[7] C. Boesch et al., Magn. Reson. Med. 20, 268, 1991.

cancel it. An eddy current measurement technique is also useful in order to evaluate the possibility of performing a given experiment with available hardware. In this chapter, a technique for measuring and analyzing the time behavior of eddy current fields is developed and experimental results are presented. Some general physical considerations of eddy currents are discussed, and existing techniques for eddy current field measurement are reviewed.

An introduction to the Bloch equations will be preliminary to a discussion of the effect of the eddy current field on the nuclear magnetization. The Bloch equations provide a phenomenological description of some aspects of the behavior of spins in a magnetic field. Let **M** be the bulk nuclear magnetization, γ the gyromagnetic ratio, B_0 the polarizing magnetic field, and B_1 the amplitude of the radio frequency excitation field which has rotational frequency ω. T_1 and T_2 are the time constants associated with longitudinal and transverse relaxation, respectively.

$$\dot{M}_X = \gamma\left(B_0 M_Y + B_1 M_Z \sin \omega t\right) - M_X/T_2 \qquad [1]$$

$$\dot{M}_Y = \gamma\left(B_1 M_Z \cos \omega t - B_0 M_X\right) - M_Y/T_2 \qquad [2]$$

$$\dot{M}_Z = -\gamma\left(B_1 M_X \sin \omega t + B_1 M_Y \cos \omega t\right) - \left(M_Z - M_0\right)/T_1 \qquad [3]$$

Instead of T_2, the symbol T_2^* is used to denote the time constant of apparent transverse relaxation when inhomogeneity in B_0 is present. Neglecting the effects of T_1 and T_2 and assuming $B_1 = 0$, the equations can be simplified.

$$\dot{M}_X = \gamma M_Y B_0 \qquad [4]$$

$$\dot{M}_Y = -\gamma M_X B_0 \qquad [5]$$

$$\dot{M}_Z = 0 \qquad [6]$$

We can introduce a complex transverse magnetization $M = M_X + iM_Y$ so that

$$\dot{M} = -i\gamma M B_0 . \qquad [7]$$

Assume that B_0 consists of a constant and a component linearly dependent on position: $B_0 = B0+gx$. $B0$ is independent of time and space, while g is quasi-static. If we define m, the magnetization in the rotating frame, by

$$M = me^{-i\gamma B0 t} , \qquad [8]$$

then

$$\dot{M} = -i\gamma B0 M + \dot{m}e^{-i\gamma B0 t} . \qquad [9]$$

Substituting back into Equation [7] gives

$$-i\gamma B0 M + \dot{m}e^{-i\gamma B0 t} = -i\gamma M(B0 + gx). \qquad [10]$$

Simplifying Equation [10] yields

$$\dot{m}e^{-i\gamma B0 t} = -i\gamma M g x . \qquad [11]$$

Combining Equation [11] with Equation [8] yields

$$\dot{m} = -i\gamma g x m , \qquad [12]$$

which has the immediate solution

$$m(t) = m(t_0)e^{-i\gamma x\int_{t_0}^{t} g dt'} . \qquad [13]$$

If the magnetization has been prepared to a non-zero $m(t_0)$ by a radio frequency pulse, the evolution described by Equation [13] is called a free induction decay (FID).

Consider the characteristics of a general eddy current field. The eddy currents give rise to a magnetic field that roughly tends to cancel the applied field of the gradient coil. The spatial dependence of the eddy current field is not exactly the same as the applied gradient field.[8]

The time behavior of the eddy current field is a multiexponential decay, which can be seen by considering the form of the solution to the differential equation governing the decay of magnetic induction due to current flow in the conductor. Maxwell's equations[9] in a vacuum in SI units are

$$\nabla \cdot \mathbf{B} = 0 \qquad [14]$$

$$\nabla \cdot \mathbf{E} = \frac{\rho}{\varepsilon_0} \qquad [15]$$

$$\nabla \times \mathbf{E} + \frac{\partial \mathbf{B}}{\partial t} = 0 \qquad [16]$$

$$\nabla \times \mathbf{B} - \mu_0 \varepsilon_0 \frac{\partial \mathbf{E}}{\partial t} = \mu_0 \mathbf{J} \qquad [17]$$

where $\mathbf{B}$ is the magnetic induction and $\mathbf{E}$ is the electric field, ρ is the charge density, ε_0 and μ_0 are the permittivity and permeability of free space, and $\mathbf{J}$ is the current density. We also assume Ohm's law, $\mathbf{J} = \sigma\mathbf{E}$, where σ is the conductivity, assumed to be isotropic and homogeneous. Taking the curl of both sides of Ampère's law, Equation [17], neglecting the displacement current, and using the identity

---

[8] R. Turner and R.M. Bowley, J. Phys E: Sci. Instrum. 19, 876, 1986.

[9] J. D. Jackson, Classical Electrodynamics, John Wiley & Sons, New York, 1975.

$$\nabla \times (\nabla \times \mathbf{A}) = \nabla(\nabla \cdot \mathbf{A}) - \nabla^2 \mathbf{A} \qquad [18]$$

gives

$$-\nabla^2 \mathbf{B} = \mu_0 \nabla \times \mathbf{J}. \qquad [19]$$

Using Ohm's law to eliminate **J** for **E**, neglecting the displacement current, yields

$$-\nabla^2 \mathbf{B} = \mu_0 \sigma \nabla \times \mathbf{E}, \qquad [20]$$

so Equation [16] allows this to be expressed as

$$\nabla^2 \mathbf{B} = \mu_0 \sigma \frac{\partial \mathbf{B}}{\partial t}. \qquad [21]$$

The decay of the magnetic induction must be a solution to this diffusion equation. Separation of variables gives solutions for the time part having an exponential time dependence. This makes it possible to correct for the linear spatial term in the eddy current field with a linear filter network. Such a network is known as a preemphasis circuit.

In a superconducting magnet, the conducting structures involved are often at very low temperatures and hence have much greater conductivity than might otherwise be expected. For example, pure aluminum at 10 K has a resistivity of 1.93×10^{-12} Ω-m, while at a room temperature of 293 K its resistivity[10] is 2.65×10^{-8} Ω-m. The time scale of the eddy current decay is directly proportional to its conductivity, as can be inferred from Equation [21], so eddy currents will persist 13,700 times longer in an aluminum

[10] D. R. Lide, (Ed.), CRC Handbook of Chemistry and Physics, 72nd Edition, CRC Press, Boca Raton, 1991.

structure at 10 K than one at 293 K. In a commercial aluminum alloy the conductivity will vary from that of the pure metal, especially at low temperature, so the effect may not be as great. In practice, the principal source of eddy current fields is generally the innermost low temperature aluminum cylinder, which is at approximately the boiling point of liquid nitrogen, 77 K. The resistivity of aluminum at 80 K is 2.45×10^{-9} Ω-m, so the time constant is about 11 times greater than it would be at room temperature.

We consider the desirable characteristics for an eddy current measurement technique. Our primary goal will be to measure the eddy current field in order to evaluate the feasibility of performing a given experiment, not to compensate for the eddy current field. Therefore dynamic range is more important than absolute accuracy. It must be possible to measure eddy currents produced by specific pulse sequences, probably by appending the eddy current measurement experiment to the end of the sequence under evaluation. It is also preferable to have a technique that is insensitive to inhomogeneity so that no shimming is necessary. Since the shim coil power supply may respond dynamically to the gradient pulse and distort the measured eddy current field, it is useful to be able to turn the shim supply off. Experiments based on Selective Fourier Transform[11] and other chemical shift imaging techniques rely

[11]H. R. Brooker et al., Magn. Reson. Med. 5, 417, 1987.

for spatial localization on the integral of the eddy current field, so it is desirable to have a measurement technique that is based upon the integral of the eddy current field. If possible, the technique should have no special hardware requirements.

Literature Review

Many workers have addressed the problem of eddy current measurement and compensation in the literature. The two aspects of the eddy current field to measure are the spatial and time behaviors. We review publications that include descriptions of eddy current measurements, although in most cases the emphasis is placed upon the preemphasis compensation process and its effectiveness, not the measurement. The measurement process can be divided into techniques that detect the derivative of the eddy current field, those that detect the eddy current field itself, and those that detect the integral of the eddy current field.

The derivative of the field is sensed by a pickup coil consisting of turns of wire through which the changing flux of the eddy current field produces an electromotive force that is proportional to the rate of change of the field.[12] A high impedance preamplifier boosts the signal. An analog integrator is usually used to convert the measured voltage into a quantity proportional to the field, although it is possible to use digital integration. When used in a magnet

[12]D. J. Jensen et al., Med. Phys. 14, 859, 1987.

at field, the pickup coil is sensitive also to any change in flux resulting from mechanical motion, which can contaminate the measurement. Since the field of the main magnet is generally about four orders of magnitude larger than the eddy current field and the time scale of mechanical modes is smaller than that of the longer time-constant eddy currents, mechanical stability of the coil is crucial. Drift in the analog electronics is another potential difficulty with the pickup coil technique. Even with digital integration, the preamplifier can experience thermal drift on time scales not too different from the eddy current field. In spite of these difficulties, pickup coils are simple to use and can be used effectively to adjust preemphasis compensation. They are used routinely to correct for eddy currents in commercial, clinical MRI installations.[13]

A different approach to measuring the eddy current field is through its effect on the NMR resonance. One advantage here is that a pickup coil and its associated hardware are not needed. These proportional techniques measure a frequency shift in the NMR resonance that is directly related to the eddy current field.[14] From Equation [13], the phase of freely-precessing magnetization in the rotating frame at time t with respect to t_0 can be written as

---

[13]Personal communication, Dye Jensen.
[14]Ch. Boesch et al., Magn. Reson. Med. 20, 268, 1991.

$$\phi = \gamma x \int_{t_0}^{t} g dt' . \qquad [22]$$

The instantaneous frequency $\omega(t)$, which can be defined as the rate of change of the phase of ϕ by $\omega(t) = d\phi/dt$, is related to the eddy current field through the Larmor equation $\omega = \gamma B$. Magnetic field homogeneity is important when using this approach, so that the FID will persist long enough to obtain a meaningful measurement.

In another approach based on the NMR experiment, the phase of the magnetization ϕ is measured at a single point in time. The phase at that point reflects the integral of the eddy current field over certain intervals in the experiment. Since only one point is sampled in each experiment, many more experiments are required to map the decay of the eddy current field than with the proportional techniques. However, T_2^* and off-resonance effects do not affect the usefulness of the technique. The experiment proposed later is a single-point acquisition technique.

All the techniques surveyed were implemented for unshielded gradient units, although preemphasis is typically used on systems with shielded gradient sets as well.[15] Boesch, Gruetter and Martin of the University Children's Hospital in Zurich[16,17] measure and correct eddy currents on a 2.35 T, 40 cm Bruker magnet. The unshielded gradient set has an inner diameter of 35 cm and a maximum gradient of 1

---

[15] R. Turner, Magn. Reson. Imag. 11, 903, 1993.
[16] Ch. Boesch et al., Magn. Reson. Med. 20, 268, 1991.
[17] Ch. Boesch et al., SMRM 1989, 965.

G/cm. They use two NMR techniques to measure the eddy current field. They interactively correct, using a 12 cm diameter glass sphere filled with distilled water, and they use no spatial discrimination in order to get all spatial components. The experiment consists of a 2.5 s gradient pulse of 0.6 G/cm followed by a train of 8 FIDs. There is a 20 ms delay between the time the gradient is switched off and the first radiofrequency (RF) pulse. The RF pulses have a 2° flip angle in order to reduce echo signals. The total eight FID acquisition time is 200 ms. They solve the Bloch equation for a sample with a single resonance frequency and decay constant and extract

$$\gamma\Delta B_z(t) = (M_y dM_x / dt - M_x dM_y / dt) / (M_x^2 + M_y^2) \qquad [23]$$

as an estimate of time-dependent B_0 shift. They claim this gives enough information for interactive preemphasis adjustment. The one measurement they publish is of an already corrected system and shows $\gamma\Delta B_z(t)$ decaying from 2 to 0 ppm as time t increases from 20 to 200 ms. Glitches are apparent at the ends of the FIDs.

To map the spatial variations, they place a stimulated echo (STE) imaging experiment following the gradient pattern of the experiment they want to analyze. The STE sequence is applied with and without the preceding gradient pattern. The difference in phase is considered to be due to the time integral of the eddy current field in the interval between the first two pulses of the STE sequence. A series of

slices tilted by multiples of 22.5° is obtained from the same 12 cm diameter phantom. The images were phase corrected. The phase of points along the z axis and on circles around the z axis was measured and used as data for a polynomial regression analysis to determine the coefficients of the various spatial harmonics. A table of the harmonic components following a 2.5 second x gradient pulse of 0.3 G/cm is presented. The delay between the end of the gradient pulse and the first RF pulse in the three pulse STE experiment is 20 ms, and the delay between the first and second RF pulse is 15 ms. The experiment was conducted following adjustment of the preemphasis unit. In decreasing order of magnitude, x, z, y, z^2, xz^2, xz, and x^2-y^2 terms were present. The value of the B_0 term was not reported. Note that after x, the dominant terms should be eliminated by the symmetry of the coil/cylinder system. Only the x and xz terms would appear in an ideal system. The presence of terms having even-order in x can be due to two reasons. First, the terms may really exist due to asymmetries in the magnet and gradient coil, crosstalk between amplifiers, etc. Second, the spherical harmonic analysis is highly sensitive to the point chosen to be the origin, and the most favorable origin may not have been employed.

A series of the phase-modulated images is presented as well, with delays of 5, 20, 50, and 100 ms between the x

gradient and the STE imaging sequence. The images are all from an already compensated system.

Van Vaals and Bergman of Philips Research Laboratories in Eindhoven, the Netherlands,[18,19] have a 6.3 T, 20 cm horizontal bore Oxford magnet with 2 G/cm non shielded gradients leaving a 13.5 cm clear bore. To measure the eddy currents, they use a 4 cm diameter spherical phantom. After shimming, they perform a simple "long gradient pulse, delay δ, RF pulse, acquire" sequence. The gradient is switched on for typically 3 s, but at least 5 times the largest eddy current time constant. For various values of δ, the magnet is re-shimmed to maximize the signal during the first 10 ms of the FID. The difference in shim values with and without the gradient pulse is interpreted to be a spherical harmonic expansion of the eddy current field. Exact values of δ are not listed, nor are tables of shim values. Instead, the amplitudes and time constants of the eddy current fields, as derived by a Laplace transform technique, are given. Only the B_0 and linear terms are given; presumably only these terms were shimmed.

Jehenson, Westphal and Schuff of the Service Hospitalier Frederic Joliot, Orsay, France, and Bruker,[20] corrected eddy currents on a 3 T, 60 cm Bruker magnet. The 0.5 G/cm unshielded gradient coils had a clear bore of 50

---

[18]J. J. van Vaals and A. H. Bergman, J. Magn. Reson. 90, 52, 1990.
[19]J. J. van Vaals et al., SMRM 1989, 183.
[20]P. Jehenson et al., J. Magn. Reson. 90, 264, 1990.

cm. They use the same type of multiple FID sequence as Boesch, Gruetter and Martin, with an exponentially increasing sampling interval and 30 sampling points. The gradient prepulse is 10 s in length. The first FID is sampled at 1.5 ms after switching off the gradient, and sampling continues for 4 s using multiple FIDs. They plot the measured field vs. the time with and without compensation. They use a 1 mm by 3 mm water-filled capillary positioned at +/- 5 cm to discriminate B_0 and linear terms. They do not consider crosstalk or higher-order terms. They use the same Laplace transform technique as van Vaals and Bergman, but they apply it iteratively to get better correction.

Heinz Egloff at SISCO (Spectroscopy and Imaging Systems, Sunnyvale, CA)[21] used a pickup coil to measure eddy current fields. To correct the B_0 component of the eddy current fields, he moved the gradient coils until the field shift was eliminated.

Riddle, Wilcott, Gibbs and Price[22] considered the performance of a Siemens 1.5 T Magnetom. They measured the instantaneous frequency $d\phi/dt$ of a 100 ml round flask (presumably filled with water) following a 256 ms, 0.8 G/cm gradient pulse. They present plots for imaging and spectroscopy shims as well as for the gradient pulse. They endorse $d\phi/dt$ as an indication of shim. It would seem to

---

[21] H. Egloff, SMRM 1989, 969.
[22] W. R. Riddle et al., SMRM 1991, 453.

work only for single-line samples, however. Following the gradient pulse, the plot of $d\phi/dt$ contains peaks that are not explained. They may be an indication of the true $d\phi/dt$, or they may be artifacts from beginnings and ends of FIDs. The sensitivity of the technique as presented here seems to be about 1 Hz.

Hughes, Liu and Allen[23] of the Departments of Physics and Applied Sciences in Medicine at the University of Alberta measured the eddy current fields of their 2.35 T, 40 cm bore Bruker magnet. After 57 delays ranging between 500 μs and 2.5 s following a 0.2 G/cm gradient pulse the FID was measured and the offset frequency of the line determined. They placed a 13 mm diameter spherical water sample at +/- 1, 2, 4 cm along the axes of the radial gradients under test. A four-exponential fit was applied to all six locations simultaneously. The shortest time constant was associated with the amplifier rise time. An interesting plot shows that the field associated with each time constant is essentially linear. The B_0 fields associated with the various time constants are different, however, suggesting a unique isocenter for each time constant.

Zur, Stokar, and Morad[24] of Elscint in Israel place a doped water sample at +/- 5 cm from the center in the direction of the gradient of the field. A train of 256 FIDs is acquired after switching off the gradient. Each FID is

---

[23]D. G. Hughes et al., SMRM 1992, 362.
[24]Y. Zur et al., SMRM 1992, 363.

Fourier transformed, bandpass filtered, then inverse transformed. The instantaneous magnetic field is obtained from $d\phi/dt$. The digital filtering points to a problem with phase measurements. The low-pass filters required to eliminate Nyquist aliasing and to improve the signal-to-noise ratio (SNR) distort the phase of the received signal. Digital filtering enables one to recover the SNR ratio of a small bandwidth without significant phase distortion.

Wysong and Lowe[25] at Carnegie Mellon and the University of Pittsburgh measured eddy current fields on a Magnex 2.35 T 31 cm magnet with unshielded gradient coils. A 1 cm diameter sphere containing water doped to $T_1 \sim T_2 \sim 1$ ms is used. A 0.9 G/cm gradient is applied for 1.0 s, then ramped down in 128 μs. A train of pulses of flip angle $\pi/2$ set 1 ms apart is applied for 1 second. One point is sampled for each FID. With the system adjusted so the FID is in-phase in the absence of a gradient field, the out-of-phase component is proportional to $\sin\left(\gamma \Delta B t e^{-t/T_2}\right) \approx \gamma \Delta B t e^{-t/T_2}$ for small values of time and gradients.

Keen, Novak, Judson, Ellis, Vennart and Summers[26] of the Department of Physics, University of Exeter, propose using a phantom slightly smaller than the imaging volume. Having switched off the gradient, they delay a variable time, then pulse and acquire the FID. The Fourier transform

---

[25] R. E. Wysong and I. J. Lowe, SMRM 1991, 712.
[26] M. Keen et al., SMRM 1992, 4029.

of the FID represents a projection of the phantom in the quasi-steady eddy current field. Measuring the distance between the peaks that appear as edge artifacts gives the eddy current field.

Teodorescu, Badea, Herrick, and Huson[27] at the Texas Accelerator Center and Baylor College of Medicine measured eddy current fields in their 4 T, 30 cm superferric self-shielded magnet. The magnet was operated at 2.19 T. They follow Riddle et al.[28] in their measurement. A small phantom is placed at various off-center locations. They use a 0.8 G/cm gradient pulse of 15 ms and a 750 μs rise/fall time. This is followed by an FID (or a series of them) that is acquired for 20 ms. They compare this to the result obtained from a pickup coil.

The eddy current field was measured with a sense coil and analog integrator by Morich, Lampman, Dannels, and Goldie.[29] They used a Laplace transform approach to derive correct parameter values for an analog inverse filter to compensate for the eddy currents. The analog inverse filter was of conventional design,[30] placed at the input of the gradient power supply. The theory was tested on an Oxford Magnet Technology whole body superconducting magnet.

The approach is based on the ease with which a linear system can be analyzed in the reciprocal space s defined by

---

[27]M. R. Teodorescu et al., SMRM 1992, 364.
[28]W. R. Riddle et al., SMRM 1991, 453.
[29]M. A. Morich et al., IEEE Trans. Med. Imag. 7, 247, 1988.
[30]D. J. Jensen et al., Med. Phys. 14, 859, 1987.

the Laplace transform. We can understand the calculation as follows. Assume the gradient field for $t>0$ in response to a unit step function is

$$g(t) = 1 - \sum_{i=1}^{N} a_i e^{-tw_i} \qquad w_i \equiv 1/\tau_i . \qquad [24]$$

The amplitudes a_i and time constants τ_i can be determined through a best-fit to experimental data. To determine the inverse filter, the first step is to deconvolve the step function to find the impulse response $h(t)$, which can more conveniently be accomplished by a multiplication in the complex frequency space, s. The equivalent function $G(s)$ is obtained by a Laplace transform

$$G(s) = \frac{1}{s} - \sum_{i=1}^{N} \frac{a_i}{s + w_i} \quad . \qquad [25]$$

Then the impulse response in the s domain, $H(s)$, is found through the relation

$$G(s) = H(s)/s, \qquad [26]$$

so that

$$H(s) = sG(s) = 1 - \sum_{i=1}^{N} \frac{a_i s}{s + w_i} \qquad [27]$$

is the impulse response. The inverse filter's impulse response is just the reciprocal of the impulse response of the eddy currents,

$$1/H(s) = \frac{1}{1 - \sum_{i=1}^{N} \frac{a_i s}{s + w_i}} \quad . \qquad [28]$$

The step response of the inverse filter, $F(s)$, is the convolution of a step function and the impulse response:

$$F(s) = \frac{1}{sH(s)} = \frac{1}{s - \sum_{i=1}^{N} \frac{a_i s^2}{s + w_i}} \quad . \qquad [29]$$

The amplitudes b_i and time constants ν_i of the inverse filter can be read directly from the inverse Laplace transform, $f(t)$, of $F(s)$:

$$f(t) = 1 + \sum_{i=1}^{N} b_i e^{-t/\nu_i} \quad . \qquad [30]$$

The inverse Laplace transform was performed by matrix inversion for a four-time-constant case using Gaussian elimination.

Now the appropriateness of these techniques to the project of following the time evolution of the eddy current field can be considered. Two of the techniques, those of Egloff and Morich, involve the use of a pickup coil, preamplifier, and integrator. We choose to confine ourselves to NMR techniques. The procedures of Boesch, van Vaals, Jehenson, Riddle, Keen, Hughes and Teodorescu require shimming to correct for the inhomogeneity of B_0. The fact that T_2^* must be reasonably long also limits the region where eddy current fields can be measured to well inside the active imaging volume. Wysong and Zur propose similar NMR techniques that do not require shimming. In general, however, it is samples with long relaxation times that are most sensitive to small eddy current fields, and the use of

a sample with especially short (T_1~T_2~1 ms) relaxation times is not an obvious way to detect low-level fields. The T_2 of the sample limits the duration of the interval in which phase can be sampled. Another drawback is that the trains of $\pi/2$ pulses will produce stimulated echoes, even if T_1 is on the order of the interpulse separation. However, this may be the most promising of the techniques surveyed.

Spin-Echo Techniques

Distortions in the phase of spectra spatially localized with a two-pulse Selective Fourier Transform technique[31] were observed by Mareci.[32] He observed that the distortions were reduced by lengthening the echo time, consistent with the known behavior of field distortions due to eddy currents induced in the metal structures of the magnet by the pulsed gradient fields used for spatial localization. We consider how a series of spin echo experiments identical except for

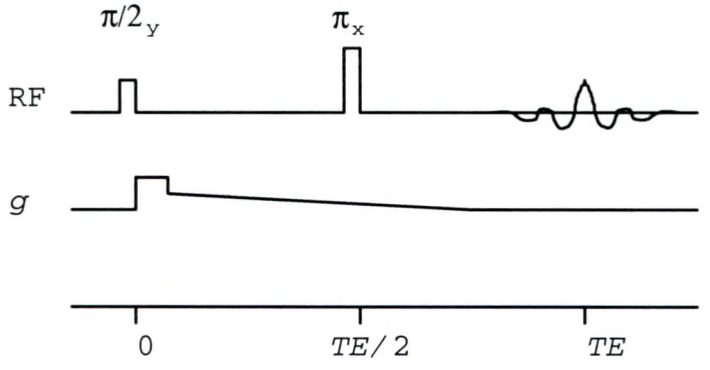

Figure 1. Two-pulse experiment with pulsed field gradient. The long trailing edge of the gradient pulse indicates distortion due to the eddy current field.

[31] H. R. Brooker et al., Magn. Reson. Med. 5, 417, 1987.
[32] T. H. Mareci, Personal communication.

increasing echo time (TE) gives an indication of the eddy current field distortion as a function of time. Consider the evolution of the rotating-frame magnetization m in the presence of the gradient field g illustrated in the pulse sequence in Figure 1. For $0<t<TE/2$, we can directly apply Equation [13] so

$$m(t) = m(0)e^{-i\gamma x\int_0^t g dt'} \qquad 0 \le t \le TE/2. \qquad [31]$$

We can also apply the result directly to describe the magnetization's evolution following the π pulse. Let $TE/2_+$ be the time just after the π pulse. Then

$$m(t) = m\left(TE/2_+\right)e^{-i\gamma x\int_{TE/2}^t g dt'} \qquad TE/2 \le t. \qquad [32]$$

The π pulse along x inverts the sign of the imaginary part of $m(t)$, equivalent to taking the complex conjugate:

$$m\left(TE/2_+\right) = m^*(0)e^{i\gamma x\int_0^{TE/2} g dt'}. \qquad [33]$$

Putting it together gives

$$m(t) = m^*(0)e^{i\gamma x\int_0^{TE/2} g dt'}e^{-i\gamma x\int_{TE/2}^t g dt'} \qquad TE/2 \le t \qquad [34]$$

$$m(t) = m^*(0)e^{i\gamma x\left[\int_0^{TE/2} g dt' - \int_{TE/2}^t g dt'\right]} \qquad TE/2 \le t. \qquad [35]$$

Measurement of the phase exactly at the center of the Hahn echo should remove off-resonance effects, whether due to chemical shift or field inhomogeneity. Now it remains to be shown that measurements of the phase at a series of echo times can be used to find $g(t)$. If ϕ_0 is the phase without a gradient pulse applied, then

$$\phi(TE) - \phi_0 = \gamma x\left[\int_0^{TE/2} g dt' - \int_{TE/2}^{TE} g dt'\right] = \gamma x\left[2\int_0^{TE/2} g dt' - \int_0^{TE} g dt'\right]. \quad [36]$$

We define a function $G(t)$ by

$$G(t) = \gamma x \int_0^t g dt' \quad , \quad [37]$$

which simplifies the expression above for ϕ:

$$\phi(TE) - \phi_0 = \gamma x\left[2G(TE/2) - G(TE)\right] \quad . \quad [38]$$

By measuring ϕ_0 and measuring ϕ at a number of echo times, we hope to be able to extrapolate the function $G(TE)$, whose rate of change gives the eddy current field. By performing a series of experiments in which the values of TE are related by successive powers of two ($TE_{i+1} = 2TE_i$), we can obtain a series of coupled equations. Using the shorthand $\phi(TE_i) = \phi_i$,

$$\phi_{i+1} - \phi_0 = \gamma x\left[2G_i - G_{i+1}\right] \qquad i = 1, 2, \ldots . \quad [39]$$

Inverting for G_i yields

$$G_i = \left[(\phi_{i+1} - \phi_0)/\gamma x + G_{i+1}\right]/2 \qquad i = 1, 2, \ldots . \quad [40]$$

For large enough i, $G_i = G_{i+1}$, and the equation has an immediate solution. The remaining G_i can be determined recursively. The rate of change of $G(TE)$ is the eddy current field.

Experiments and subsequent data analysis have pointed to several drawbacks in this approach. The first is that the echo time TE limits the maximum length of the gradient pulse. A gradient pulse long in comparison to the eddy current decay time approximates a step function, which

simplifies the analysis of the eddy current response.[33] However, lengthening the *TE* reduces the time resolution of the experiment. Placing the gradient pulse before the excitation pulse as in Figure 2 eliminates the problem and decouples the length of the gradient pulse from the echo time.

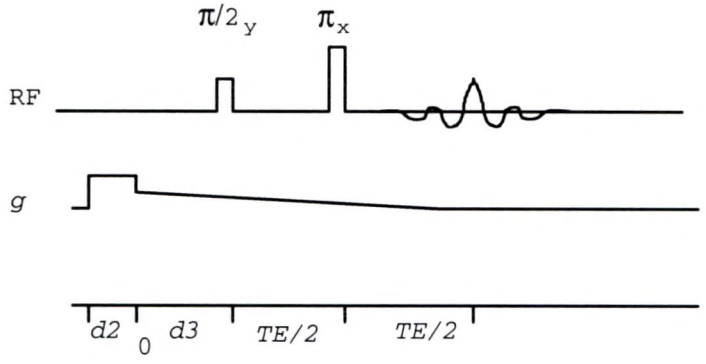

Figure 2. Gradtest v.1.2 is a spin-echo experiment for measuring the eddy current field following a pulsed field gradient.

The above analysis assumes a point sample. Any real sample has finite extent and will experience some dephasing, and associated signal loss, as its phase evolves in the gradient field. By not subjecting the transverse magnetization to the gradient pulse but only to the eddy current field, the dephasing effect is reduced. Another drawback proved to be that the signal decayed due to T_2 relaxation before G_i stabilized. With the gradient pulse before the excitation, the condition $G_i = G_{i+1}$ could be met for small values of *TE*. However, for large *TE* we could

[33] M. A. Morich et al., IEEE Trans. Med. Imag. 7, 247, 1988.

assume that $g = 0$ while for small TE, $g \neq 0$. To solve for the G_i it is necessary to know one of them in advance, so to determine G_i for large TE, another experiment was performed. TE was held fixed at a large value and $d3$, the interval between the end of the gradient pulse and the RF excitation pulse, was varied in steps of $TE/2$. A system of simultaneous equations describes the phase obtained by varying $d3$ in steps of $TE/2$, starting with $d3 = 0$:

$$\phi(TE + d3) - \phi_0 = \gamma x[2G(TE / 2 + d3) - G(TE + d3) - G(d3)] \quad . \qquad [41]$$

The problem of signal decay due to T_2 is thus circumvented. This technique could be used by itself or, as we used it, only to obtain a starting point for varying TE.

A remaining difficulty is the ambiguity of phase measurement. Phase can be directly measured only modulo 360°, but the accumulated phase in our experiment may be much greater. One way around this difficulty is to reduce the applied gradient so that we can be sure that our sample rate is above the Nyquist limit, so that $\phi_{i+1} - \phi_i < 180^o$. To get an upper bound that guarantees no phase ambiguity, assume that the eddy current field has the same amplitude as the applied field before the π pulse and zero amplitude following the π pulse. Protons precess at 4258 Hz/G. To get a measurement for $TE/2$ = 512 ms without phase ambiguity would, for a sample 1 cm from the center, require a gradient pulse no greater than 0.000229 G/cm. Such a small gradient

pulse would result in no detectable phase accumulation in practical cases. Experimental experience showed that it was not simple to choose in advance a gradient amplitude that would result in measurable phase accumulation, but no phase ambiguity, at all echo times. Instead, we repeated the experiment for a series of increasing gradient amplitudes. For phase changes of less than 360°, the phase doubles as the gradient doubles. We could keep track of phase accumulations greater than 360°, thereby decreasing the minimum detectable eddy current field.

Stimulated Echo Techniques

The stimulated echo (STE) has advantages over the spin echo as the basis of an eddy current field measurement experiment. Consider the stimulated echo sequence Gradtste in Figure 3. The "e" at the end of the pulse sequence name indicates that this is a stimulated echo experiment. A third pulse is required to excite a stimulated echo. The magnetization of interest is flipped into the transverse plane by the first RF pulse, where it accumulates phase

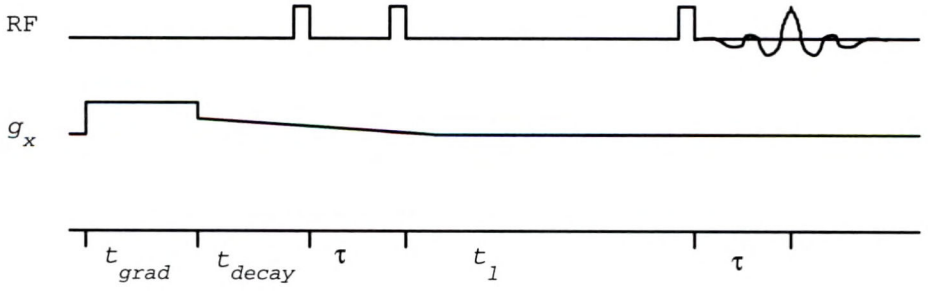

Figure 3. Diagram for Gradtste, a three pulse stimulated echo experiment for measurement of the eddy current field.

shift due to static field inhomogeneity and eddy current fields. Then, stored by the second RF pulse along the z axis, the magnetization accumulates no more phase until the final RF pulse tips it back into the transverse plane. The phase accumulation due to static inhomogeneity now unwraps, resulting in the stimulated echo. If t_1 is long enough, there is essentially zero eddy current field in the second τ, so the phase accumulated due to eddy current fields in the first τ is preserved.

It is possible to follow the eddy current decay by incrementing either t_{decay} or τ between experiments. If τ is incremented, the procedure for determining the eddy current field is similar to that for spin echo experiments. The phase shift for two experiments with different τ is subtracted to get the integral of the eddy current field in the time between the earlier and later τ. A more direct approach is to increment t_{decay} between experiments, keeping τ small. Using this approach, each experiment yields the integral of the eddy current field over a short interval τ. Dividing by τ yields the average eddy current field in the interval.

Two advantages of the STE are immediately evident. A single STE experiment can be directly related to phase accumulation in a single interval, eliminating the need for the recursive data analysis or simultaneous equations associated with the spin echo technique. This would also seem to make the choice of gradient pulse amplitude more

straightforward. Since t_1 is limited by T_1, which is generally longer than T_2, it is possible to sample with smaller residual gradient field than in the spin echo experiment.

The eddy current field is subject to a multiexponential decay. The integral of a multiexponential decay is another multiexponential decay. We can expect these functions to be reasonably smooth. That is, if we notice that the phase is not changing much between delay increments, we could either increase the delay increment or increase the amplitude of the gradient pulse. This is a form of adaptive sampling, since the sampling strategy for the gradient field depends upon its behavior. The sampling technique should be capable of following the residual field decay when preemphasis is used, and in this situation the field will not in general decay monotonically, since some of the decay components may be overcompensated. Therefore the adaptive sampling must also be able to decrease sensitivity when needed.

Since the eddy current field generally changes most rapidly at short times, varying τ to keep the measured phase shift approximately constant for each value of t_{decay} yields less densely spaced measurements when the field is changing slowly. We have implemented such an adaptive sampling technique by writing a recursive macro Adgrad in the Varian MAGICAL language to perform a series of measurements in which τ is varied to "lock" the phase shift to 45°. The macro functions as a command to the Varian program "VNMR"

through which the spectrometer is controlled. Adgrad allows the automatic measurement of the eddy current field over a large dynamic range. Forty-five degrees is large enough to measure with enough precision and yet small enough to minimize the possibility of aliasing. The values of phase

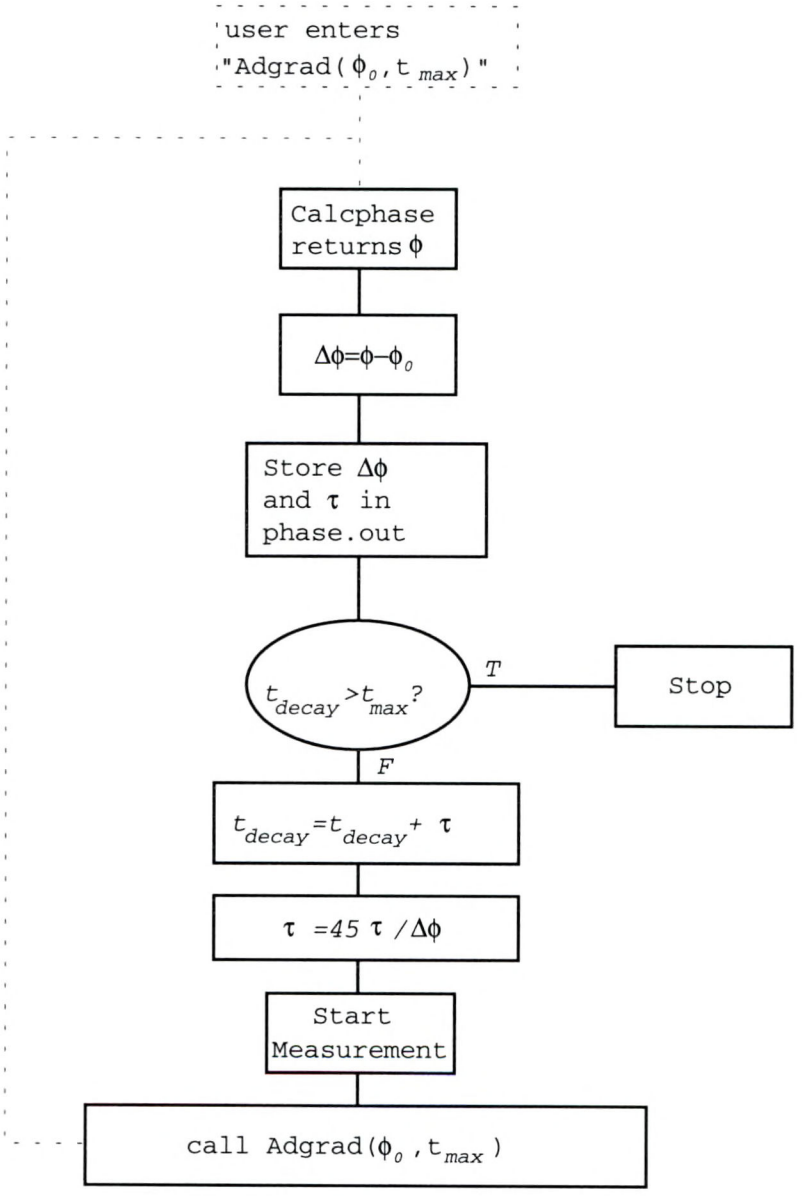

Figure 4. Flow chart of the macro Adgrad, which executes adaptive sampling of the eddy current field. The dotted portion is not part of the macro.

shift $\Delta\phi$ and τ are easily reduced to a plot of the eddy current field vs. time. A flow chart of Adgrad is found in Figure 4. It is most easily explained in the context of the whole experimental procedure. The user notes the phase of the STE for an experiment with g_{ph}, the value of the gradient pulse, set to zero. He then selects a combination of τ, t_{decay}, and g_{ph} that results in phase accumulation of about 45° and acquires an FID. He also removes the file "phase.out" if it remains from a previous session. Then he executes the macro Adgrad(t_{max}, ϕ_0), where t_{max} is the value of t_{decay} at which the macro will stop and ϕ_0 is the phase with $g_{ph} = 0$.

Adgrad first calls the macro Calcphase to compute the phase $\Delta\phi$ at the center of the acquisition window (that is also the center of the FID) for the data already in memory. Adgrad then stores the values of $\Delta\phi$ and τ as the first line in the output file "phase.out." Next, Adgrad tests to find if $t_{decay} > t_{max}$. If so, it ends the experiment. This should not occur on the first pass through the test. In the following two steps, Adgrad sets up the timing for the next experiment. The new t_{decay} is set to be greater than the old by τ, to provide for a contiguous series of intervals τ. The new τ is set so that if the eddy current field remains constant, the next measurement will yield a phase $\Delta\phi$ of 45°. Now the measurement is started. Following the measurement, the macro calls itself and the process repeats. When the

$t_{decay} > t_{max}$ test is passed, Adgrad returns control to the operator.

Two other adaptive sampling macros have been developed for eddy current testing. Adgrad2 changes both τ and g_{ph} to lock the phase to 45°. The resulting series of experiments are more closely spaced in time than Adgrad. Using Adgrad2, it is possible to follow the eddy current field over a wider range of values than with Adgrad. However, linearity error in the digital-to-analog converter or nonlinear amplifier response will be reflected in error in the eddy current field. Adgrad180 locks the phase to 180°. It can only work when the phase accumulation is monotonically decreasing yet never changes sign, which is true for the uncompensated gradients. Otherwise, Adgrad180 may lose its lock. If the error in the measured angle is constant, the accuracy of the technique, when applicable, should be about 5 times better than for Adgrad or Adgrad2.

In the preliminary data analysis, we assumed that the eddy current field was essentially constant over the sampling interval τ, so that $g = \Delta\phi/\gamma x\tau$. An Excel spreadsheet was used to reduce and analyze the data and plot the results. An example is shown in Figure 5. It is a plot of the average field in each of the measurement intervals. Since the field is dropping exponentially, not linearly, fits to the mean value will have systematic errors. A better way is to assume a multiexponential decay of the eddy current field, and then calculate what phase will be

measured in the STE experiment. If we define $\Phi(t)$ as the total phase shift from $t = 0$ to t_n for $g_{ph} = 1$, then

$$\Phi(t) = \sum_{i=1}^{n} \phi_i \quad . \qquad [42]$$

This phase shift is just, for a single experiment,

$$\Phi(t) = \gamma x \int_0^t g(t')dt' \quad . \qquad [43]$$

Now we assume that the eddy current field can be described by a three-time-constant decay,

$$g(t) = Ae^{-t/t_a} + Be^{-t/t_b} + Ce^{-t/t_c} \, . \qquad [44]$$

Integration gives a function to which the measured phase can be fit:

$$\Phi(t) = \gamma x \left[t_a A\left(1 - e^{-t/t_a}\right) + t_b B\left(1 - e^{-t/t_b}\right) + t_c C\left(1 - e^{-t/t_c}\right) \right]. \qquad [45]$$

Results

Eddy current measurements were made on several gradient coils of practical interest. Tests of the Oxford gradient coils in the 2 and 4.7 T magnets were conducted. For the 4.7 T magnet, the eddy current measurements were used to adjust the preemphasis network. Measurements of the eddy current fields associated with home-built gradient coils were also made. The detailed design and construction of the coils, on 9 and 15 cm formers, is described in the following chapter.

Initial measurements were made using the spin-echo technique of Gradtest v1.2. A 5 mm NMR tube with about 5 mm

of H_20 trapped by a vortex plug was used as a sample and placed 1.7 cm from the center of a 2 T, 31 cm horizontal-bore magnet (as measured from an image). The Oxford Z gradient in the Oxford 2 T magnet was pulsed to a value of 1000 units or 1 G/cm. The manufacturer-installed preemphasis filter was in place. A d3 array with four elements was used to establish the phase value for large echo times via matrix inversion of simultaneous equations. An echo time array resulting in a series of coupled equations was used to work back to 1 ms. The resulting plot is shown in Figure 5. The bumpiness of the plot may be due to the preemphasis. Data points are plotted in the center of the interval for which they represent the average gradient.

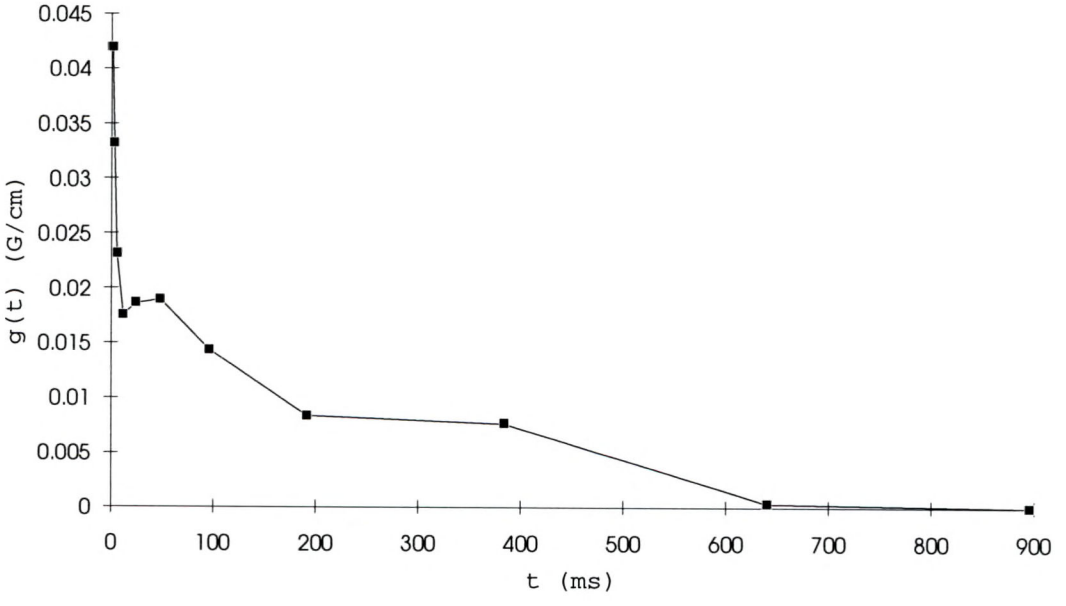

Figure 5. Eddy current field as a fraction of applied field for Oxford gradient coil.

Stimulated echo measurements using the pulse sequence Gradtste and the macro Adgrad were conducted for the Oxford gradients as well as for the 9 cm home-built gradient coil in the 2 T, 31 cm diameter magnet. The eddy currents for the Oxford gradients were measured with the manufacturer-installed preemphasis filter in place. The 9 cm coils had no preemphasis. A 5 mm NMR tube with about 5 mm of H_2O trapped by a vortex plug was used as a sample and placed between 1 and 2 cm from the center of the magnet. The center of the sample was determined from an image. In all cases, t_{grad} = 2 s, $d1$ = 2 s, t_1 = 0.5 s, and two averages were acquired. The parameter τ was set to 4 ms and t_{decay} was 1 ms for the initial experiment. The data were analyzed in Excel spreadsheets. In the plots of field vs. time given in Figures 6 and 7 for the Oxford and 9 cm coils respectively, the average of the eddy current field over the sampling interval is plotted against the middle of each sampling interval. The eddy current field is represented as a percentage of the applied gradient. Note that without preemphasis, the eddy current field due to the 9 cm coil declines monotonically, while the preemphasis filters contribute to the measured field of the Oxford coils. For the 15 cm coil tested in the 2.0 T magnet, eddy current measurement was used to calculate values for an inverse filter. The coils and samples were removed between the experiments before and after preemphasis. The Techron 7540 amplifiers were used to drive the coils in current mode.

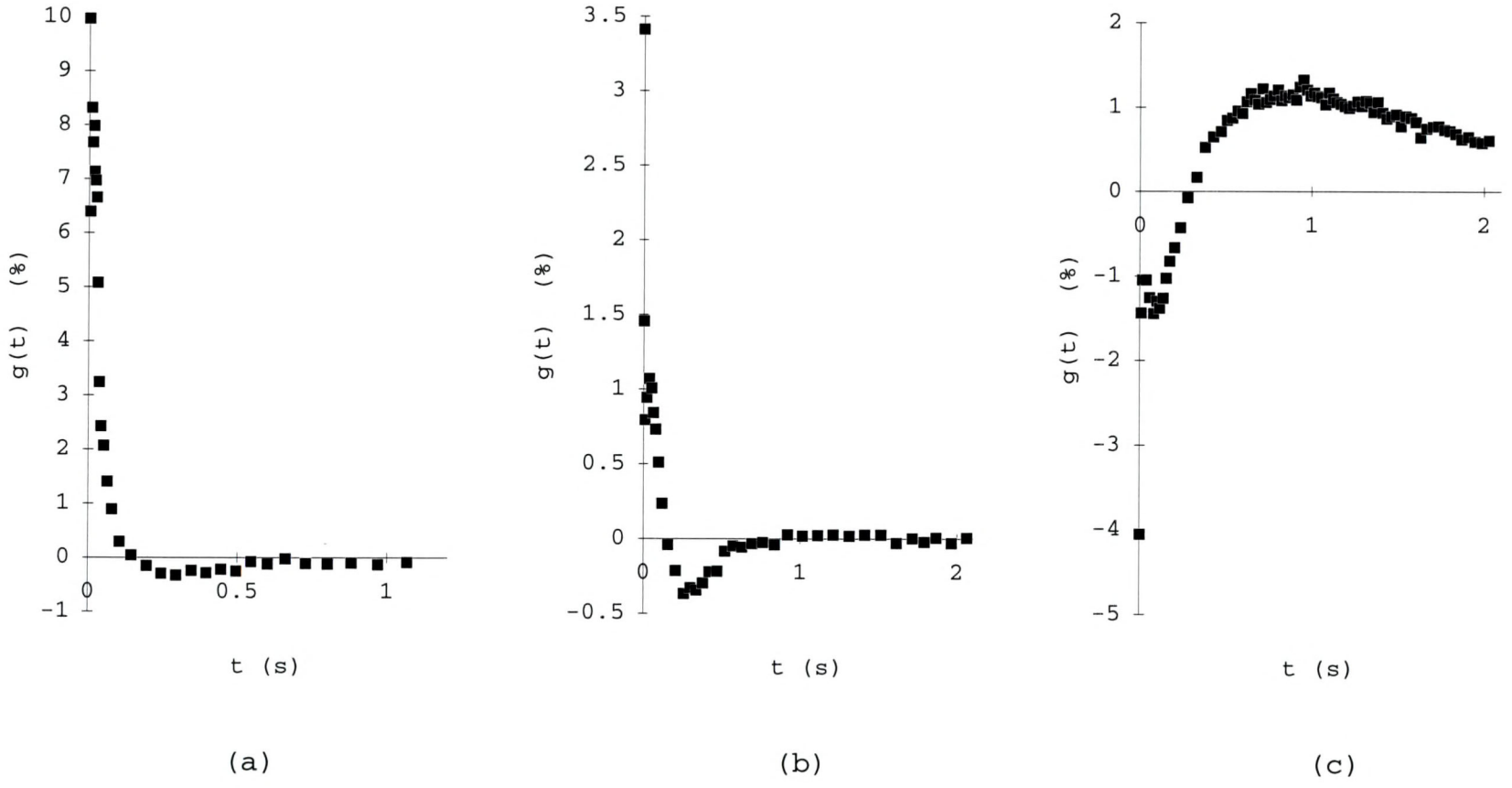

Figure 6. Eddy current field of Oxford gradient coil in 2 T 31 cm magnet as measured with Adgrad. The manufacturer-installed preemphasis filter was in place. a) X coil; b) Y coil; c) Z coil.

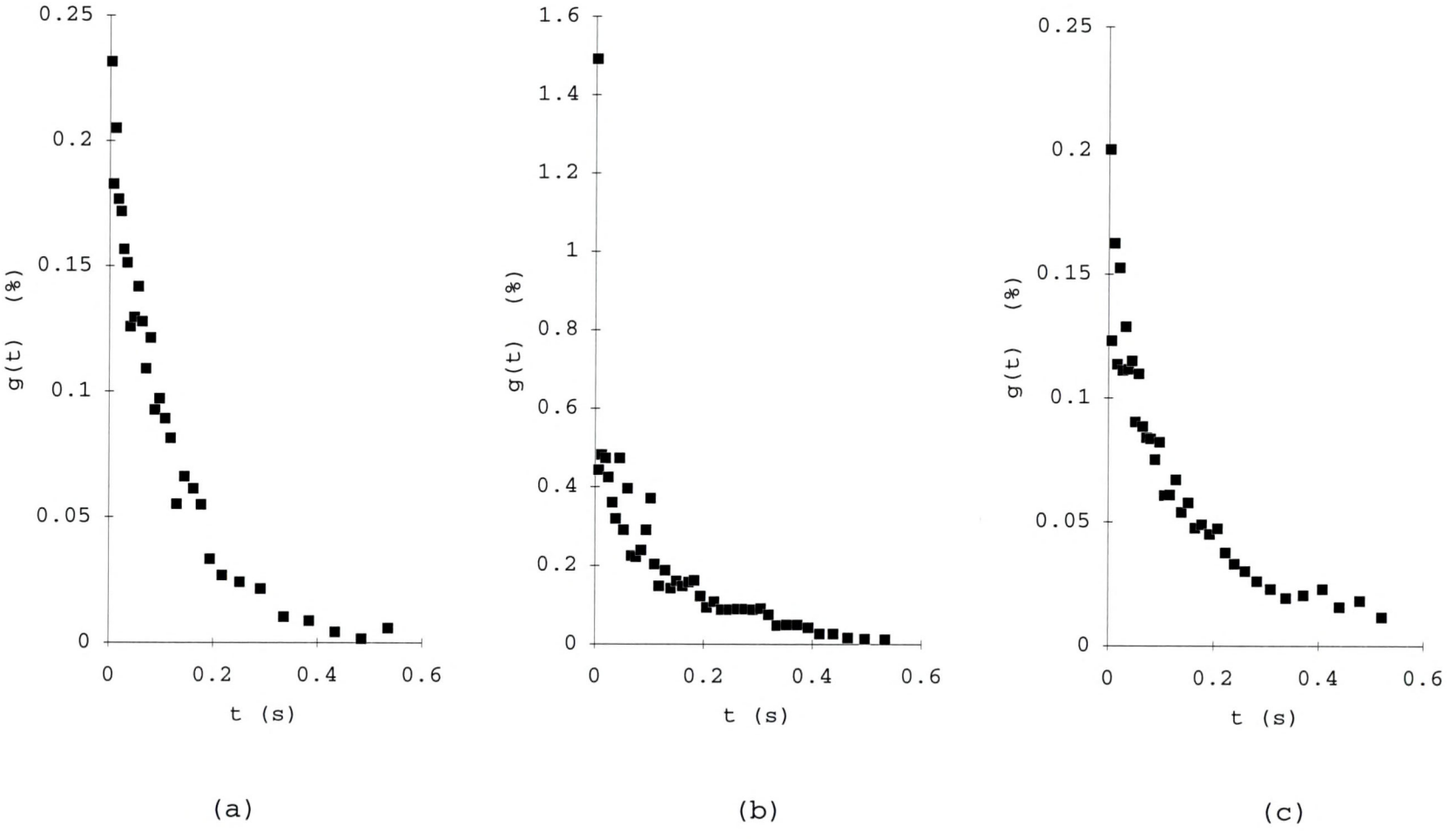

Figure 7. Eddy current field of home-built 9 cm gradient coil in 2 T 31 cm magnet as measured with Adgrad. No preemphasis filter was used. a) X coil; b) Y coil; c) Z coil.

The same sample and RF coil were used as in the Oxford and 9 cm tests. In all cases, t_{grad} = 0.5 s, t_1 = 0.5 s, the sample position was between 1 and 2 cm from the center, and the position was measured in an image. The data were

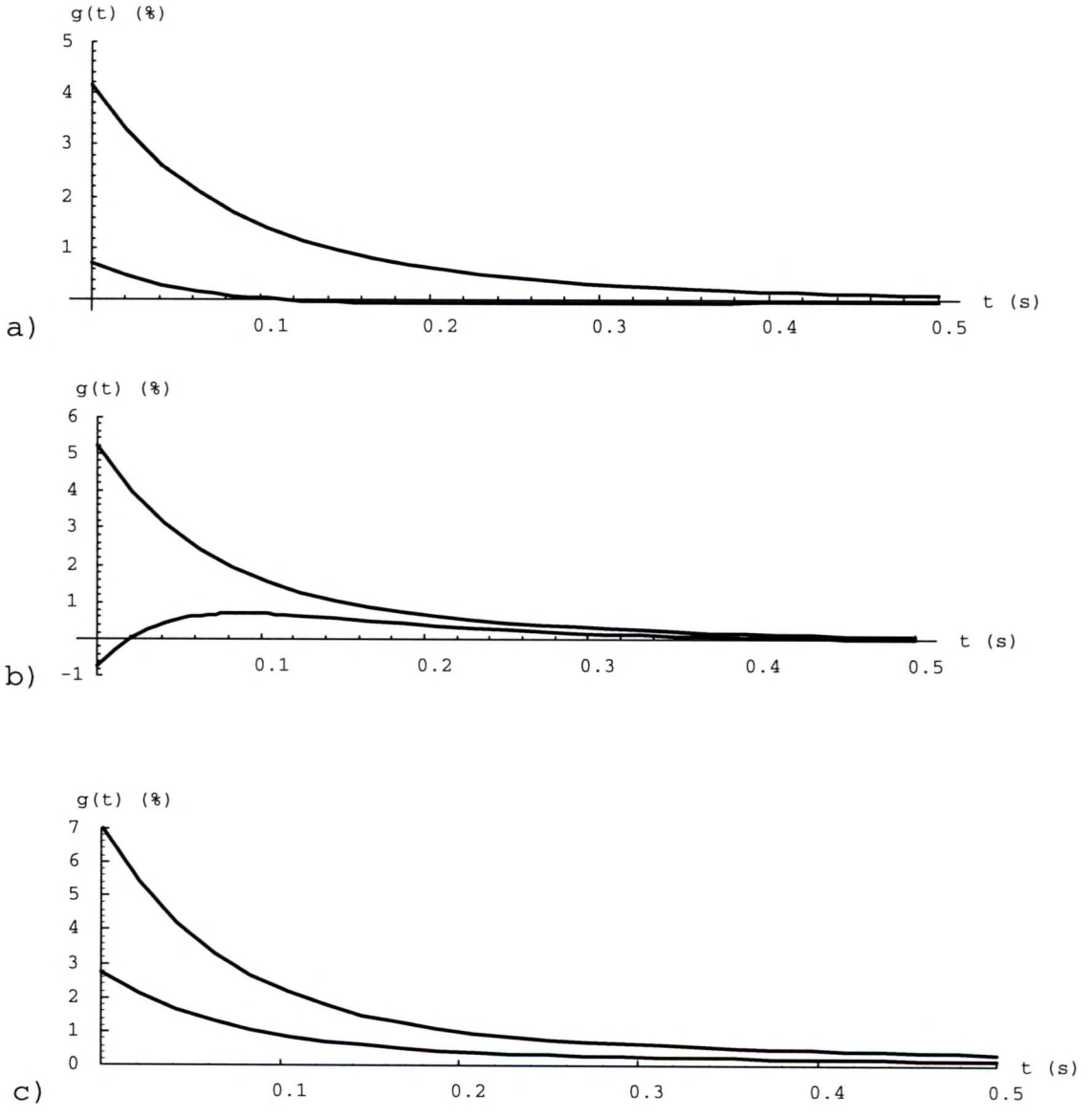

Figure 8. Eddy current field of 15 cm gradient coil set in 2.0 T magnet system before (upper curve) and after compensation (lower curve). a) X coil; b) Y coil; c) Z coil.

acquired with Adgrad2, that changes g_{ph} as well as τ to keep the phase locked. Eight averages were acquired. The eddy current field was measured out to 1 s, although the plots in Figure 8 only show 0.5 s. The data were analyzed both with the average-field technique used in the Excel (Microsoft, Inc.) spreadsheet and with a multiexponential curve fit in Mathematica (Wolfram Research, Inc.). The curve fits seemed more satisfactory, and are shown in Figure 8. The lower curves represent the eddy current field after compensation. The curves plotted are the derivatives of the exponential curves that were fitted to the raw data. The preemphasis filter amplitudes and time constants were taken to be those of the eddy current field itself. This procedure should

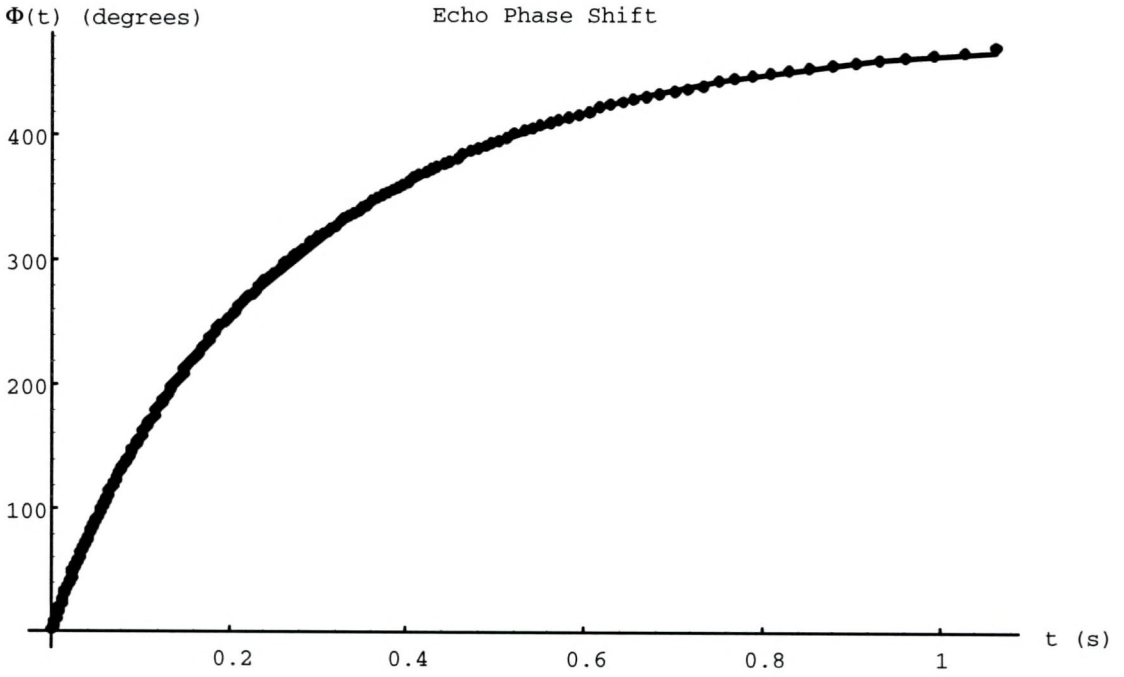

Figure 9. Fit to raw data of eddy current field of Oxford Z gradient field for 4.7 T magnet system before compensation.

tend to underestimate the preemphasis required, but since the unshielded eddy current fields were already less than 5% of the applied field, the error is not severe.

The 4.7 T magnet that replaced the 2 T 31 cm magnet did not have manufacturer-installed preemphasis, so the eddy current measurement techniques were applied to design an appropriate preemphasis filter. Since the uncompensated eddy currents were on the order of 50% of the applied field, the approximation used to compensate the 15 cm coil would not be effective. An inverse Laplace transform technique was used to design the filters. The technique was implemented through the symbolic inverse Laplace transform capability of Mathematica. An example of a multiexponential fit to the raw phase accumulation performed with Mathematica is shown in Figure 9. Eddy current fields before and after compensation are presented in Figure 10. The upper curves represent the field before, and the lower curves after, preemphasis. For the Y coil, the procedure was repeated a second time to obtain an additional reduction of the eddy current field. The lowest curve in Figure 10 (b) represents the eddy current field after the second pass of eddy current correction.

Conclusion

A technique to measure the eddy current field of a pulsed field gradient based on the phase of the stimulated-echo NMR signal has been proposed. Experimental

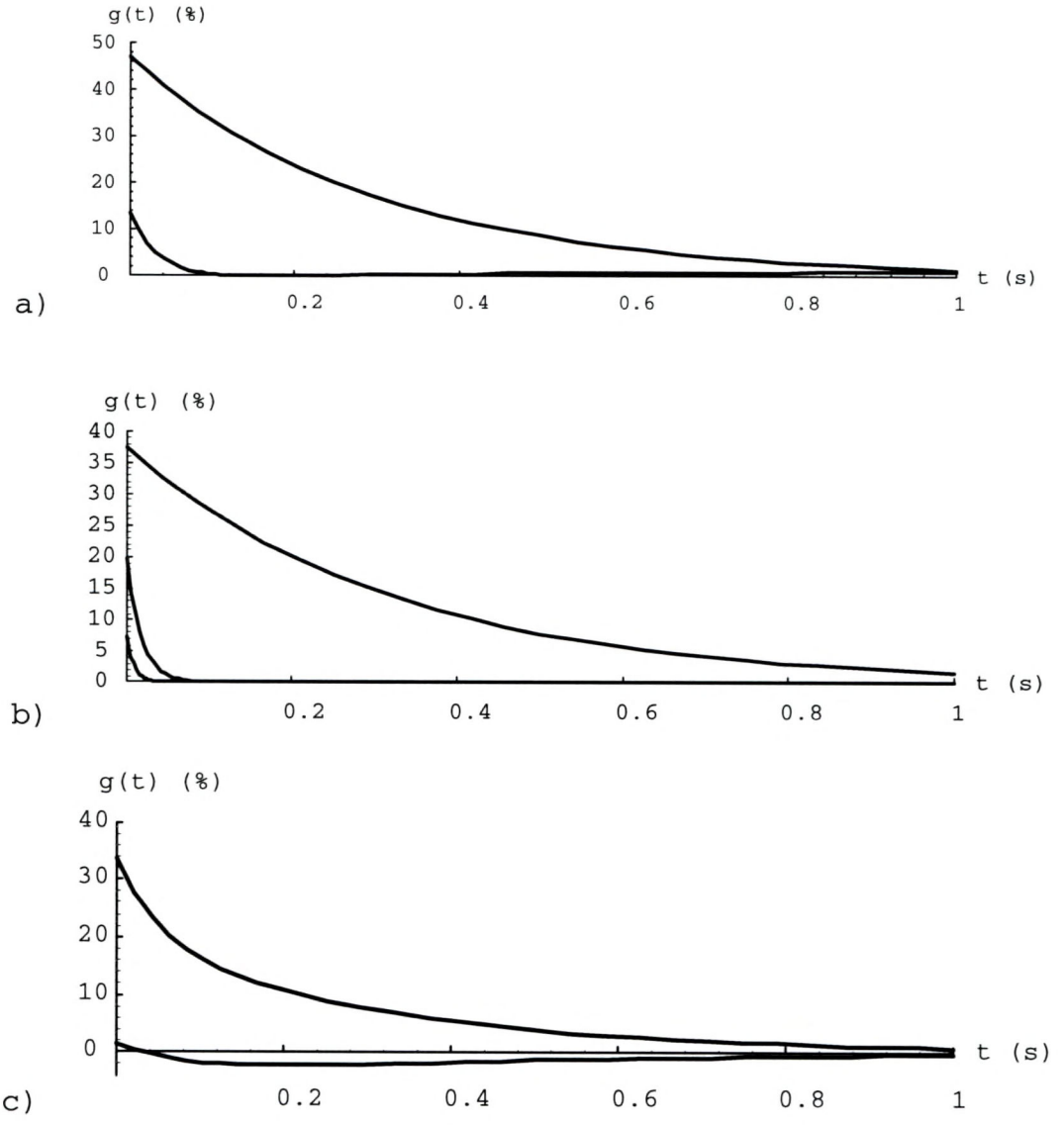

Figure 10. Eddy current field of Oxford gradient coil in 4.7 T magnet system before (upper curve) and after compensation (lower curve). a) X coil; b) Y coil. Lowest curve was acquired after second-pass preemphasis; c) Z coil.

verification consists of measurements of the eddy current field before and after preemphasis. The level of the eddy current field after preemphasis can be interpreted as an upper limit on the error bar of the measurement. It is only an upper limit, since other errors also contribute to the

residual eddy current field. Any error in the values of timing components in the preemphasis filter will add to the residual eddy current field. Also, any distortion in the amplifier will reduce the effectiveness of the compensation, since the filter was designed based on the assumption that the amplifier is linear. Error in the eddy current measurement technique itself might be due to other echo terms than the stimulated echo contributing to the signal. However, experiments have shown that other echoes are essentially negligible due to a combination of favorable timing and phase cycling. In the case of Adgrad2, which scales g_{ph} as well as τ, it is clear that some error is due to inaccuracies in the digital-to-analog converter (DAC) output level. The applied gradient is then not proportional to the DAC code, and so there is an error in normalizing to the applied gradient. Error in the curve fits may be significant, since in a multiple-exponential fit it is difficult to get an accurate fit if the time constants are not widely separated. Note that second-pass adjustment of the preemphasis was more effective in reducing the residual eddy current field.

The technique came out of a need to quantify phase distortions in localized spectroscopy. It is therefore better-suited to measuring the time integral of the eddy current field than the field itself, and it is the integral of the field that gives rise to errors in phase-sensitive techniques such as SFT. It is often useful to employ the

basic stimulated echo experiment without adaptive sampling to quantify the integral of the eddy current field over an interval, and allow one to predict the resulting phase distortion directly.

The adaptive sampling algorithm is able to follow eddy current fields that are not simply monotonically decreasing. I found experimentally that if the angle became much different than 45°, the values for τ would bounce around a lot before stabilizing. This is probably due to the control being purely proportional. Introducing an integral term might help.

The relatively large eddy current field produced by the 15 cm Z gradient compared to the X and Y channels is due to its extended-linearity design, which locates the currents farther from the region of interest than a Maxwell pair. The relatively large eddy current field produced by the 9 cm Y gradient compared to the X and Y channels may be due to a problem with centering the gradient coils in the bore. The measured field gradient would then depend strongly on the position of the sample.[34]

The contrast in eddy current field between the large and small coils is clear. There is a factor of about 10 in eddy current field between the 15 cm coil and the larger Oxford coil. There is a factor of about 180 in eddy current field between the 9 cm coil and the Oxford gradient coil set

[34]D. J. Jensen et al., Med. Phys. 14, 859, 1987.

in the X and Z channels. Experimental evidence demonstrates the advantage in eddy current field obtainable with reduced size gradient coils.

GRADIENT COIL DESIGN

Introduction and Theory

Although virtually all NMR measurements rely on auxiliary field coils, there has been comparatively little published work on the design and analysis of shim and field gradient coils compared to that for radio frequency coils. However, high levels of performance have become increasingly important for these low-frequency room-temperature coils on several frontiers of the NMR technique. Three of these areas are gradient coils for NMR microscopy, coils for spatial localization of spectra, and local gradient coils for functional imaging of the human brain.

The simple forms of discrete element coil designs have linear regions that are about 1/3 of the coil radius.[35] Therefore the gradient coil must be considerably larger than the sample. Increasing the linear region would allow smaller coils to be used, generally improving efficiency and decreasing eddy current fields. Several approaches are available to increase the region of linearity. Adding discrete elements to cancel more high-order terms in the harmonic expansion has been done successfully by Suits and Wilken.[36] Continuous current density coils have also been

[35]F. Romeo and D. I. Hoult, Magn. Reson. Med. 1, 44, 1984.
[36]B. H. Suits and D. E. Wilken, J. Phys. E: Sci. Instrum. 23, 565, 1989.

designed with linear regions that are a large fraction of the radius.[37] We have tried to take a fresh approach, combining aspects of both continuous and discrete designs. For a solenoidal main magnet, available radial gradient coil designs are longer and less efficient than axial designs, so we have chosen to concentrate on the radial case.

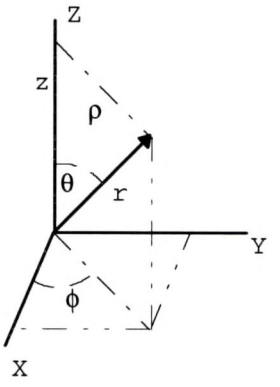

Figure 11. The coordinate system used in the text.

An appropriate starting point to find a new radial gradient coil design might be: what current distribution on the surface of an infinitely long cylinder would produce a field in which the axial component is linearly proportional to the radial position, $B_z \propto x$? To describe surface currents and fields, we introduce the three coordinate systems described by Figure 11. Any point can be described in any of three orthogonal coordinate systems. In the Cartesian system a point is described by its location along the three axes (x, y, z). In the spherical system, it is described by two angles and the distance from the origin:

[37] R. Turner, J. Phys. D: Appl. Phys. 19, L147, 1986.

(r, θ, ϕ). In the cylindrical system, the point is described by (ρ, ϕ, z). It can be easily shown that an azimuthal component of the surface current, J_ϕ, proportional to $\cos\phi$ and independent of z produces the desired spatial dependence. Neglecting for the moment the problem of current continuity, there are two possible approaches to achieving the $\cos\phi$ angular dependence. First, it can be approximated by superimposing azimuthal currents with no axial component. The solutions are exactly the same as for discrete filamentary currents. The first approximation, the 120° arc familiar from the so-called Golay double-saddle design,[38,39] is shown in Figure 12(a). This class of designs has been called the "Golay Cage" because of its correspondence to the double-saddle design. Higher-order approximations utilizing superimposed arcs are derived by Suits and Wilken.[40] The other approach is to use our freedom to choose any axial current to meet $J_\phi \propto \cos\phi$ by varying the current direction, for example, $J_\phi \propto \cos\phi$, $J_z \propto \sin\phi$. This approach leads to the Cosine Coil shown in Figure 12(b). Note that in Figure 12 the return paths are located away from the active volume of the coil. For a coil of practical length, the current return paths can significantly reduce and distort the gradient field.

---

[38] F. Romeo and D. I. Hoult, Magn. Reson. Med. 1, 44, 1984.
[39] M. J. E. Golay, Rev. Sci. Inst. 29, 313, 1958.
[40] B. H. Suits and D. E. Wilken, J. Phys. E: Sci. Instrum. 23, 565, 1989.

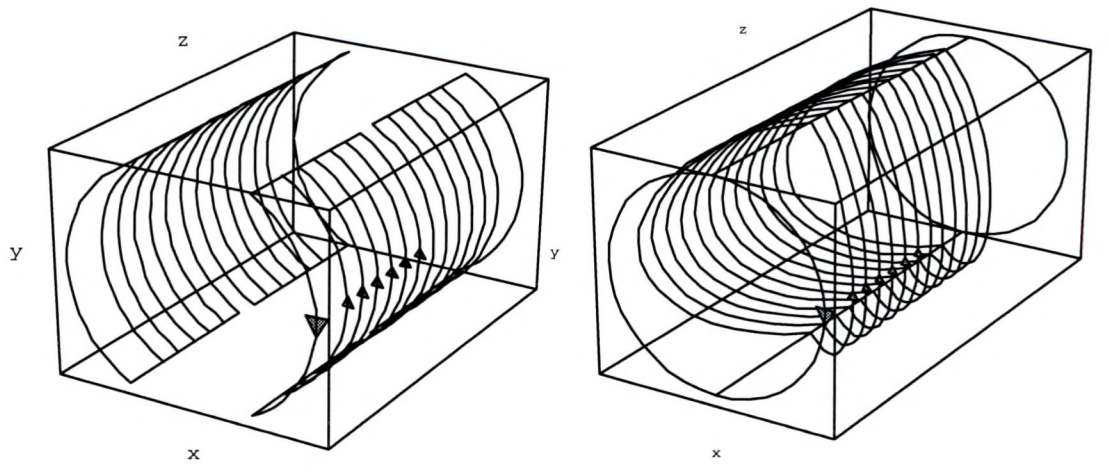

Figure 12. Two radial gradient coils. a) The Golay Cage Coil; b) Cosine Coil.

Another approach to current return paths is possible if we relax the requirement that the current is confined to the surfaces of cylinders. The current return paths can be located in the same plane as the azimuthal current paths. A gradient coil can be constructed of a stack of planes approximating a current sheet, such as shown in Figure 34 (a) on page 111. The planes include radial as well as azimuthal current elements. The radial currents do contribute to the axial magnetic field. It happens that the third-order harmonic terms eliminated by using 120° arcs are independently zero for the radial currents connecting the arcs. These Concentric Return Path (CRP) Coils can have a linear region that can be increased in length by stacking more planes together. The overall combined coil structure can also be very short, since the return paths do not require extra length. In order to improve the linear region

beyond that produced by a constant current density along z, we can adjust the relative current or position of each planar unit.

Literature Review

This literature review will be focused on efforts to increase the useful volume of a gradient coil, to optimize its performance, and to understand the eddy current field associated with a switched gradient it produces. The specific requirements of coils of interest for functional imaging of the human head are discussed, along with several approaches to meeting those requirements.

Gradient coils can be grouped into two broad categories: those made up of discrete current elements as in Figure 13, and those approximating a continuous current density. The former include the original NMR shim coil designs,[41,42] while the latter approach has been used to make possible actively shielded gradient coils.[43]

Anderson described a set of electrical current shims for an NMR system based on an electromagnet.[44] The coils were located in two parallel planes, one against each poleface, to allow access to the sample. Each coil was designed to produce principally one term in the spherical harmonic expansion of the field. The orthogonality of the

---

[41] W. A. Anderson, Rev. Sci. Inst. 32, 241, 1961.
[42] M. J. E. Golay, Rev. Sci. Inst. 29, 313, 1958.
[43] P. Mansfield and B. Chapman, J. Magn. Reson. 66, 573, 1986.
[44] W. A. Anderson, Rev. Sci. Inst. 32: 241 1961.

expansion ensured relatively independent adjustment of the current in the various coils.

Techniques for designing higher-order shim coils for solenoidal magnets were set forth by Romeo and Hoult.[45] Coils are designed by expanding the Biot-Savart integral for B_z, the axial component of the field, in a spherical harmonic series about the center of the coil for simple filamentary building block currents.

$$B_z(r,\theta,\phi) = \sum_{l=0}^{\infty} \sum_{m=-l}^{l} A_{l,m} P_l^m(\cos\theta) e^{im\phi}. \qquad [46]$$

The functions $P_l^m(\cos\theta)$ are the associated Legendre functions. As building blocks are added in the form of arcs on the surface of a cylinder, more terms in a spherical harmonic expansion of the field can be set to zero. The designer connects the building blocks in such a way as to satisfy the requirement of current continuity, which is not built into the Biot-Savart law. By setting each undesired term in the harmonic series to zero, a system of equations results. The solutions are the current, length, and position parameters of the coil designs. A Maxwell pair, as shown in Figure 13(b), is composed of a loop placed at θ = 60° and another having opposite current direction placed at θ = 120°. This separation is required to cancel the (l, m) = (3, 0) term, while the odd symmetry cancels the (2, m) and (l, $m \neq 0$) terms. The desired (1,0) term remains. The

[45] F. Romeo and D. I. Hoult, Magn. Reson. Med. 1, 44, 1984.

simplest coil producing a gradient perpendicular to the axis of the cylinder is the double saddle or "Golay" coil illustrated in Figure 13(a). The arcs all subtend 120° and are placed at the four angles θ_1 = 68.7°, θ_2 = 21.3°, 180°-θ_1, and 180°-θ_2, where they produce an (*l*, *m*) = (1, 0) term but no (*l*, *m*) = (3, 0) term. The relative current directions are shown in Figure 13(a). A family of solutions exists for which the sum of the (*l*, *m*) = (3, 0) terms produced by the arcs cancels, but the (*l*, *m*) = (3, 0) terms produced by each arc are not necessarily zero. We designate such coil designs by the two angles θ_1 and θ_2, so that the design above would be described as 68.7°/21.3°. Adding additional current elements to the coils adds degrees of freedom to the system of simultaneous equations, and makes it possible to cancel more terms.

Adding another pair of loops adds two more degrees of freedom (the current and position of the new loops), and makes it possible to cancel higher-order terms including (5, 0). Note that the equations are not linear, so for a large number of current elements the procedure becomes unwieldy. For shim coils, it is less important to improve the linear region of a first-order or gradient coil than to design additional coils whose lowest-order terms are of increasingly high order. The simple saddle coil in Figure 13(a) designed by this technique has a useful volume with a radius of about 1/3 that of the cylinder.

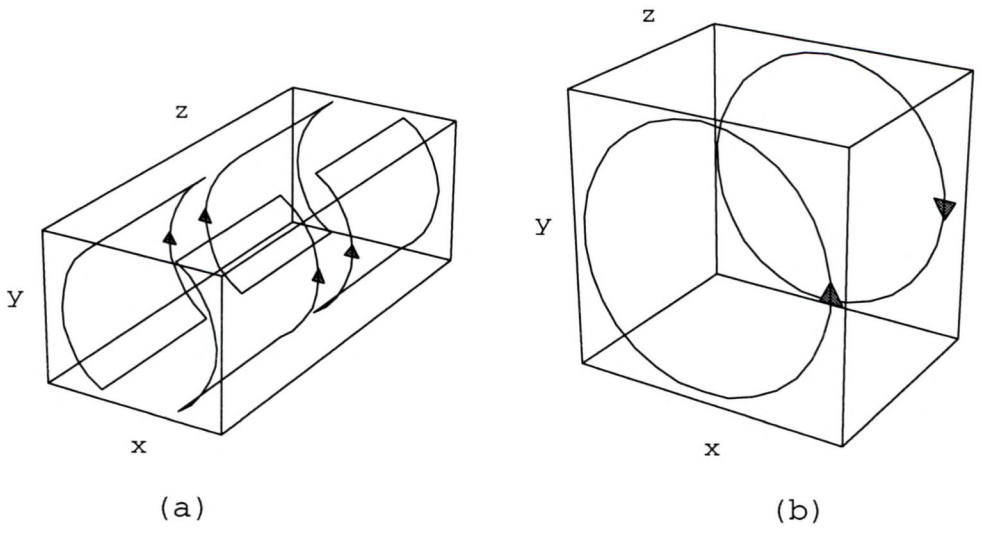

Figure 13. Field gradient coils that use discrete filamentary current elements. a) Double-saddle 68.7°/21.3° coil to produce the radial field gradient x or y; b) Maxwell pair produces the axial, or z, field gradient.

The approach is best suited to cases where the gradient coil is much larger than the sample, since the harmonic series approximation to the field converges more rapidly near the center of the coil. Although in theory the current elements are lines, in practice they do have finite dimensions, especially where large field intensity is required. Including the wire diameter would greatly complicate the design procedure. It is natural to use this technique to design the shim coils mentioned above, where it is conventional to have separate adjustments for as many as twelve or more terms in the harmonic series. The coils designed this way have the advantage of simplicity of construction.

The building block approach was successfully extended by Suits and Wilken[46] to use discrete wires to produce a constant field gradient over an extended region. They evaluated designs for cylinders with the polarizing field both parallel and perpendicular to the axis. To improve the useful volume of the radial gradient coil, they superimposed four saddle coils. The available degrees of freedom then included the number of turns in each of the four coils, the angular width of the four arcs, and the axial positions of the arcs. Systems of nonlinear equations result that were solved to null desired terms in an expansion of the field in orthogonal functions. Numerical plots demonstrate that the useful volume was extended to about eight times that of the simple saddle coil. In each case, the volume was nonspherical. The problems of extending this approach further are that larger systems of nonlinear equations are increasingly difficult to solve, and that the orthogonal expansions do not converge rapidly away from the center of the coil.

Bangert and Mansfield[47] designed a gradient coil in which the wires were included in two intersecting planes. The wires in each plane formed two trapezoids symmetrically placed about the z axis. By setting the angle between the planes to 45°, the third-order terms in the magnetic field are canceled.

---

[46]B. H. Suits and D. E. Wilken, J. Phys. E: Sci. Instrum. 23, 565, 1989.
[47]V. Bangert and P. Mansfield, J. Phys. E: Sci. Instrum. 15, 235, 1982.

Approaches based on a continuous current density are most often used for gradient coils, where performance and linear volume are more important than simplicity. The impetus for these coils was the echo-planar imaging technique of Mansfield,[48] which requires high intensity field gradients switched about an order of magnitude faster than conventional Fourier imaging. Also, shielded coils are useful in other imaging experiments that require rapidly switched gradient fields, and in volume localized spectroscopy. Without shielding to cancel the external field, the higher frequency and intensity lead to greater eddy currents in the cryostat and magnet, that in turn distort the linearity and time response of the field. Using current on two concentric cylinders, it is possible to produce a linear field inside the inner cylinder and zero field outside the outer cylinder. Continuous current density coils can be designed to have a large linear region, and, since current flows on the surface of the whole cylinder, high efficiency.

A Fourier transform technique was applied by Turner to design gradient coils that approximate a continuous current distribution. The approach arose from consideration of the eddy currents induced on cylindrical shields concentric to gradient coils made up of discrete arcs.[49] Expansion of the Green's function in cylindrical coordinates was a natural

---

[48]P. Mansfield and I. L. Pykett, J. Magn. Reson. 29, 355, 1978.
[49]R. Turner and R. M. Bowley, J. Phys. E: Sci. Instrum. 19, 876, 1986.

approach to calculating the eddy current distribution. It was then possible to write the field produced by a general current distribution on the surface of a cylinder as a Fourier-Bessel series.[50] An inverse Fourier transform of the Fourier-Bessel series allowed the current to be expressed in terms of the desired field on the surface of an imaginary cylinder. The field must satisfy Laplace's equation to allow the existence of the inverse Fourier transform. So by specifying the inverse Fourier transform of the desired field, the current distribution required to generate that field could be calculated. The continuous distribution of current is approximated by discrete wires. The wires are placed along the contour lines of integrated current. Although the principal application of the technique was shielded gradients, unshielded coils having extended linearity were also designed. For example, a radial gradient coil is reported to have a gradient uniform to within 5% over 80% of the radius and a length of twice the radius. The overall length of the coil is about 9 times the radius.

It was pointed out by Engelsberg et al. for the case of a uniform solenoid that the homogeneity of the coil depends strongly on the radius of the target cylinder.[51] They note that the field has the target value only on the surface of the target cylinder. For example, in order to achieve a

---

[50]R. Turner, J. Phys. D: Appl. Phys. 19, L147, 1986.
[51]M. Engelsberg et al., J. Phys. D. 21, 1062, 1988.

homogeneous field along the axis of the solenoid, the target cylinder should be as narrow as possible. The effect is especially pronounced at the ends of the target cylinder.

The importance of functional imaging of the human brain and its reliance on the echo planar imaging technique puts special demands on the rise time and field of the gradient coil. The fact that smaller coils will be more efficient and less affected by eddy currents has motivated several workers to design gradient coils that will fit closely over the head. To use a small gradient coil it is necessary to have extended linearity in the radial and axial directions. For a head coil, extended axial linearity is especially important to allow the diameter of the coil to be smaller than the width of the shoulders.

Wong applied conjugate gradient descent optimization to the design of gradient coils with extended linearity.[52] He allows the position of current elements to vary to minimize an error function. It is possible to define the error function as desired, so it is simple to optimize over regions of any shape, or for coil formers of any shape. It is also simple to include parameters such as coil length. Repeated numerical evaluation of the Biot-Savart law for the test wire positions would limit the application to coils with a fairly small number of elements. Wong applied the technique to the design of a local gradient coil for the

---

[52]E. C. Wong et al., Magn. Reson. Med. 21, 39, 1991.

human head.[53] Its overall length was 37 cm, diameter 30 cm. The region of interest is a cylinder 18.75 cm in diameter and 16.5 cm long, over which the RMS (root mean square) error in the field was less than 3% for all three axes. The gradient coil was symmetric to avoid torque. In order to make still shorter coils, Wong placed the return paths on a larger cylinder.[54] The wires on the inner cylinder were connected to the return paths on the outer cylinder over both endcaps. A coil was designed of 30 cm length, 30 cm inner diameter, and 50 cm outer diameter. The optimization region was a cylinder 24 cm long and 20 cm in diameter, and the RMS error over the cylinder was 7.2%. The symmetry of the coil eliminated the torque that arises in other short designs. Additional points on a cylinder 70 cm in diameter were added to the region of interest to force some partial shielding.

Another approach to the design of gradient coils that will fit over the head is to design a coil that has its linear region at one end. Myers and Roemer[55] used only half of a conventional coil to move the linear region to the end. A target field approach was used by Petropoulos et al. to design an asymmetric coil with low stored energy.[56] The coil simulated was 60 cm long and 36.4 cm in diameter. The "center" of the coil was 14.5 cm from one end. The stored

---

[53]E. C. Wong et al., SMRM 1992, 105.
[54]E. C. Wong and J. S. Hyde, SMRM 1992, 583.
[55]C. C. Myers and P. B. Roemer, SMRM 1991, 711.
[56]L. S. Petropoulos et al., SMRM 1992, 4032.

energy for a gradient of 4 G/cm was calculated to be 7.93 J. Since these coils can be made much smaller than the bore of the magnet, eddy currents are not a serious problem and neither of these coils is shielded. Unlike symmetric designs, these coils experience a net torque in the magnetic field that is potentially dangerous.

Another coil at a larger radius can be used to cancel the torque experienced by an asymmetric gradient coil. Petropoulos et al.[57] took this approach to design a head coil with an inner diameter of 36.4 cm, the same as their single-layer coil described above, and an outer diameter of 48 cm. The length of both inner and outer coils was 60 cm. The coil was designed to have a useful region that is a sphere of 25 cm diameter. There is a price to pay in increased stored energy, which increases over the single layer coil value of 7.93 J to 19.2 J. Torque-compensating windings can be added to the same cylinder as the primary coil, resulting in a long structure one end of which is placed over the head of the patient. Abduljalil et al.[58] developed such a coil set for echo-planar imaging. The diameter of the two radial coils was 27.2 cm and 31.2 cm. The center of the linear region was 17 cm from the end. The overall length was not reported, but based on artwork for the wire pattern, it seems to be about 116 cm.

---

[57]L. S. Petropoulos et al., SMRM 1993 1305.
[58]A. M. Abduljalil et al., SMRM 1993, 1306.

Turner has suggested that the best approach to a compact gradient head coil design is that of Wong, in which the return paths are placed on a larger cylinder.[59] He points to the trapezoidal gradient coil designed by Bangert and Mansfield,[60] and discussed above, as a starting point for this approach. The concept for such a gradient coil is described in a patent by Frese, for a cylindrical geometry.[61] It can be thought of as a Bangert and Mansfield coil in which the inner and outer wires have been stretched into arcs on concentric cylinders. This is the design independently developed by Brey and Andrew and dubbed the Concentric Return Path Coil (CRPC). Frese suggested using a stack of the planar CRPC units with spacing along the cylinder's axis varied to improve size of the linear region. He also suggested that the angle of the arcs could be varied from plane to plane. No specific information on the spacing or angle of the arcs is provided.

A survey of the literature suggests that it is desirable to design a short gradient coil using the basic concentric return path geometry to be used for the human head. A direct error-minimization technique is appropriate for two reasons. First, the Fourier-Bessel transform technique, although computationally efficient, limits the shape of the region of optimization to the surface of a

---

[59] R. Turner, Magn. Reson. Imag. 11, 903, 1993.
[60] V. Bangert and P. Mansfield, J. Phys. E.: Sci. Instrum. 15, 235, 1982.
[61] G. Frese and E. Stetter, U. S. Patent 5,198,769, 1993.

cylinder, and axial linearity is important for the head coil. Second, the currents are not confined to the surface of a cylinder, and the transform technique in its present form allows only for current on the surface of a cylinder.

Field Linearity

An extended linear region is one of the goals of a reduced-size gradient coil. In order to evaluate a coil design in terms of its linear region, it is necessary to define the boundary of the linear region. An appropriate definition for the error associated with a field gradient reflects the purpose of the gradient coil. In an error minimization technique, the error definition is central to the coil design. A reasonable parameter to use is the error in the field, $B.E. = \frac{B_z(\mathbf{x})}{\mathbf{G} \cdot \mathbf{x}}$ where the desired gradient, $\boldsymbol{G}$, is measured at the center of the coil. Another error parameter is the error in the gradient, $G.E.$, defined by $G.E. = \frac{1}{|\mathbf{G}|} \frac{dB_z(\mathbf{x})}{dx}$. In an NMR image, error due to the gradient coil simply produces an error in the mapping between the sample and the image. The absolute mapping error is simply the error in the field, $B.E.$ In practice, samples are usually centered in the gradient coil, so we may want to weight the error toward the center of the coil. We use an error parameter that corresponds to the mapping shift relative to the component of the distance to the center in

the direction of the gradient, the relative error $R.E.$, defined by $R.E. = \frac{B_z(\mathbf{x}) - \mathbf{G} \cdot \mathbf{x}}{\mathbf{G} \cdot \mathbf{x}}$.

Efficiency

In order to make use of the efficiency the reduced size of an extended-linearity gradient coil design can provide, it is necessary to construct the coil in such a way that it can be driven efficiently by an amplifier. By adjusting the number of turns, it is possible to trade maximum gradient for switching time. We will show that to obtain optimal switching time, the amplifier should be current-controlled to compensate for the inductance of the coil. To reduce switching time with such an amplifier, the coil resistance per turn should be as low as possible, even though the time constant of the coil will be lengthened. A time-domain model for the coil and amplifier will be used to explore the tradeoff between maximum gradient and switching time.

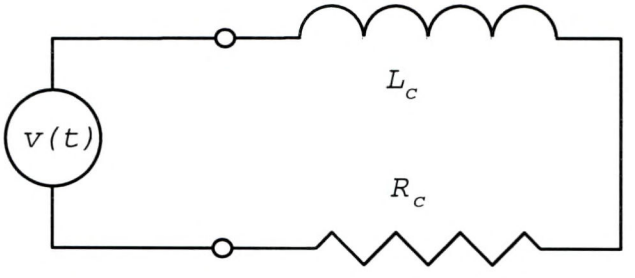

Figure 14. Time-dependent voltage source $v(t)$ drives inductive load.

We show that a current-controlled amplifier gives better switching performance into an inductive load than a

voltage source. The amplifier, modeled by a time-dependent voltage source, $v(t)$, is connected to a load with resistance, R_c, and inductance, L_c, as shown in Figure 14. When a demand is applied to a current-controlled amplifier for some current, i_0, it will by definition change its output voltage, $v(t)$, as much and as rapidly as possible to change the current through an inductance across the output. If the maximum output voltage of the amplifier is V_0, and we define the steady state output voltage $v_0 = V_0 / R_c$, where $V_0 > v_0 > 0$, then the amplifier output voltage and current as a function of time will be

$$v(t) = \begin{cases} 0 & t < 0 \\ V_0 & 0 < t < t_0 \\ v_0 & t_0 < t < \infty \end{cases} \qquad i(t) = \begin{cases} 0 & t < 0 \\ \dfrac{V_0}{R_c}\left(1 - e^{-t/\tau}\right) & 0 < t < t_0 \\ i_0 & t_0 < t < \infty \end{cases}, \tag{47}$$

where t_0 is the time at which the output current reaches the desired current i_0, and $\tau = L_c/R_c$. It is straightforward to calculate that

$$t_0 = \tau \ln\left(\frac{V_0}{V_0 - v_0}\right). \tag{48}$$

The smaller the ratio of V_0 to v_0, the greater the switching time t_0 will become. If the amplifier is a voltage source, the desired current will never be exactly reached. It is more desirable to use a current-controlled amplifier for which $V_0 >> v_0$.

It will be shown that, with a current-controlled amplifier, additional series resistance per turn always decreases performance. Therefore, the series resistance should be reduced as much as possible, for example, by using a larger cross-sectional area for the winding in a coil of fixed radius. Consider again the time response of a current-controlled amplifier from Equation [47]. Any internal amplifier resistance can be included in R_c to avoid any loss of generality. Assume there is some finite, positive R_c that maximizes $i(t)$. Then for that R_c, $\frac{di}{dR_c} = 0$. Solving for R_c:

$$\frac{di}{dR_c} = -\frac{V_0}{R_c^2}\left(1 - e^{-t/\tau}\right) + \frac{V_0}{R_c}\left(-\frac{t}{L_c}\right)\left(-e^{-t/\tau}\right) = 0 \ , \qquad [49]$$

and assuming that R_c and V_0 do not vanish,

$$-\left(1 - e^{-t/\tau}\right) + {R_c t}/{L_c}\left(e^{-t/\tau}\right) = 0. \qquad [50]$$

This can be written as

$$(1 + x)e^{-x} = 1 \quad \text{where } t/\tau = x, \qquad [51]$$

therefore

$$e^x = 1 + x \, . \qquad [52]$$

There is no positive value of x that satisfies Equation [52]. Hence $\frac{di}{dR_c} < 0$ for all $t>0$, $R_c>0$. A lower R_c is always an advantage when using a current-controlled amplifier, although the time constant $\tau = L_c/R_c$ of the gradient system increases as R_c decreases. It is then

appropriate to maximize the cross-sectional area of the windings subject to considerations of linearity and available space.

Next we consider how the number of turns of wire in a coil of fixed cross-sectional area can be varied to achieve the desired performance. It is important to note that the time constant of a coil, for a fixed area, can properly be considered to be independent of the number of turns. This result follows from consideration of a gradient coil at low frequencies, as described by the equivalent circuit of a series resistor R_c and inductor L_c as shown in Figure 15.

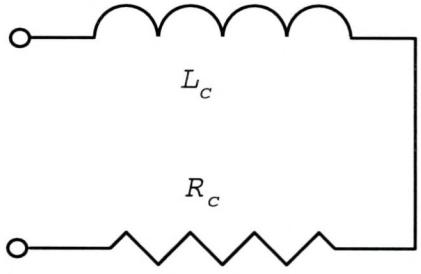

Figure 15. Equivalent circuit of a gradient coil in the low-frequency limit.

Let R_1 be the resistance, and let L_1 be the inductance of a single turn coil. It is well known that the inductance of a coil increases as the square of the number of turns of wire N.[62] The resistance also increases as the square of the number of turns if the area is held constant, since as the number of turns increases, the area of each turn diminishes.

---

[62] T. N. Trick, Introduction to Circuit Analysis, p. 256, John Wiley and Sons, New York, 1977.

The total resistance and inductance are then

$$R_C = R_1 N^2 \qquad L_C = L_1 N^2 . \qquad [53]$$

The time constant τ of the coil is just the ratio

$$\tau = {}^{L_C}\!/_{R_C} = {}^{L_1}\!/_{R_1} . \qquad [54]$$

Perhaps surprisingly, τ is independent of N. The result does not apply when additional turns of wire are added to an existing coil, thus increasing the area. However, since the area should already be as large as possible to maximize the performance, it will not be possible to increase N without decreasing the size of the wire.

To determine how many turns of wire N should be used in the gradient coil, we consider how rapidly and to what value the current rises for various N, holding the area constant. It will be shown that with a current-controlled amplifier, the coil is optimized to switch to the field at which it reaches a saturation current, I_0, which is the maximum that the amplifier can supply. Consider an amplifier with negligible output impedance switching at time $t = 0$ from zero current to maximum current, I_0, through a gradient coil, reaching I_0 at t_0. Assume that $R_C < V_0/I_0$. The current as a function of time is:

$$i(t) = \begin{cases} \dfrac{V_0}{R_C}\left(1 - e^{-t/\tau}\right) & 0 \le t \le t_0 \\ I_0 & t \ge t_0 \end{cases} . \qquad [55]$$

We define a current efficiency k for a single turn so that the gradient field $G(t) = kNi(t)$. R_C varies as N^2, and the

magnetic field G varies as N, so

$$G(t) = \begin{cases} \frac{kV_0}{R_1 N}\left(1 - e^{-t/\tau}\right) & 0 \le t \le t_0 \\ kNI_0 & t \ge t_0 \end{cases} . \qquad [56]$$

A plot of $G(t)$ for various values of N is shown in Figure 16. All three curves have the same time constant, so

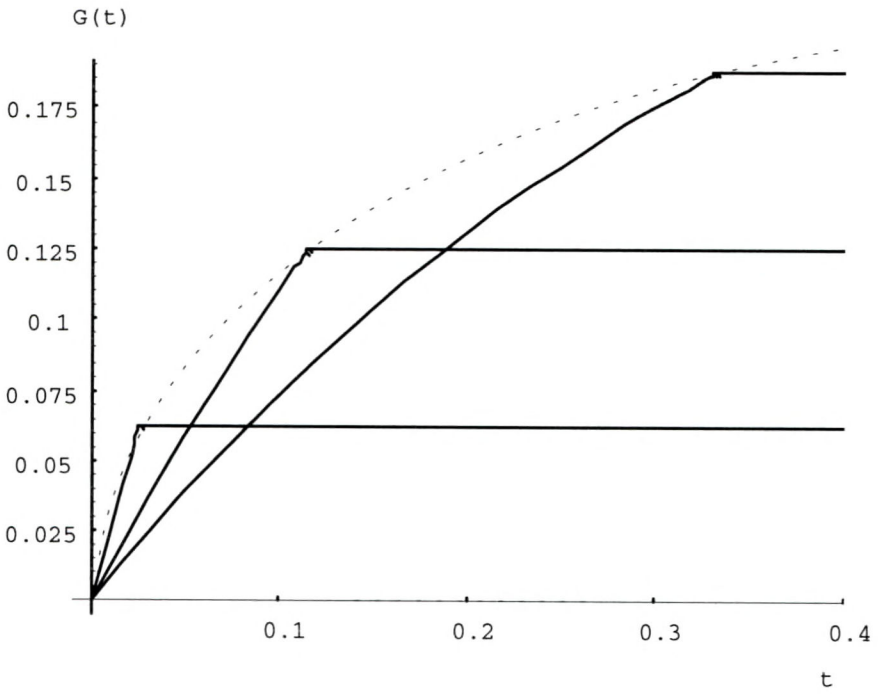

Figure 16. Magnetic field produced by a current controlled linear amplifier coupled to a coil of fixed dimensions. Each curve represents a different number of turns.

the difference in slope is due to the relative amplitude of the maximum gradient. The dotted line connects all the current-limit points. Since at the current-limit point t_0 the amplifier is both a voltage and a current source, we can eliminate $G(t_0)$ in favor of N and t_0, yielding an optimum number of turns for a given switching time.

$$N_{opt}(t_0) = \left({V_0}/{I_0 R_1} \left(1 - e^{-t_0/\tau} \right) \right)^{1/2} \qquad [57]$$

By substituting [57] back into [56], we obtain an expression for $G_{max}(t_0)$, the maximum field attainable at a given switching time for a class of coils having the same design except for the number of turns.

$$G_{\max}(t_0) = k\sqrt{\frac{V_0 I_0}{R_1}\left(1 - e^{-t_0/\tau} \right)} \qquad [58]$$

$G_{max}(t_0)$ is just the dotted line in Figure 15. The tradeoff between switching time and field strength is described by the plot of $G_{max}(t_0)$.

In summary, a design procedure has been developed for optimizing the switching performance of a gradient coil. Use of a current-controlled amplifier reduces switching time. The cross-sectional area of the winding is maximized subject to constraints that include linearity and available space. Then the number of turns is computed from Equation [57], given the desired switching time t_0. The resulting coil will give the largest possible gradient for the desired switching time.

Eddy Currents

Shielding efficiency of self-shielded gradient coils is typically evaluated using a screening factor, a ratio of the magnetic field outside the unshielded coil to the field outside the shielded coil.[63] It is possible to take this

[63] R. Turner, Magn. Reson. Imag. 11, 903, 1993.

type of approach further and evaluate the ratio of the gradient at the center of the coil with and without the shield. This would seem to be a useful approach when evaluating reduced-size gradient coils and comparing them to shielded coils. For small eddy current fields, as in the case of reduced-size coils, an iterative approximation technique described below can be used to solve the integral equation for the eddy current field. This technique is best suited to situations where the eddy current field is much smaller than applied field, so that a first-order approximation can be used. However, it is simple and flexible.

To estimate the eddy current field due to a gradient coil, we assume that there is a passive shield surrounding the coil. The shield is typically part of the cryostat. The boundary conditions at the shield will be

$$(\mathbf{B}_2 - \mathbf{B}_1) \cdot \hat{n} = 0 \qquad [59]$$

$$\hat{n} \times (\mathbf{H}_2 - \mathbf{H}_1) = \mathbf{K} \qquad [60]$$

where $\mathbf{B}_1$ and $\mathbf{H}_1$ are the magnetic induction and field inside the shield, $\mathbf{B}_2$ and $\mathbf{H}_2$ outside the shield, $\mathbf{K}$ is the surface current on the shield, and $\hat{n}$ is an outwardly directed unit vector normal to the surface of the shield.[64] We assume the shield is perfectly conducting, so that with $\mathbf{H}_2 = 0$,

$$\mathbf{H}_1 \times \hat{n} = \mathbf{K}, \qquad [61]$$

---

[64] J. D. Jackson, Classical Electrodynamics, p. I.5, John Wiley & Sons, New York, 1975.

or more conveniently,

$$\mathbf{K} = \frac{1}{\mu_0} \mathbf{B} \times \hat{\rho} \quad , \qquad [62]$$

since $\mathbf{B} = \mu_0 \mathbf{H}$ and $\hat{n} = \hat{\rho}$ at the cylinder. Recall the Biot-Savart law:

$$\mathbf{B}(\mathbf{x}) = \frac{\mu}{4\pi} \int \mathbf{J}(\mathbf{x}') \times \frac{\mathbf{x} - \mathbf{x}'}{|\mathbf{x} - \mathbf{x}'|^3} d^3x' . \qquad [63]$$

Let $\mathbf{B}_0(\mathbf{x})$ be the free-space field from the gradient coil. Then

$$\mathbf{B}(\mathbf{x}) = \mathbf{B_0}(\mathbf{x}) + \frac{\mu}{4\pi} \int \mathbf{K}(\mathbf{x}') \times \frac{\mathbf{x} - \mathbf{x}'}{|\mathbf{x} - \mathbf{x}'|^3} d^2x' \quad , \qquad [64]$$

and substituting Equation [62] for the surface current, for $\mu = \mu_0$,

$$\mathbf{B}(\mathbf{x}) = \mathbf{B_0}(\mathbf{x}) + \frac{1}{4\pi} \int \left[\mathbf{B}(\mathbf{x}') \times \hat{\rho}' \right] \times \frac{\mathbf{x} - \mathbf{x}'}{|\mathbf{x} - \mathbf{x}'|^3} d^2x' \qquad [65]$$

where $\hat{\rho}' \equiv \hat{\rho}(\mathbf{x}')$. This is an integral equation for $\mathbf{B}$. We can solve it iteratively. If we define $\mathbf{B}_n(x)$ as the field to nth order, then the first-order solution is

$$\mathbf{B}_1(\mathbf{x}) = \mathbf{B_0}(\mathbf{x}) + \frac{1}{4\pi} \int \left[\mathbf{B}_0(\mathbf{x}') \times \hat{\rho}' \right] \times \frac{\mathbf{x} - \mathbf{x}'}{|\mathbf{x} - \mathbf{x}'|^3} d^2x' . \qquad [66]$$

The first-order solution does not take into account eddy currents induced by eddy currents. When the coil and shield are in close proximity, not only are the eddy currents larger but they are also closer to the coil, so the second-order effect can be important. To second-order,

$$\mathbf{B}_2(\mathbf{x}) = \mathbf{B_0}(\mathbf{x}) + \frac{1}{4\pi} \int \left[\mathbf{B}_1(\mathbf{x}') \times \hat{\rho}' \right] \times \frac{\mathbf{x} - \mathbf{x}'}{|\mathbf{x} - \mathbf{x}'|^3} d^2x' . \qquad [67]$$

The expressions to first- and second-order for the eddy current field will be used to evaluate numerically the eddy current field of several coil designs. Although the result is not exact, the expressions can easily be integrated for coils and shields of totally arbitrary shape, assuming they are not too close together.

The first-order calculated eddy current field of a 68.7°/21.3° radial gradient coil is plotted in Figure 17. The first-order approximation breaks down for ratios of shield-to-coil radius of less than about 1.5.

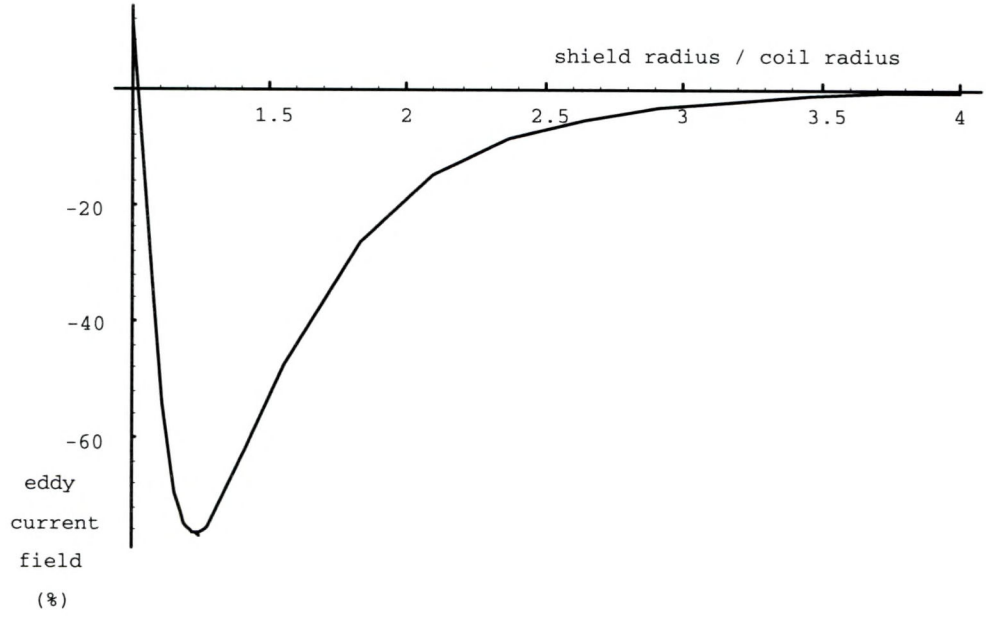

Figure 17. Eddy current field of 68.7°/21.3° double-saddle radial gradient coil. The field as a percentage of applied field is plotted against the ratio of shield radius to coil radius.

Coil Projects

Coil projects were intended to meet experimental needs while exploring some aspect of coil design. The 15 cm, 9 cm and 16 mm NMR microscopy coils are well separated from any sources of eddy currents, and demonstrate the results that can be achieved with simple filamentary designs and without shielding. The CRP coil development was begun to produce a coil with good axial linearity for NMR microscopy, so that long, narrow samples could be observed. It seemed to be well-suited for use as a head coil for echo planar imaging, and we turned the development toward that possible application.

Amplifiers

Three Techron 7540 dual-channel amplifier units (Crown International, Elkhorn, Illinois) are used to drive the three-axis gradient coil sets. Each axis of the gradient coil set is split into two halves, and one channel of each amplifier unit is wired to each half. The plane in which the field is always zero can be shifted slightly by varying the relative gain in the amplifiers. This is particularly useful in the 51 mm, 7 T magnet, since the sample is inaccessible once loaded, and mechanical centering is difficult. The amplifiers are rated to produce 23.8 A at 42 V direct current output. The maximum slew rate is 16 V/μs. The output impedance is less than 7 mΩ in series with less than 3 μH, which is negligible. The power response into a 4

Ω load is +/- 1 dB up to 25 kHz for 265 W. The noise is rated to be 112 dB below the maximum output from 20 Hz to 20 kHz.[65]

Tests of the Techron 7540 were conducted into six loads consisting of wire-wound resistors between 1 and 9 Ω. The amplifiers were pulsed to saturation at low duty cycle. 10-90% rise times were between 4 and 6.5 μs, and so are essentially independent of load. Thus the amplifier was bandwidth limited, not slew-rate limited, and it is appropriate to use a linear model. The voltage and current

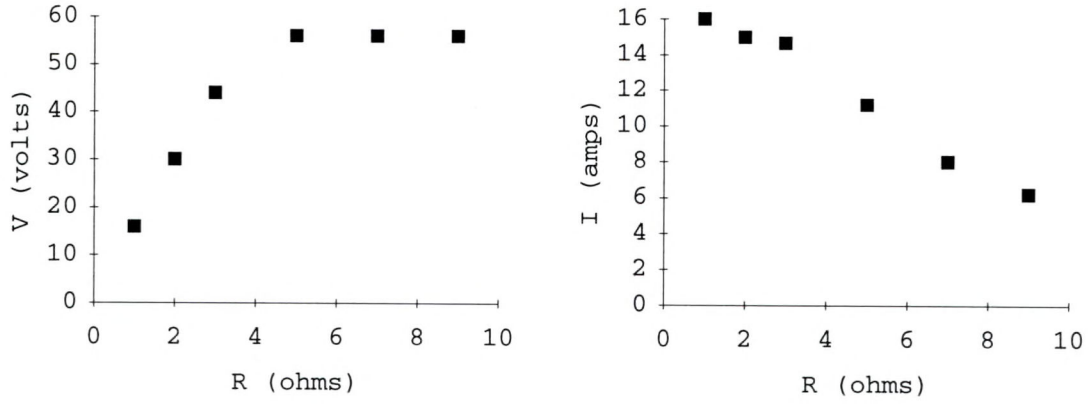

Figure 18. Output of Techron 7540 measured into load. a) Measured voltage; b) Calculated current.

produced are shown in Figure 18. For load resistance of four ohms or more, the amplifier at saturation can be modeled by a 56 V voltage source. For a load resistance of

[65]Crown International, Techron 7540, Elkhorn, Illinois.

four ohms or less, it can be modeled as a 15 A current source.

The Techron amplifiers are equipped with optional current-control modules. With current control switched on, an amplifier behaves like a voltage-controlled current source. With current control switched off, an amplifier behaves like a voltage-controlled voltage source. Current control serves two functions when driving gradient coils. It compensates for any variation in temperature of the gradient coil due to resistive heating. More importantly, it enables the coil to be switched to low fields much more rapidly than the coil's time constant would otherwise allow. The current-control module compares the demand (or input signal) to the voltage across a small shunt resistor in the output circuit. With a highly inductive load such as a gradient coil, at high frequencies the amplifier's output voltage is shifted almost $\pi/2$ with respect to the coil current, and the amplifier is unstable and will oscillate. The voltage and current response of one of the Techron amplifiers in current mode is shown in Figure 19. The controlled voltage overshoot reduces the current switching time. Approximately 5 A is being switched into a 7 Ω load. An adjustable resistor-capacitor (RC) network in parallel with the coil rolls off the high frequency gain to compensate for the instability. The values of the RC network are determined by the inductance of the coil. Since the 7540 amplifiers are used with more than one coil, the

current-control units were modified so the RC networks can be plugged in and out when gradient coils are changed.

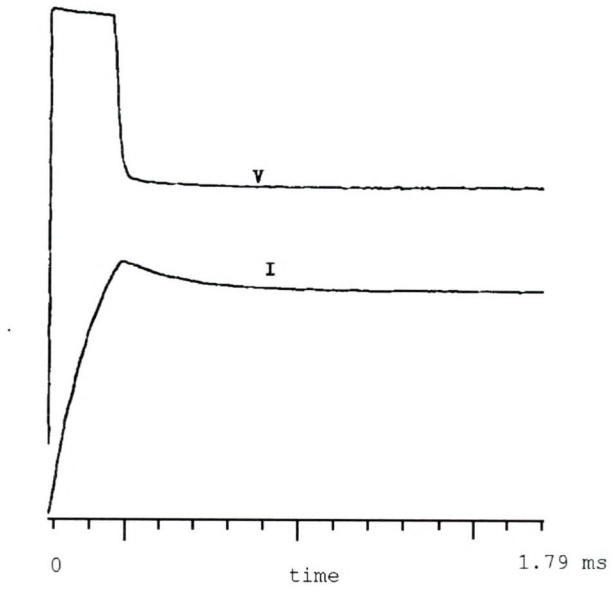

Figure 19. Output voltage and current of Techron 7540 amplifier with current-control module. The load is the highly inductive 9 cm field gradient coil.

The amplifier rack was equipped with wheels and shared between the NMR microscopy and small-animal spectrometers. It was used in voltage-control mode with the NMR microscopy system, and current-control mode with the small animal system where the coil inductance was much higher. Input and output connectors were standardized to facilitate quick conversion. A fully-shielded output cable terminated in a fuse-and-filter chassis eliminated interference from the RF coils.

16 mm Coil for NMR Microscopy

The 16 mm gradient coil was developed as part of the NMR microscope development project described below. Earlier NMR microscopy gradient coils described in the literature were located outside of the RF probe insert, as part of the shim coil set. A simple and straightforward approach to improving the coil switching time, increasing the field strength, and decreasing the eddy current field is to integrate the gradient coils with the RF probe. This also allows the use of a narrowbore (51 mm) magnet. Drawbacks to this approach include a lack of flexibility. If the gradient coil is outside the RF probe, then any RF probe can be used. In our approach, one gradient coil is required for each RF probe. Also, since one of the dewars associated with the variable-temperature (VT) control system is replaced by an acrylic tube, the range of the VT system is reduced. Our probe did not contain any VT control capability. The fact that the coil former was so small encouraged us to choose a simple design to ease the assembly.

Since the sample-tube inner diameter was 4.5 mm and the first metal tube, or shield, had an inner diameter of 33 mm, this was a favorable case for using a reduced-size gradient coil. A simple 68.7°/21.3° radial gradient coil as described above has a useful volume with a diameter of about

1/3 that of the coil,[66] so the gradient former was chosen to have a diameter of about 15 mm, or 5/8". A factor of two remains in the ratio of the coil to the shield diameter. This results in an eddy current field for the 68.7°/21.3° Golay radial gradient coil, based on Figure 17, of about 20% of the applied field.

The NMR microscope gradient coil set is of the conventional Maxwell and Golay design described above. It was constructed to accommodate standard 5 mm tubes used in analytical NMR work. The 10 turns of 36 AWG enameled magnet wire are wound on a 5/8" nominal outer diameter acrylic tube (15.9 mm). Using a value of 1.36 Ω/m for the wire[67] and a length of 0.135 m per turn, the resistance of each side of the coil is 1.84 Ω. The coil inductance can be estimated[68] to be about 8 μH. The time constant of the coil is then about 4 μs. The current efficiency of a 68.7°/21.3° Golay radial gradient coil is $0.918/a^2$ G/cm-A, where a is the coil radius,[69] so the coil has a current efficiency of 14.1 G/cm-A. A Maxwell pair has a current efficiency of $0.808/a^2$ G/cm-A, so the coil has a current efficiency of 15.3 G/cm-A. The typical figure for the linear region of 1/3 the diameter of the coil is then enough to accommodate a sample. The coil is driven by the Techron 7540 amplifier set. The coil

---

[66]F. Romeo and D. I. Hoult, Magn. Reson. Med. 1, 44, 1984.
[67]D. Lide,(Ed.), CRC Handbook of Chemistry and Physics, 51st Edition, CRC Press, Boca Raton, 1970, p. 15-29.
[68]F. E. Terman, Radio Engineers' Handbook, McGraw-Hill, New York, 1943.
[69]F. Romeo and D.I. Hoult, Magn. Reson. Med. 1, 44, 1984.

has a small time constant, so using the Techron in voltage mode does not limit the switching time. The two halves of each gradient coil are driven separately. Since the voltage gain of the amplifiers can be adjusted manually, it is convenient to vary the relative gain in the coils to shift the zero point of the magnetic field to make up for sample misregistration.

The details of the coil construction are visible in Figure 47 in the following chapter. The radial coils were wound on a flat winding former, then removed and attached to the acrylic tube with epoxy. To eliminate any solder connectors within the coil, the winding former allowed two loops to be wound at once, held apart at the correct distance. General Electric #7031 varnish was used to hold the wires together while the coil was being clamped to the former. No attempt was made to arrange the wire into a packed structure. The Maxwell pair was wound around the radial coils. The whole assembly was potted in epoxy to secure the coils to the former, and the 36 AWG wires were run down to a small printed circuit board mounted to the structure of the probe. It was necessary to pot the fine wires to keep them from moving in the magnetic field when a current pulse is applied.

An example of the results obtained with the coil is reproduced in Figure 60. Although the coil is capable of about 150 G/cm, in routine operation, the coil was operated at a full-scale field gradient of 5 G/cm for the radial

gradients, and 10 G/cm for the axial gradient, to allow sufficient resolution.

9 cm Coil for Small Animals

An NMR magnet is frequently used for samples or animals significantly smaller than the available bore size. It is possible to take advantage of this fact and scale the size of the gradient coil to match the size of the sample. One advantage that accrues is reduced eddy current fields, since the coil and the source of eddy currents are better separated. Another is the increased efficiency possible with smaller coils, since efficiency scales as the fifth power of the diameter.[70] Many applications require more rapidly switched and more intense gradient fields than are generally available. Diffusion-weighted imaging and localized spectroscopy are two examples. Also, to achieve the same bandwidth per pixel, small samples require larger gradient fields.

The 31 cm 2 T small-animal imaging spectrometer was supplied with a gradient coil set manufactured by Oxford instruments that has a clear bore of 22.5 cm, and is capable of producing a maximum gradient of 2 G/cm with a switching time of 1 ms. Although rat, mouse, and lizard studies, do not require the full 22.5 cm bore, they benefit from the horizontal orientation and will not fit into other available magnets. Additionally, localization techniques such as

[70] R. Turner, Magn. Reson. Imag. 11, 903, 1993.

selective Fourier transform[71] typically require better gradient performance than is available with a large, unshielded gradient coil set.

To meet some of these needs, a conventional Maxwell and 68.7°/21.3° Golay radial gradient coil set was designed and constructed with a clear bore of 8.3 cm in diameter. The useful region is a sphere of about 1/3 the diameter of the coil, or about 3 cm. The coil was designed to accommodate rats up to 150 g, and was able to achieve 12 G/cm with a 200 μs switching time. The intense gradients are needed for imaging experiments on smaller samples. The coil was used for projects involving lizards, and for development of techniques to produce diffusion images of the spinal cord of a rat model.

We can consider the application of the time-domain model to the 9 cm coil. As wound, the coil will produce the field shown in Figure 20 when driven to saturation. The Maxwell pair, Z-axis coil, is the most efficient, followed by the inner radial, or X-axis coil, which has better performance than the outer radial, or Y-axis coil, because of its smaller radius. The Maxwell pair reaches the 16 A current limit of the amplifier, and does not increase in field beyond that point. The radial gradient coils never reach the current limit.

---

[71]T. H. Mareci and H. R. Brooker, J. Magn. Reson. 57, 157, 1984.

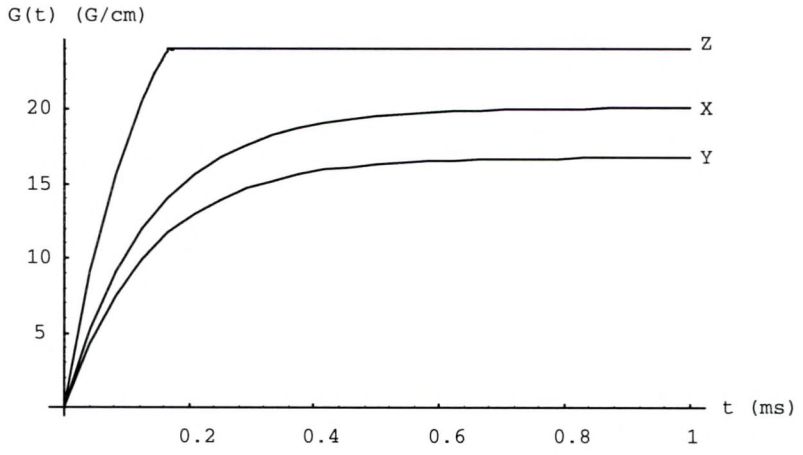

Figure 20. The gradient produced by the 9 cm gradient coil set following a demand that saturates the amplifier.

Figure 21 describes the maximum field $G_{max}(t_0)$ possible for switching time t_0 for each of the three coils. The

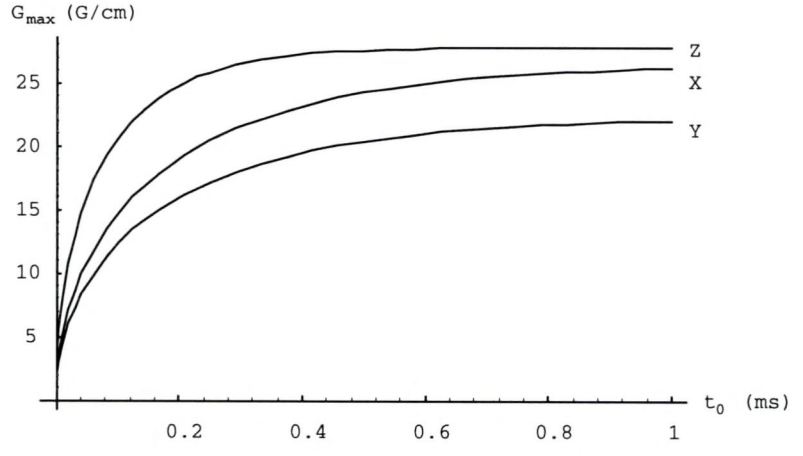

Figure 21. The maximum gradient that could be achieved by a coil identical to the 9 cm coil, with the same cross-sectional area, but with varying number of turns.

inherently lower inductance and resistance of the Maxwell pair are reflected in its greater field. The actual and optimal fields obtainable at 200 μs are compared in Table 1. The Maxwell pair has about the optimal number of turns, and its field is about the same as the optimum. The Golay coils

have about twice as many turns as optimum, and yield fields about 80% of optimum level.

Table 1. Gradient fields for 9 cm coil set.

Gradient channel	Actual no. of turns	Gradient after 200 μs (G/cm)	Optimal no. of turns	Gradient after 200 μs (G/cm)
X	52	15.2	27.9	19.0
Y	52	12.3	26.9	15.9
Z	52	24.0	53.6	24.8

The radial and axial gradient coils consist of 52 turns of AWG 27 enameled magnet wire. The wire was wound in a 7-6-7-... close-pack configuration to minimize the cross-sectional area of the winding, which is reduced by a factor of 0.866 from a square winding pattern. The resulting winding cross-section is about 2.6 mm on a side, only about 6% of the coil radius, so the winding approximates a filament. The mean radius of the coils is 4.6 cm, 4.8 cm, and 5.1 cm. The Maxwell pair is wound on the outside because it is inherently more efficient and will hold down the other coils. The two halves of each coil are wound separately, and one channel of a stereo amplifier is wired to each. It is driven in current mode from the Techron 7540 amplifiers. The current-control circuit helps to buck the inductance of the coil. The coil resistance for the radial windings is predicted to be about 6.7 Ω for the inner set. The measured resistances and time constants including the

leads and filters are given in Table 2. The time constant of the shorted power cable with filters and fuses was too short to measure with the amplifier, so it can be assumed to be negligible. The last column is the inductance estimated from the Bowtell and Mansfield formulation for coils on the surface of cylinders.[72] To adapt for the thick winding, the height is added to the width of the winding. Calculations for loops of square cross section compare closely to heuristic formulas.[73]

Table 2. Comparison of measured and predicted inductance for 9 cm gradient coil set.

Coil	Measured Resistance (Ω)	Measured Time Constant (μs)	Experimental Inductance (μH)	Theoretical Inductance (μH)
X1	7.02	175	1229	1727
X2	7.08	175	1239	1727
Y1	7.57	195	1476	1866
Y2	7.61	190	1446	1866
Z1	3.50	150	525	330
Z2	3.53	150	530	330

The difference between the theoretical and experimental inductance is not due to the inductance of the power cable, which was measured by the same technique to be about 18 μH. It is primarily due to poor control of the cross-sectional

[72]R. Bowtell and P. Mansfield, Meas. Sci. Technol. 1, 431, 1990.
[73]F. E. Terman, Radio Engineers' Handbook, McGraw-Hill, New York, 1943.

dimensions of the winding, which expands when it is removed from the winding former. The maximum operating field as the system has been installed is 12.83 G/cm for X, 12.28 G/cm for Y and 8.80 G/cm for Z. By limiting the gradient field to a value below that corresponding to the steady state current, the switching time is better controlled.

A drawing of the coil that illustrates how the Faraday shield and RF coil fit together is shown in Figure 22.

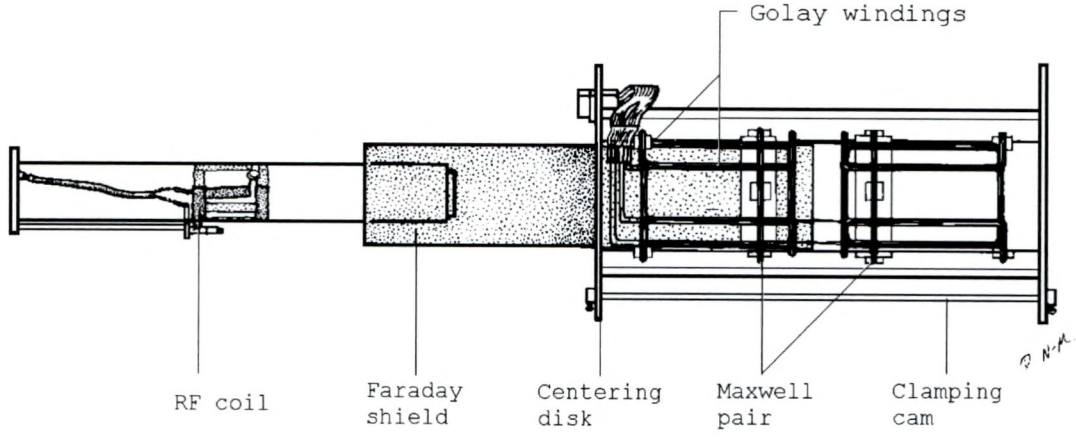

Figure 22. Drawing of 9 cm gradient coil set with Faraday shield and RF coil.

Figure 23 is a photograph of the assembly. The former is an acrylic tube of 3.5" (89 mm) nominal outer diameter and 1/8" (3.2 mm) wall thickness. The radial gradient coils are wound on rectangular bobbins made from three flat pieces of acrylic. The wires are held together in a hexagonal matrix by General Electric varnish #7031 diluted in acetone. After winding, the bobbin is disassembled and the coil is glued onto the cylindrical former with epoxy. A variety of

Figure 23. Photograph of 9 cm gradient coil set. The power cable and water supply cables are visible at left. The axial and radial gradient coils are visible through the cooling tubing.

RF coils were developed as inserts for the probe, including ^{19}F, ^{1}H birdcage, $^{31}P/^{1}H$ double-tuned saddle coil, and my own ^{1}H saddle coil. A pair of cams connected by a rod and mounted on the edge of the mounting flanges served to lock the probe into the magnet. A Faraday shield was used in addition to the filter/fuse box to isolate the RF coils from the gradient coils. The shield consisted of strips of Reynolds heavy-duty aluminum foil approximately 2" wide, overlapped by about 1/2", and insulated from the other strips by masking tape that also secured the strips to manila card stock. At one end, all strips contacted a header strip. Provision was made to ground the shield, but

in practice it was not used. The interdigitated geometry reduced eddy currents from the gradient coil, but allowed the shield to serve as a barrier to the RF field. The Maxwell pair is on the outside, which helps to hold the radial gradient coils in place. Epoxy was initially used to hold the windings to the former and pot the windings, but the epoxy did not withstand the temperatures developed by the coil and depolymerized. Polyester was selected as a casting resin that would outperform the acrylic former under warm conditions, and the coils were potted in polyester.

In order to cool the unit, approximately 25 m of 1/8" O. D. by 1/64" wall polypropylene tubing was wound around the coils. It was connected to a Neslab circulating system that is capable of producing a pressure head of 40 psi. Supply tubing consisted of about 30 m of 1/4" O. D. by 1/32" wall polypropylene. Assuming laminar flow, the water flux through a tube[74] of radius r (cm) is

$$flux = \frac{\pi r^4 \Delta p}{8 \mu l} \quad ,$$

where Δp is the pressure in dyne/cm^2, l is the length of the tube in cm, and μ is the viscosity in poise. The resulting flux for a 40 psi drop is 8.6 cm^3/s. One KW of power transferred to the water in the tube will raise its temperature by about 28° C. Measurement of the motion of bubbles in the tubing reveals a flow of about 3.5 cm^3/s.

---

[74]D. Lide,(Ed.), CRC Handbook of Chemistry and Physics, 51st Edition, CRC Press, Boca Raton, 1970, p. F-34.

The difference is almost certainly due to quick-release connectors that allow the probe to be removed or inserted at operating pressure.

15 cm Coil for Small Animals

The 15 cm coil was designed to accommodate larger rats and other medium-sized laboratory animals and still produce a higher field and faster switching time than the Oxford gradient set. Like the 9 cm and the NMR microscope coil set, it is based on filamentary winding design. Since it is also driven by the Techron 7540 amplifier set, which is under-powered for a coil of this diameter, switching performance was at a premium. So, in contrast to the 9 cm coil, the 15 cm coil was designed to have optimal switching performance for the chosen switching time. In order to provide more flexibility in choosing either high field intensity or fast switching time, the windings were split and could be driven either in series or parallel. Since the coil would tend to become somewhat unwieldy as an insertable unit, its length was the shortest that would give essentially undiminished field intensity. Plots of the relative error in Figures 26 and 27 illustrate the linear region of the radial coil design. In order to avoid aliasing signals from long animals, the axial coil was based on an extended linearity design by Suits and Wilken.[75] The

[75]B. H. Suits and D. E. Wilken, J. Phys. E: Sci. Instrum. 23, 565, 1989.

coil and amplifiers were capable of developing 9 G/cm in a 100 μs switching time on X, Y and Z channels.

The arcs in the 15 cm coil were arranged to have the minimum length without losing a significant amount of efficiency in the static limit. The standard solution of 68.7°/21.3° for the arc positions arc1/arc2 leads to no third order component from either arc, but a family of solutions for which the third order components cancel is available. These solutions are graphed in Figure 24.

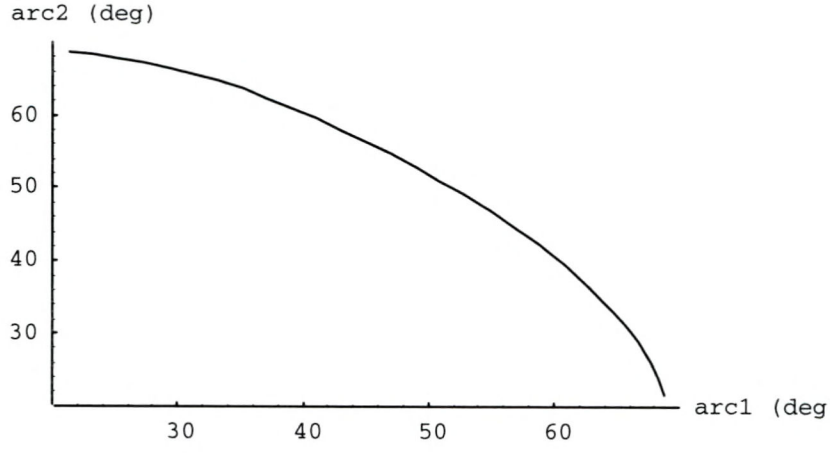

Figure 24. The solutions to the arc position of the double-saddle radial gradient coil.

Each solution is graphed twice, since exchanging arc1 and arc2 results in the same coil design. To improve the relative size of the linear region to the coil, one would like to make the coil shorter than the 68.7°/21.3° solution. The current efficiency decreases with the length, since the return arcs tend to cancel the desired field, and moving them closer increases the effect. However, in order to

include the effect of reducing resistive loss in the coil, one must divide the current efficiency by the square root of the length. The resulting measure is an indication of the relative field that can be produced with an amplifier of a given power. Figure 25 illustrates the relative power efficiency as a function of the position of the return arc.

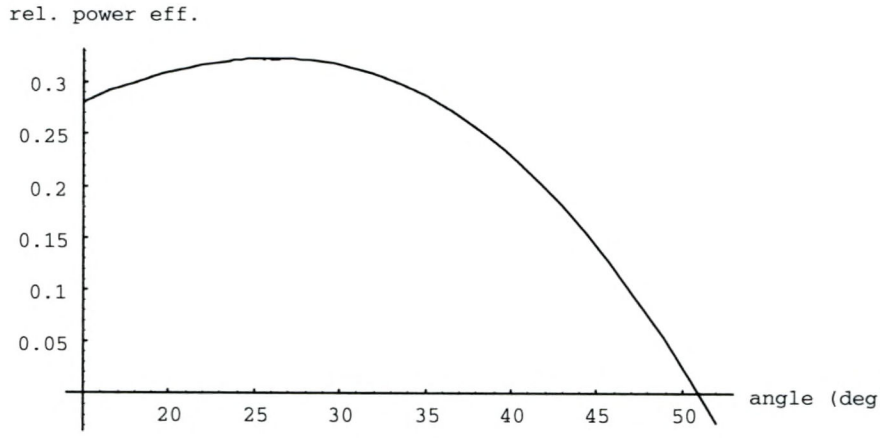

Figure 25. The relative power efficiency of the double-saddle radial gradient coil as a function of the angle between the z-axis and the current return path.

The peak efficiency is achieved at 26°, but efficiency is a weak function of angle and much shorter coils can be used with little loss of performance. Based on this curve, the arcs of the 15 cm radial coil were placed at 30.2° and 66.1° from the axis of the coil, compared to 21.3° and 68.7° for the Golay coil. The overall length of the coil is reduced by 33%. The current efficiency is $0.819/a^2$ G/cm-A compared to $0.808/a^2$ G/cm-A for the 68.7°/21.3° Golay coil. It would be even better to use a variant of the field-versus-switching-time approach to determine the change in

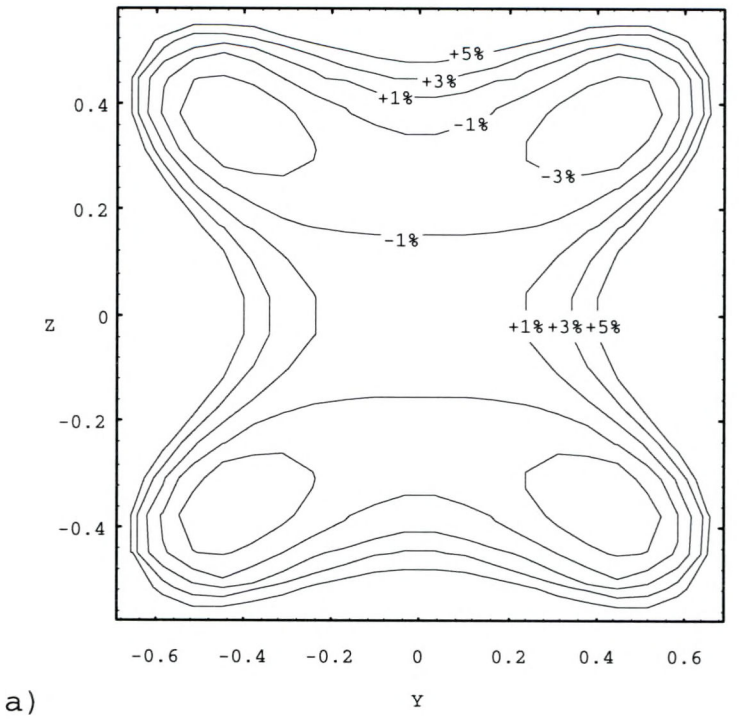

a)

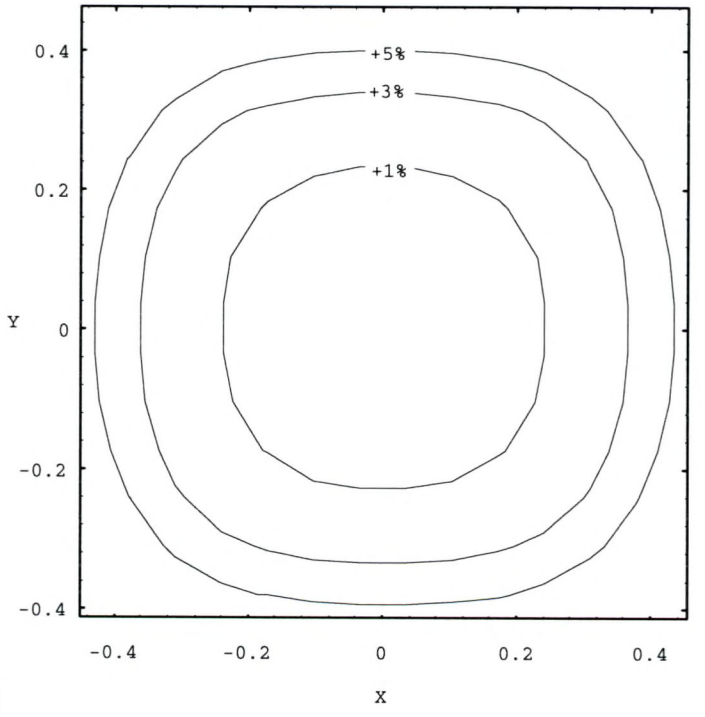

b)

Figure 26. Relative error plots of 30.2°/66.1° radial gradient coil. Radius of coil corresponds to 1 on scale. a) YZ plane; b) XY plane.

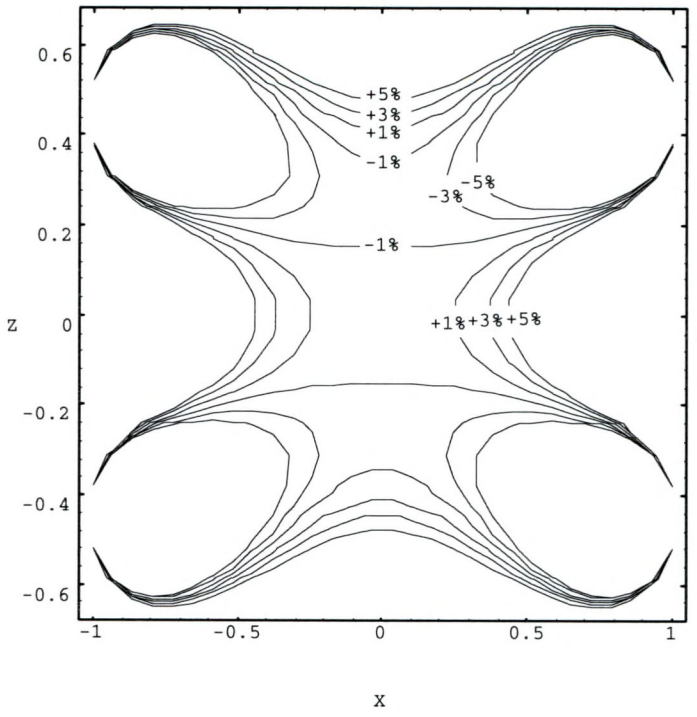

Figure 26--continued. Relative error plots of 30.2°/66.1° radial gradient coil. Radius of coil corresponds to 1 on scale. c) XZ plane.

performance for coils of different lengths, taking the changing inductance into account.

The size and shape of the linear region of the 66.1° /30.2° radial gradient coil design is described by the plots of Figures 26 and 27. It is not greatly different from the longer 68.7°/21.3° design. Note from Figure 26 that the regions of equal relative error are not simply connected. A three-dimensional plot of a region as large as that in the two dimensional plots would give a false impression of the size of the linear region, since the apparently solid volumes would contain large holes. To avoid these "bubbles" of linearity and give a true picture of the useful volume,

the region displayed in Figure 27 is truncated. As a result of the truncation, it is possible to see through the linear region. All plots were produced by direct evaluation of the Biot-Savart law.

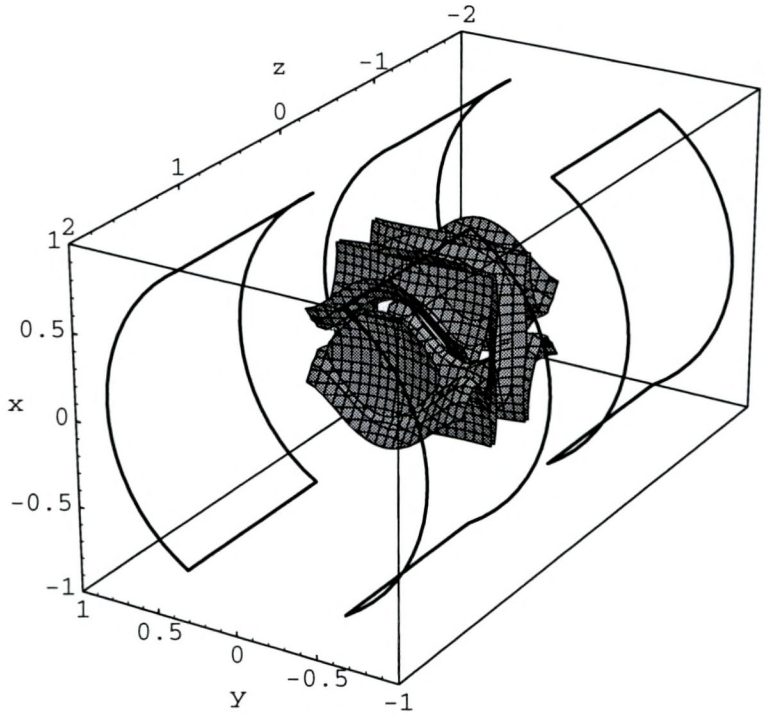

Figure 27. Perspective rendering of the 5% relative error region of 30.2°/66.1° radial gradient coil.

The axial coil was built to an extended-linearity design proposed by Suits and Wilken.[76] It consists of loops at both 40.0° and 66.3° from the z axis. The outer loops carry 7.5 times more current than the inner loops. Using the additional degrees of freedom of the second-loop position and the ratio of current in the loops, the fifth

[76]B. H. Suits and D. E. Wilken, J. Phys. E: Sci. Instrum. 23, 565, 1989.

and seventh order terms are canceled, resulting in about eight times the useful volume of a Maxwell pair. For a coil with more turns in some loops than others, the current efficiency does not have an unambiguous definition. With respect to the current in the outer loops, the current efficiency of the coil is $0.635/a^2$ G/cm-A.

The 15 cm coil was matched to the Techron 7540 amplifiers in our laboratory using the time-domain model of gradient performance described above. The height and width of the windings was set to be 1 by 1 cm for the radial and 1 by 2 cm for the outer axial, to ensure that the assumption of filamentary wires in the calculation of angle position would be valid. The width of the outer axial winding was increased from 1 to 2 cm, since it is farther from the center than the others, and it was necessary to increase it to match the radial performance. Inductance of the radial and axial coils was calculated using a Fourier-Bessel approach.[77] The available combinations of switching time and maximum gradient are shown in Figure 28.

In order to improve the switching time to smaller fields, the 15 cm coil is constructed from split windings. All the gradient coils described have the two sides driven by separate amplifiers so that the magnetic center of the coil can be moved. The 15 cm coil has each side split further into two identical but electrically separate

[77]R. Bowtell and P. Mansfield, Meas. Sci. Technol. 1, 431, 1990.

windings. Placing the windings in parallel trades field intensity for switching time; placing them in series reduces switching time at the expense of lower field intensity.

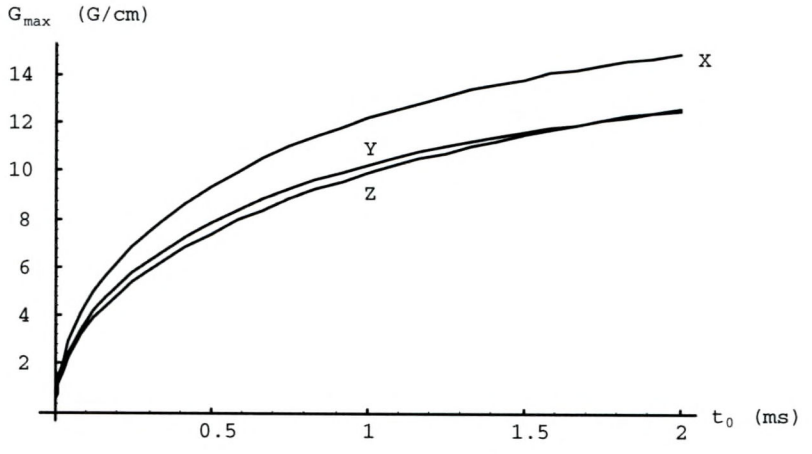

Figure 28. Maximum field G_{max} (G/cm) vs. switching time t_0 (ms) for the 15 cm field gradient coil set as driven by the Techron 7540. Points along the curves represent designs with different numbers of turns, increasing from left to right. The top curve represents the inner radial coil. The lower curves represent the outer radial coil and the axial coil. A "slower" coil has a larger maximum field.

All three coils are optimized to approximately 10 G/cm for the series mode. The exact number of turns for the desired field is not used, due to the limited number of standard wire sizes and the use of rectangular winding cross sections. For the number of turns actually used, t_0 and G_{max} based on the time domain model are tabulated in Table 3.

A photograph of the 15 cm coil assembly is shown in Figure 29. The coil is wound on an acrylic former having a nominal O. D. of 6" (152 mm) and a wall thickness of 1/4" (6.4 mm). The overall length was 38 mm. The radial coils

Table 3. Predictions for 15 cm coil set based on time-domain model.

	Series			Parallel		
	Turns	t_0 (μs)	G_{max} (G/cm)	Turns	t_0 (μs)	G_{max} (G/cm)
X	52	735	10.9	26	150	5.5
Y	52	816	9.5	26	164	4.8
Z	75	717	9.9	37.5	157	5.7

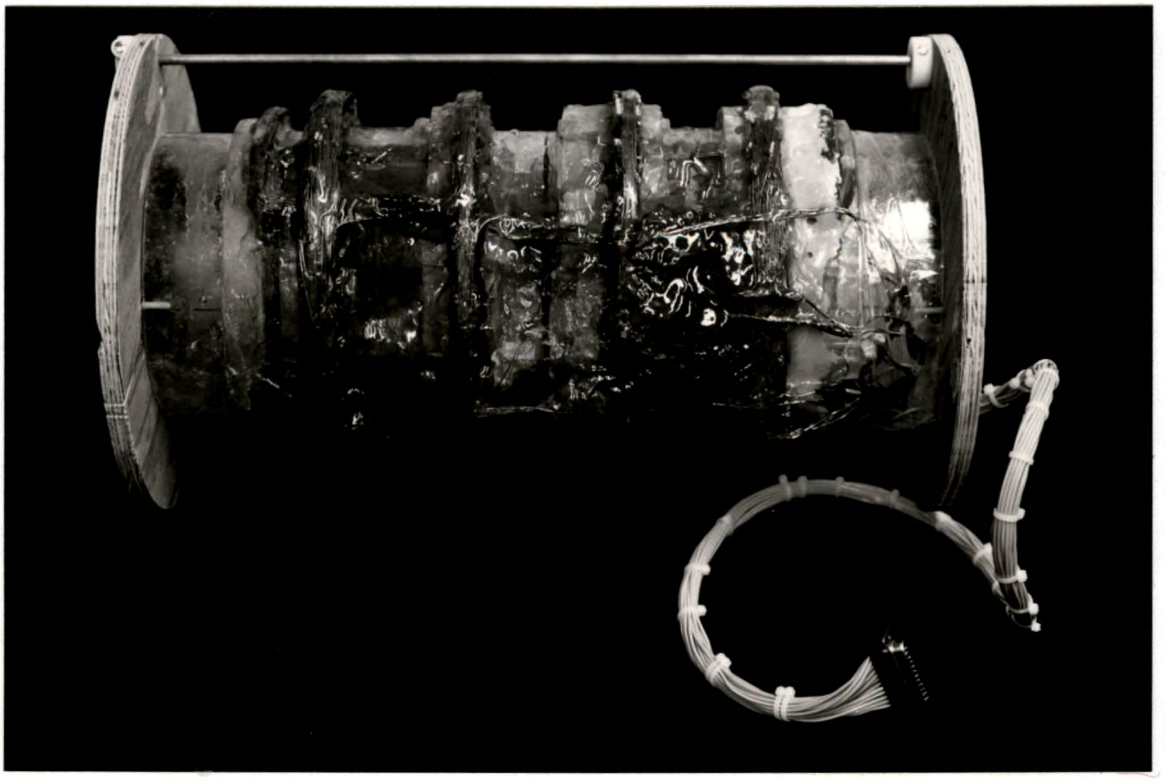

Figure 29. Photograph of the 15 cm gradient coil assembly.

consist of 52 turns of 20 AWG enameled magnet wire in 7-6 close-pack matrix. The wire is first wound onto a rectangular bobbin as described above, then cemented to the former. The axial coil, consisting of 75 turns 18 AWG magnet wire, is wound over the radial coils. The assembly

was potted in polyester resin to hold the coils in place. Each of the windings is split so that it can be driven either in series or in parallel. A simple adapter installed between the power cable and the filter box enabled the coil to be driven in series. The hardware and software have not been designed to change configurations during an experiment.

Measurements have been made of the resistance and time constant of the load that the 15 cm coil, cable, and filter box present to the amplifier. Tables 4 and 5 allow the measured values to be compared to predictions. The experimental and theoretical inductance are reasonably close. The inductance of coils constructed in this way is not well controlled, since the cross section of the winding can expand somewhat when the winding former is disassembled.

Table 4. Comparison of measured and predicted inductance for 15 cm gradient coil set in series configuration.

Coil	Measured Resistance (Ω)	Measured Time Constant (μs)	Experimental Inductance (μH)	Theoretical Inductance (μH)
X1	2.48	740	1835	2000
X2	2.47	700	1729	2000
Y1	2.59	680	1761	2184
Y2	2.62	720	1886	2184
Z1	1.70	1120	1904	2120
Z2	1.50	1300	1950	2120

Table 5. Comparison of measured and predicted inductance for 15 cm gradient coil set in parallel configuration.

Coil	Measured Resistance (Ω)	Measured Time Constant (μs)	Experimental Inductance (μH)	Theoretical Inductance (μH)
X1	0.95	440	418	500
X2	0.96	440	422	500
Y1	0.96	440	422	546
Y2	0.96	460	441	546
Z1	0.84	560	470	488
Z2	0.70	640	448	488

The first order calculation for the eddy current field of the 66.1°/30.2° radial gradient coil as plotted in Figure 30 is about the same as for a 68.7°/21.3° Golay coil of the same diameter shown in Figure 17.

This project demonstrates application of the time-domain performance model to optimize the number of turns in the coil. It also shows that is possible to reduce the length of the coil without significantly reducing the size of the linear region or the coil efficiency. A further refinement of the optimization of performance would be to include the coil length as a second parameter in the time-domain optimization procedure. This project also illustrates how using split windings allows the user to trade off switching time for field strength as needed for a given experiment.

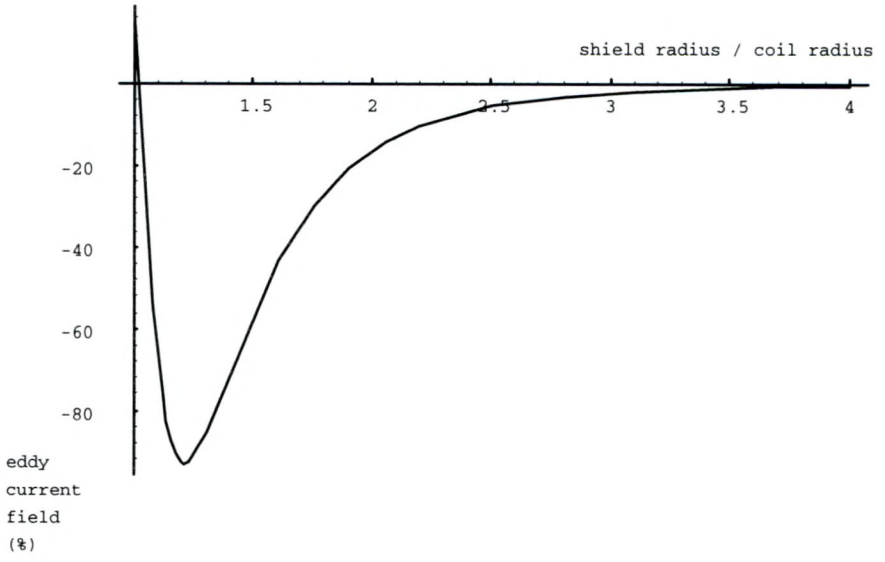

Figure 30. Eddy current field of 30.2°/66.1° radial gradient coil, as calculated to first order.

The field produced by an optimal coil increases with the cross-sectional area of the winding, as the current is distributed over a larger area, so designing the coil in a filamentary approximation is fundamentally not conducive to high performance. A better approach that preserves some of the simplicity of design and construction would be to include the arc width in the coil design process. The appropriate terms in the spherical harmonic expansion of the field would be set to zero for arcs of desired, non-zero width, on the surface of a cylinder.

Concentric Return Path Coil

The development of functional imaging[78] and diffusion-weighted imaging[79] of the human brain in vivo has created a

[78]J. Frahm et al., Magn. Reson. Med. 29, 139, 1993.
[79]P. Gideon, et al., J. Magn. Reson. Imag. 4, 185, 1994.

demand for gradient systems that produce a field that is high in intensity and can be switched rapidly on and off. Since smaller coils of a given design are more efficient, and gradient coils designed specially for the head can be made smaller than those that accommodate the whole body, such coils are useful in high-performance applications. Another benefit of smaller designs is the reduced interaction with the cryostat and other metal structures in the magnet, and the smaller resulting eddy currents. The need for shielding is thereby reduced. Some smaller designs incorporate shielding, but many do not. The principal problem associated with designing gradient coils for the human head is that the linear region of traditional designs is a rather small fraction of the length of the assembly and is located at the center of the assembly. A traditional coil design will not fit over the human shoulders. A successful alternative has been to design asymmetric coils in which the linear region is pushed to one end of the coil.[80] In general such coils experience a torque in the main magnetic field that is not experienced by symmetric coils. These coils must be mechanically fixed in place. Torque-free coils have been designed by imposing extra constraints.[81]

We have taken an approach that results in a symmetric coil that has a linear region that extends quite close to

---

[80]C. C. Myers and P. B. Roemer, SMRM 1991, 711.
[81]L. S. Petropoulos et al., SMRM 1993, 1305.

the ends of the coil. This is possible because the current return paths are located on a larger concentric cylinder, as shown in Figure 31. The coil is inherently torque free. In fact, since each planar unit of the CRP coil is independently torque free, axially asymmetric CRP coils will also be torque free. Radial volume efficiency is traded for axial volume efficiency. This new approach can lead to a family of new designs; here we explore only two simple possibilities.

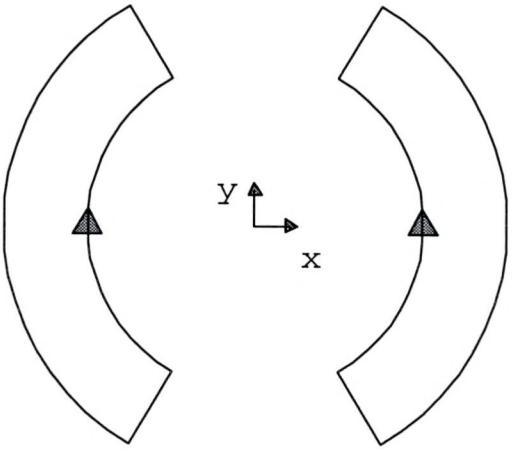

Figure 31. A planar unit of a Concentric Return Path Coil. Inner and outer arcs subtend 120°. The ratio of the outer radius to the inner radius is 1.5. Current direction is indicated by arrows.

One way to understand the topology of the CRP coil is to start with a double-saddle radial gradient coil as shown in Figure 13(a). The only part of the coil that makes a useful contribution to the field is the set of four inner arcs. The longitudinal elements and the outer arcs make up the current return paths that are needed to provide for

current continuity. Unfortunately, the current return paths make the coil much longer. How could such a coil be shortened? The quality of the field produced by the coil might not be greatly affected by moving the current return paths off the cylinder and bringing them into the planes of the four inner arcs, but at a larger radius. This results in a simple CRP coil. All the current lies in two planes, each of which we call a planar unit.

Another approach to understanding the CRP coil is to ask if there is a way to make a radial gradient coil that is indefinitely long, as a linear field analog to a solenoid. In such a coil the current cannot depend on the axial coordinate. The obvious place to start is with the inner arcs, that now can be thought of as surface currents independent of z, not filamentary currents. The width of the inner arcs must be the same as for the double-saddle coil, since the analysis used for the width of the arcs in the double-saddle coil did not consider their axial position. In the double-saddle design, the outer arcs are the same width as the inner arcs; carrying this over to the indefinitely long coil leads to arcs with a larger radius concentric with the inner arcs. Radial elements naturally connect these nested arcs. The problem is that an infinitely long CRP coil with uniform current distribution has zero external field! This can be seen through a simple application of Ampère's law. Consider a single solenoid of arbitrary cross section with surface current **K** as shown in

Figure 32. We apply Ampère's law $\oint \mathbf{B} \cdot d\mathbf{l} = \mu_0 I_{enclosed}$, where $I_{enclosed}$ is the current enclosed by an Amperian loop in the YZ plane outside of the solenoid. Since $I_{enclosed} = 0$,

$$\oint \mathbf{B} \cdot d\mathbf{l} = \int_1 \mathbf{B} \cdot d\hat{\mathbf{r}} + \int_2 \mathbf{B} \cdot d\hat{\mathbf{z}} + \int_3 \mathbf{B} \cdot d\hat{\mathbf{r}} + \int_4 \mathbf{B} \cdot d\hat{\mathbf{z}} = 0. \qquad [68]$$

The current density is independent of z, so the magnetic field **B** must also be independent of z and the integrals over 1 and 3 must cancel leaving

$$\oint \mathbf{B} \cdot d\mathbf{l} = \int_2 \mathbf{B} \cdot d\hat{\mathbf{z}} + \int_4 \mathbf{B} \cdot d\hat{\mathbf{z}} = 2B_z L = 0, \qquad [69]$$

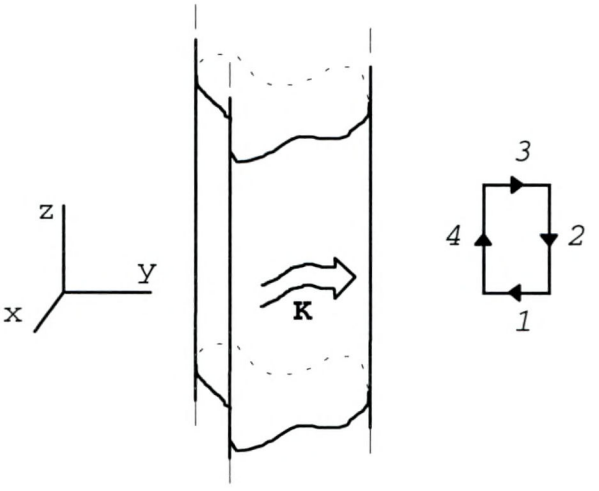

Figure 32. Ampère's law applied to a solenoid of infinite length. The solenoid has an arbitrary cross-sectional shape. The arrow indicates the direction of current flow. An Ampèrian loop is drawn at right.

where L is the length of sides 2 and 4 of the loop. So $B_z = 0$. Therefore, outside any infinitely long solenoid of arbitrary shape, the component of magnetic field parallel to the axis of the solenoid vanishes. An infinitely long CRP coil would consist of two such solenoids and have zero field parallel to its axis. Therefore, we cannot approximate a

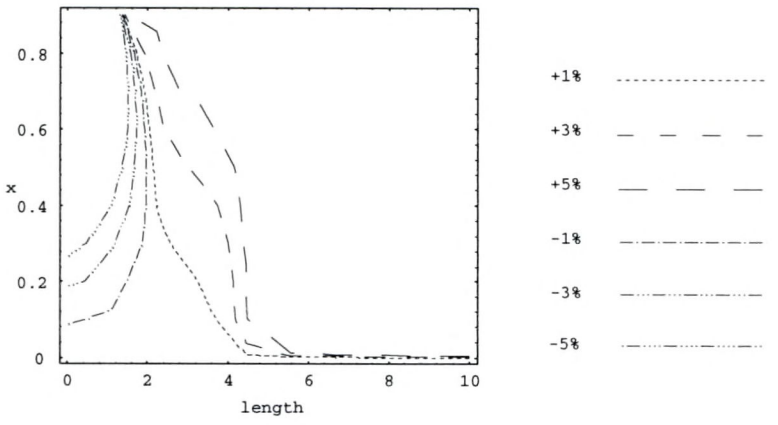

a)

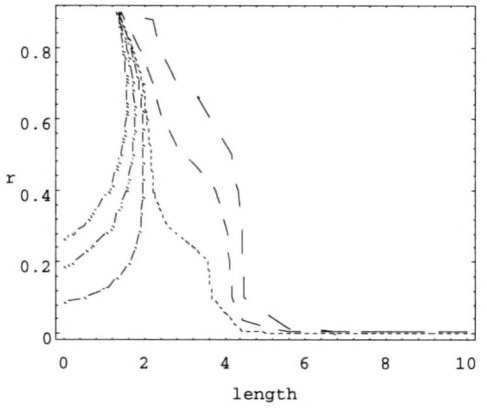

b)

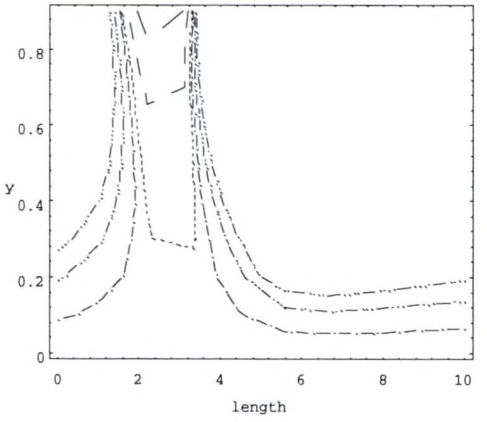

c)

Figure 33. Relative Error of CRP coils with uniform current density. Length and distance are in units of inner radius. Outer radius is 1.5 times inner radius. a) *R. E.* along *x* axis; b) *R. E.* along *x* = *y*; c) *R. E.* along y axis.

CRP coil as being infinitely long. We are led to consider the effect of length on the linear volume of a CRP coil having constant current density over its finite length. Plots in Figure 33 of the linear region vs. coil length demonstrate that the linear volume of such a coil is a very strong function of length. Along both the x axis and x = y, the linear region is strongly peaked at a length that is twice the inner radius. This is in contradistinction to the homogeneous region inside a solenoid, which would grow with the length. For the CRP coil with uniform current density, as the length grows both the field intensity and the linear volume decline.

We consider the design of the CRP coil in two steps. First is the design of the planar unit. Second is the adjustment of current between planar units to optimize the axial extent of the linear region. Since the magnetic field in the coil must be a solution to Laplace's equation, which is separable in cylindrical and spherical coordinates, we can separate the axial and radial parts of the solution. To design the planar unit we follow the spherical harmonic approach of Romeo and Hoult.[82] Starting with a definition of the vector potential $\mathbf{A}$ by $\mathbf{B} = \nabla \times \mathbf{A}$, where $\mathbf{B}$ is the magnetic field, we use the well-known result that in free space $\mathbf{A} = \frac{\mu_0}{4\pi} \int \frac{\mathbf{J}}{r} dv$ where $\mathbf{J}$ is the current density, r is the distance between the current and the observer, and dv is an

[82] F. Romeo and D. I. Hoult, Magn. Reson. Med. 1, 44, 1984.

infinitesimal volume element. For wires, we write $\mathbf{J} = Id\mathbf{s}$, where I is the current and d$\mathbf{s}$ is a unit vector in the direction of the current. Then the vector potential of an infinitesimal current element is $d\mathbf{A} = \frac{\mu_0 I d\mathbf{s}}{4\pi r}$. Now we expand $d\mathbf{A}$ in associated Legendre polynomials to find that

$$d\mathbf{A} = \frac{\mu_0 I d\mathbf{s}}{4\pi} \sum_{n=0}^{\infty} \sum_{m=-n}^{n} \frac{(n-m)!}{(n+m)!} P_{nm}(\cos\alpha)\left(\frac{r}{f}\right)^n P_{nm}(\cos\theta) e^{im(\varphi-\psi)}, \quad [70]$$

where f is the distance between the current element and the origin. The Neumann factor $\varepsilon_m = 1$ if $m = 0$, and otherwise $m = 2$. All variables are defined as in Romeo and Hoult, who derive the magnetic field of an arc element to be

$$dB_z = \sum_{n=0}^{\infty} \sum_{m=-n}^{n} \frac{\mu_0}{\varepsilon_m} \left\{ F_{n,m-1} G_{n,m-1} + F_{n,m+1} J_{n,m+1} \right\} r^n P_{nm}(\cos\theta) e^{im(\varphi-\psi)} \quad [71]$$

where

$$F_{nm} = I(\sin\alpha)\varepsilon_m (n-m+1)!\, P_{n+1,m}(\cos\alpha)/4\pi(n+m+1)! \quad [72]$$

$$G_{nm} = -\left(1 + \delta_{m,0}\right)/2f^{n+1} \quad [73]$$

$$J_{nm} = \left(1 - \delta_{m,0}\right)(n+m+1)(n+m)/2f^{n+1}. \quad [74]$$

A finite arc of constant radius and axial position can be trivially integrated from $\psi = \psi_1$ to ψ_2 to give

$$B_z = \sum_{n=0}^{\infty} \sum_{m=-n}^{n} \frac{\mu_0}{\varepsilon_m} \begin{Bmatrix} F_{n,m-1} G_{n,m-1} \\ + F_{n,m+1} J_{n,m+1} \end{Bmatrix} r^n P_{nm}(\cos\theta) \frac{1}{m} e^{im\varphi} e^{im(\psi_2 - \psi_1 - \pi/2)}. \quad [75]$$

To make a term of given m vanish, we only must make $e^{im(\psi_2-\psi_1-\pi/2)}$ purely imaginary, i.e. we set

$$m\left(\psi_2 - \psi_1 - \pi / 2\right) = (2n + 1)\pi / 2 \qquad [76]$$

for n some nonnegative integer. The linear term, which is needed in the field gradient coil, has $n = 1$, $m = 1$. The arc widths that do not contribute m=3 terms are $\psi_2 - \psi_1 = 0$, $\pi/3$, $2\pi/3$, π. The arc width $2\pi / 3$ is employed in the classical radial gradient coil designs.

A similar analysis can be applied to the radial current elements. The result is

$$dB_z = \frac{-i\mu_0}{2} \sum_{n=0}^{\infty} \sum_{m=-n}^{n} \frac{m}{|m|\varepsilon_m} \left\{ \begin{matrix} L_{n+1,m-1}\left(1 - \delta_{m,0}\right)\left(1 + \delta_{m,1}\right) + \\ L_{n+1,m+1}(n + m + 2)(n + m + 1) \end{matrix} \right\} r^n P_{nm}(\cos\theta) e^{im(\varphi - \psi)}, \qquad [77]$$

where

$$L_{nm} = \varepsilon_m \frac{Ids}{4\pi f^{n+1}} \frac{(n - m)!}{(n + m)!} P_{nm}(\cos\alpha). \qquad [78]$$

To eliminate terms with a given m, the radial currents must be placed at positions that make dB_z completely imaginary: $m\psi = n\pi$ for n a nonnegative integer. For m = 3 we obtain ψ = 0, $\pi/3$, $-\pi/3$, $2\pi/3$, $-2\pi/3$, π as the only positions that do not contribute term with m = 3. But these include exactly the solutions for the arcs! Note that the solutions for the radial currents are valid independent of length. We can choose the lengths as desired, or use the length to cancel higher order terms. We might also be able to find solutions in which the arcs and the radial currents contribute m = 3 terms of equal magnitude but opposite sign. Perhaps this would allow arc widths of approximately $\pi/2$, which would be most convenient for coil construction.

Notice above that arc widths of $\pi/3$ also meet the criterion of nulling $m = 0$ terms, and would have large advantages for coil construction since the radial gradient coils would not overlap.

The radial part of the linearity has been accomplished by using a spherical harmonic expansion for the field and choosing current elements that do not give undesired terms. It seems reasonable to try the same approach with the axial linear region. One can space the current on the z axis so that undesired harmonic terms are canceled. Unfortunately, the terms in the expansion of the field for the radial currents are not as easily evaluated as those in the expansion for azimuthal currents. However, coils have been designed using a computational approach to null higher-order harmonics terms. To eliminate the undesired terms, there are two degrees of freedom available for each planar unit: its position and its current. Since the field strength depends linearly on the current, but nonlinearly on the position, it is computationally more efficient to vary the current. We chose to leave the units evenly spaced at 0.2 of the inner radius and vary only the current. Biot-Savart simulations showed that this spacing reasonably well approximated a continuous current distribution, so that the field does not fluctuate with the period of the spacing. However, the designs exhibited regions of linearity that were disappointingly small. Since we expect to be able to design coils with arbitrarily long linear regions, and the

interior expansion does not converge rapidly unless $r << f$, a target field approach was tried.

Turner defined a target consisting of points evenly spaced on a cylinder, so that he could perform the coil optimization in a reciprocal space.[83] We perform a minimization of the mean square relative error of the field at a list of points freely chosen in the region of interest, similar to a method used by Wong.[84] The points are chosen opportunistically to push out the region of linearity in the desired directions. Typically, points are evenly spaced in two lines. One line is close to the z axis and one is slightly inside the edge of the desired linear region. As in the harmonic term nulling procedure, only the currents are varied. In principle, if the number of degrees of freedom is equal to the number of constraints, it is possible to find a solution with zero error at the target points. In practice, there are drawbacks to this approach. Since the target points define the periphery of the linear region, the field will naturally have a small error there, so the constraints are not well related to the parameters of interest. Solutions having large currents of opposite sign in adjacent planes are apt to occur, which in practice would give very poor power efficiency. A better approach is to use more constraints (points in the target field) than degrees of freedom (number of planar units). The

---

[83]R. Turner, Magn. Reson. Imag. 11, 903, 1993.
[84]E. C. Wong et al., Magn. Reson. Med. 21, 39, 1991.

minimization starts with equal current in each planar unit, which is in some sense the most power-efficient solution. The current in the planes is then varied to minimize the error. We hope to find a local minimum of the relative error that is as close as possible to the uniform current starting point.

The target-field approach yields noninteger currents in the various planes. In practice, one would like to vary the current in the planes by varying the number of turns of wire, which requires integer currents. Then all the planes can be wired in series, so the current is precisely controlled and independent of the quality of the connections in the coil. A simple way to choose the smallest integral currents that give essentially the same performance as the minimal error design is described below. If I_i is the nonintegral current of plane i in the solution, we generate trial practical solutions $I'_i = Round(aI_i)$ where I'_i is the integral current in the plane, a is an adjustable parameter, and $Round()$ is a function that rounds a number to the nearest integer. By varying a and plotting the error that results, we can choose the smallest value of a that yields acceptable error.

We have designed CRP coils with length:inner diameter:outer diameter ratios of 1.8:2:3 and 6:2:3, as shown in Figure 34(a) and 35(a), respectively. Both utilize an inner-radius to outer-radius ratio of 1:1.5. Both have a spacing between planar units of 0.2 of the inner radius.

The difference in the coils is in the number of planar units utilized, and in the relative current in the planes. A short coil containing 10 planes was designed to have a generally spherical linear region. A second design of 30 planar units illustrates the flexibility in length of the CRP topology. Figures 34(b)-(f) and 35(b)-(f) exhibit the field and relative error associated with the coils. The linear volumes extend to a large fraction of the coil length. The 1.8:2:3 coil has 10 planar units, with a turn ratio of 20, -2, 11, 6, 8, 8, 6, 11, -2, 20. The turn ratio rationalization procedure did not work satisfactorily with the 6:2:3 design, so we present the exact solution: 50.45, 1.44, 3.94, 3.24, 3.86, 3.96, 4.28, 4.47, 4.60, 4.83, 4.99, 5.09, 5.09, . . . , 50.45. The size of the linear region in relation to the size of the coil can be most clearly visualized from Figure 36, a three-dimensional rendering of the 5% relative error contour.

For a coil constructed on a single cylinder, Lenz's law guarantees that any eddy current field generated on a concentric shield will oppose the field produced by the coil. The CRP coil is a different case. The field outside the coil is dominated by the outer arcs. The outer arcs tend to cancel the field due to the inner arcs. The Lenz's law argument applied to the CRP coil results in an eddy current field that actually reinforces the applied field. The single-cylinder coil's transfer function is a low-pass filter, whereas the CRP coil transfer function is that of a

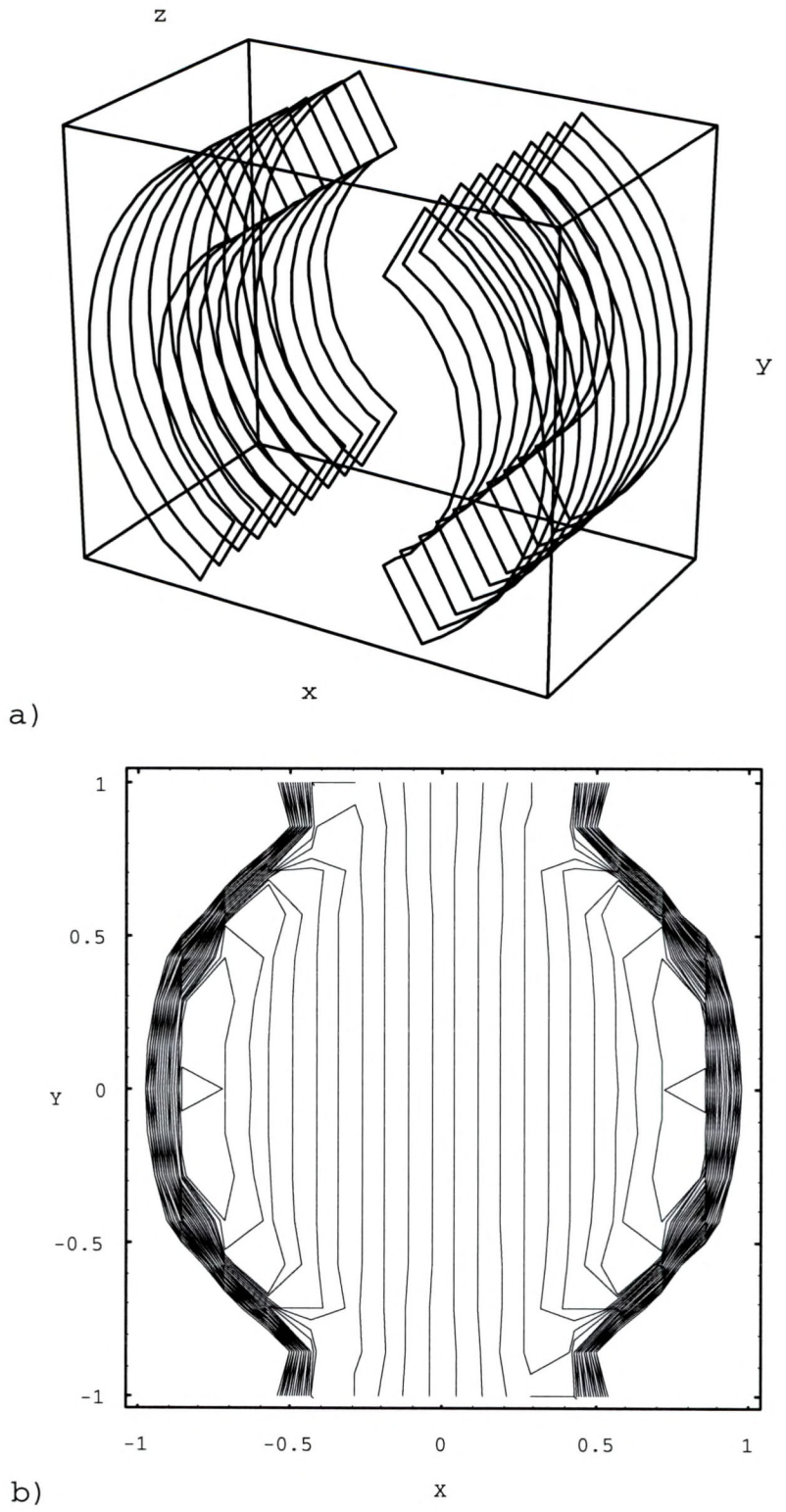

Figure 34. A Concentric Return Path Coil with 10 planar units. The ratio of length:inner diameter:outer diameter is 1.8:2:3. a) Wire configuration. b) Contour plot of the field in the Z = 0 plane.

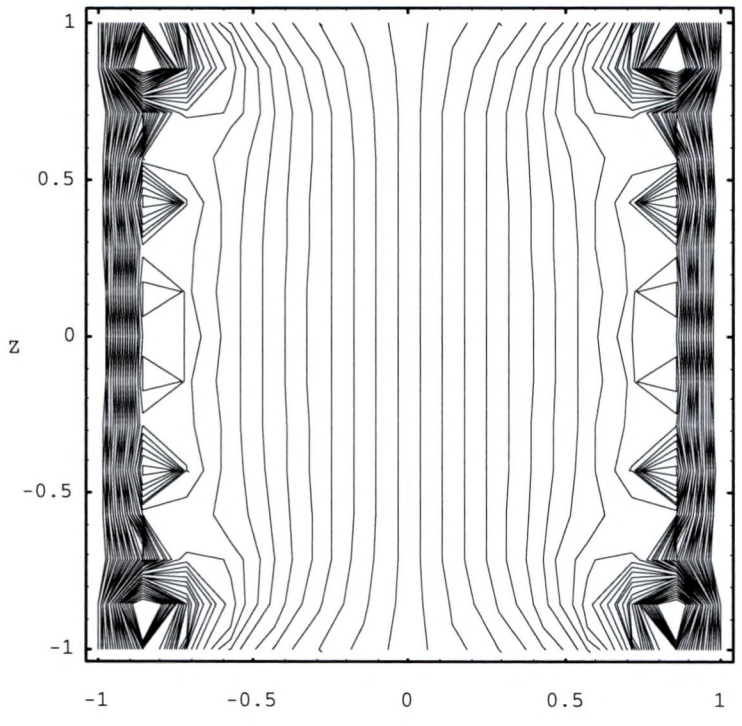

c)

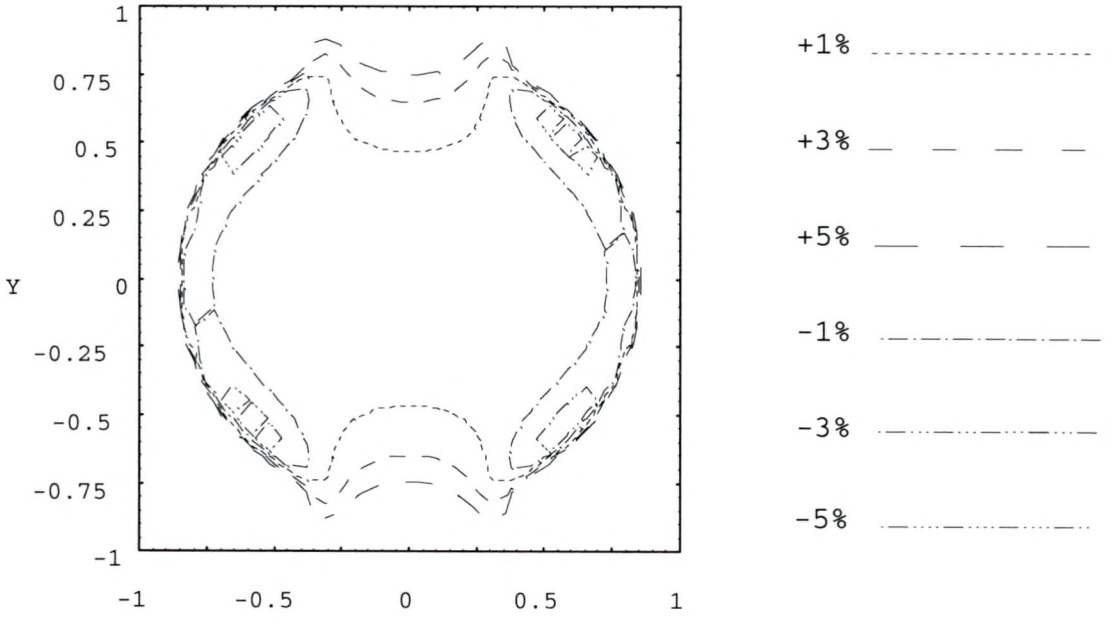

d)

Figure 34--continued. c) Contour plot of the field of the 10 unit CRP Coil in the Y = 0 plane. d) Contour plot of the relative error of the 10 unit CRP Coil in the Z=0 plane.

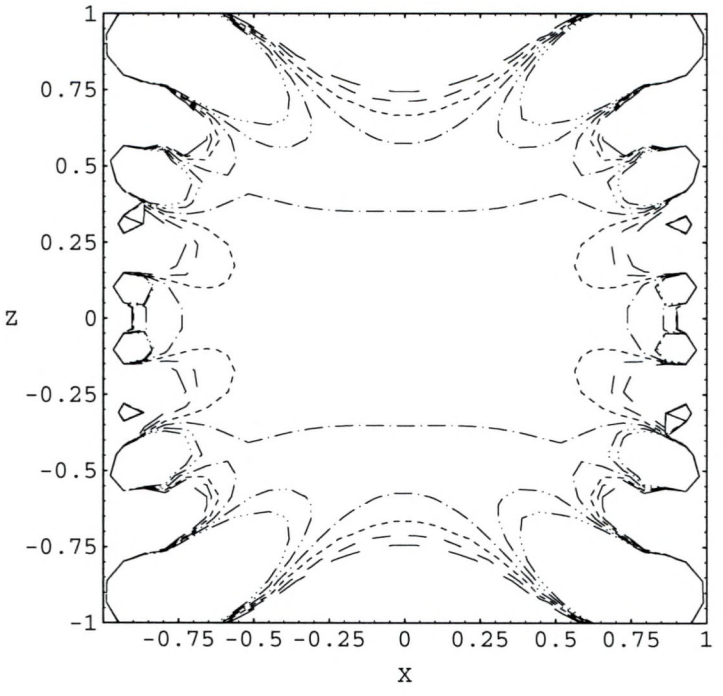

e)

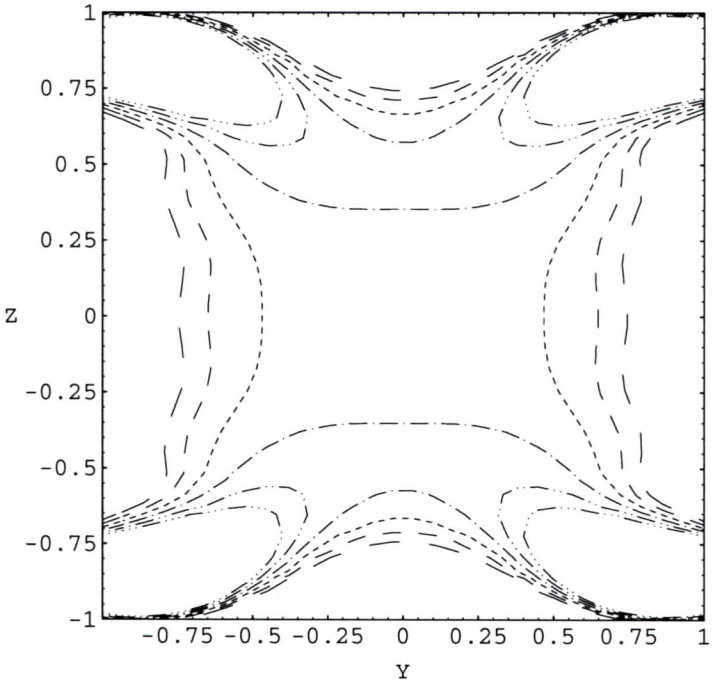

f)

Figure 34--continued. Contour plot of the relative error of the 10 unit CRP Coil. e) Y = 0 plane; f) X = 0 plane.

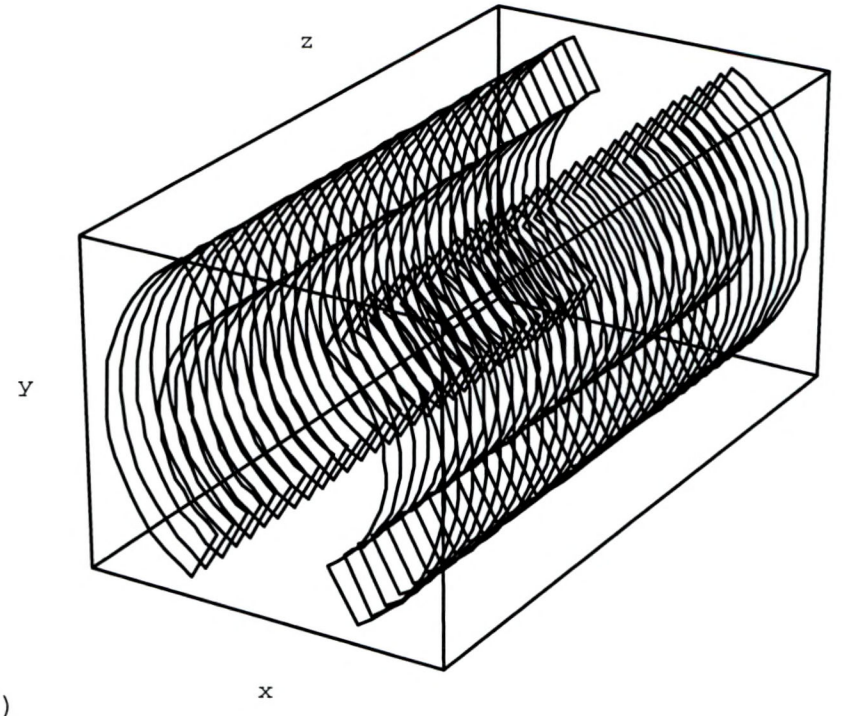

a)

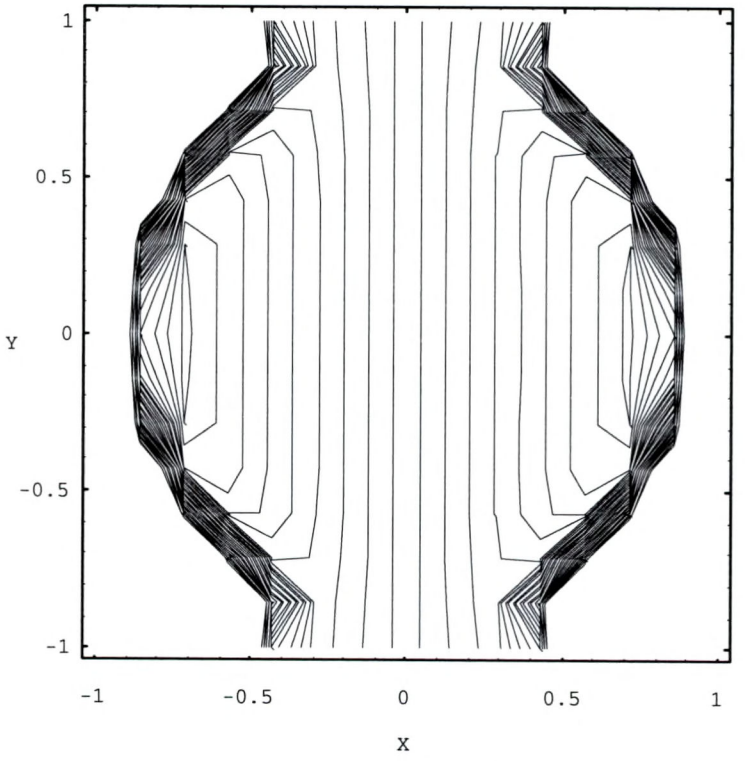

b)

Figure 35. A Concentric Return Path Coil with 30 planar units. The ratio of length:inner diameter:outer diameter is 6:2:3. a) Wire configuration. b) Contour plot of the field in the Z = 0 plane.

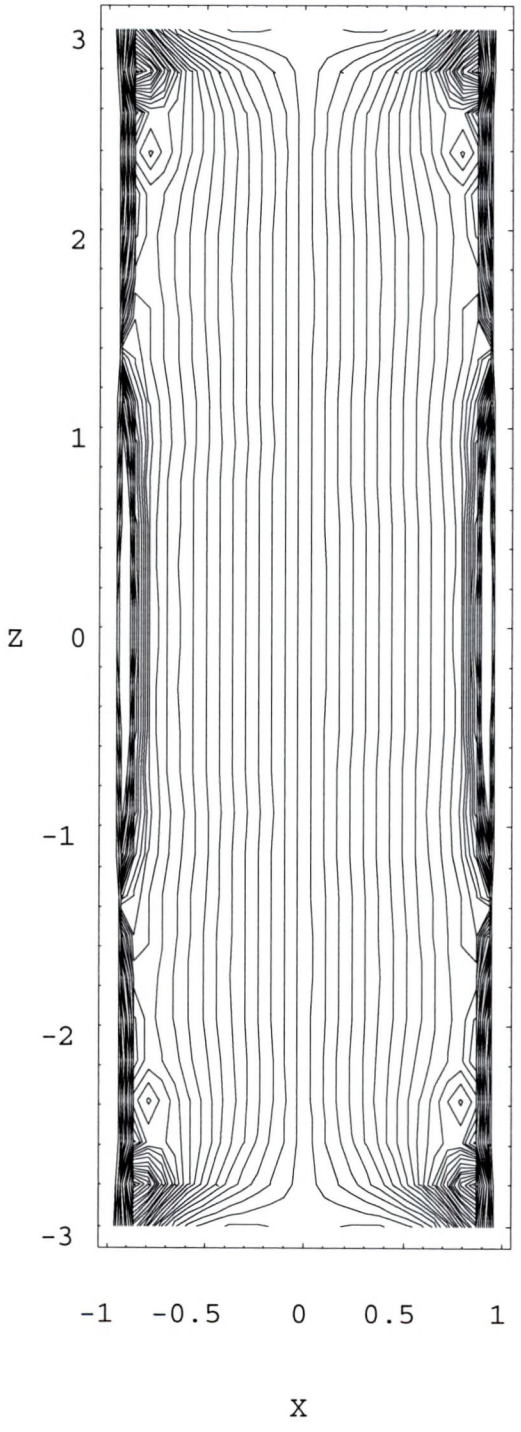

Figure 35--continued. c) Contour plot of the field of the 30 unit CRP Coil in the Y = 0 plane.

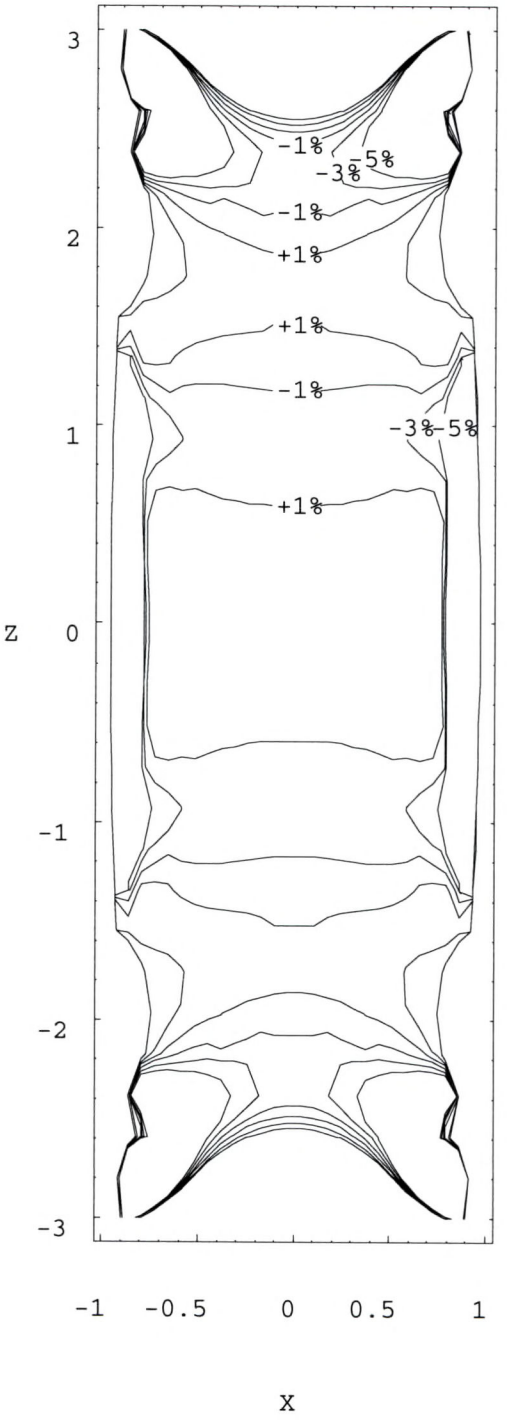

Figure 35--continued. d) Contour plot of the relative error of the 30 unit CRP Coil in the Y = 0 plane.

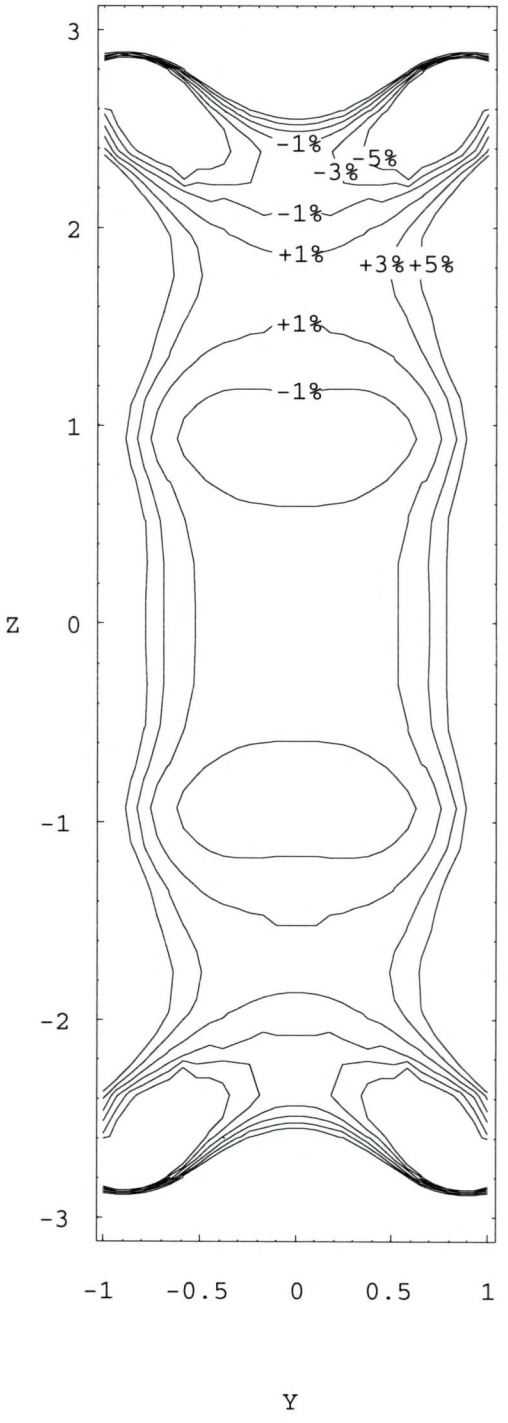

Figure 35--continued. e) Contour plot of the relative error of the 30 unit CRP Coil in the X = 0 plane.

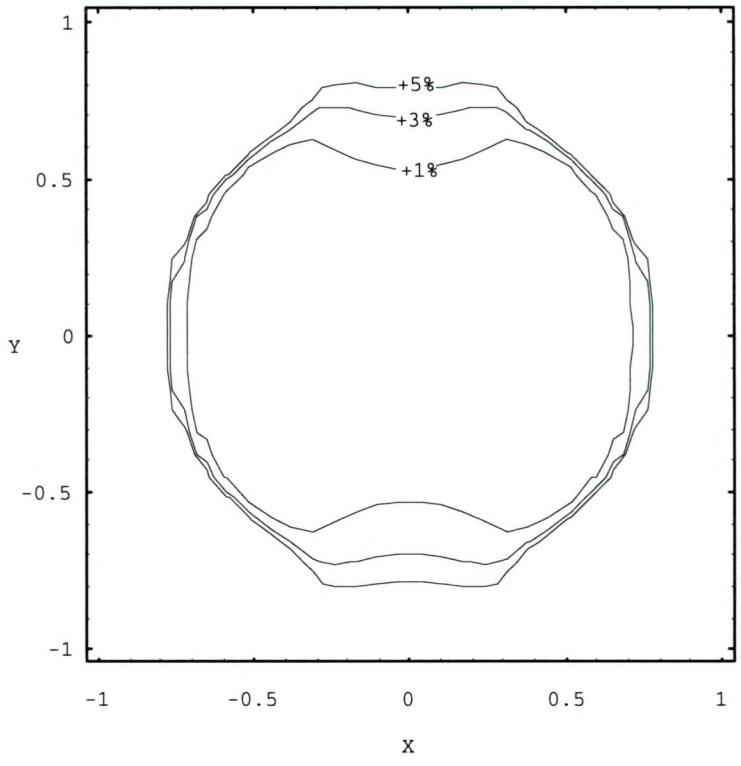

Figure 35--continued. f) Contour plot of the relative error of the 30 unit CRP Coil in the Z = 0 plane.

high-pass filter. Rather than applying preemphasis, a high-pass filter, to cancel the eddy current field, it would be appropriate to apply a low-pass filter. Any estimate of the amplifier specifications required to drive a CRP coil should take the above distinction into account, since it is easier for the amplifier to reproduce the low-pass current waveform.

The results from a first-order calculation of the gradient at the center of the coil due to the eddy current field from a concentric cylinder are given in Figures 37 and 38. This shows that there is a large difference in eddy current performance between the 30-plane and the 10-plane versions of the coils. Note that the sign of the eddy

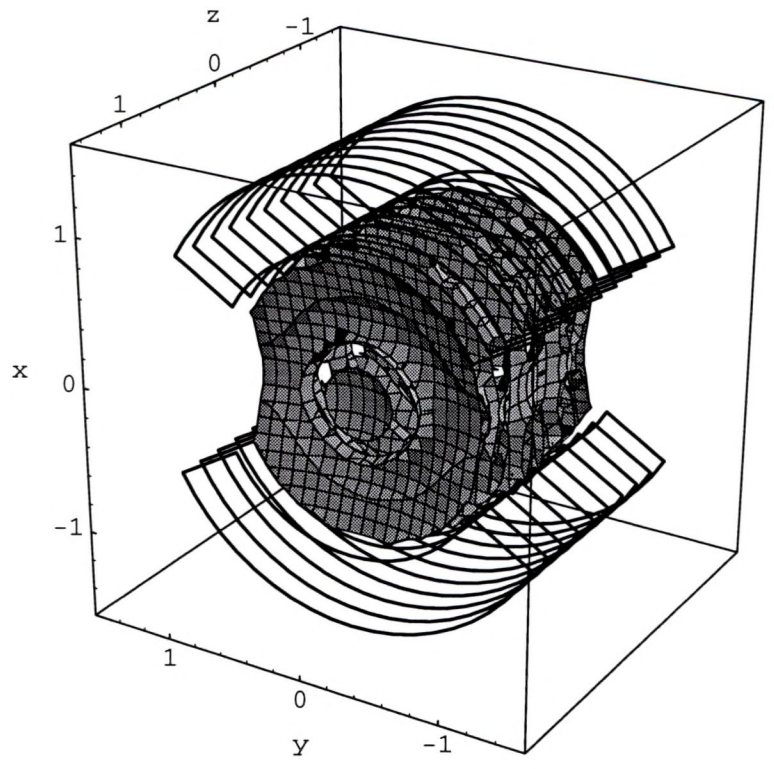

Figure 36. Three-dimensional plot of useful volume of 10-plane CRP coil. The shaded surface is the 5% relative error contour.

current field is opposite to that for the single-cylinder gradient coils.

A prototype of the 10-plane CRP coil was constructed. It was designed to fit into the bore of our 31 cm 2 T magnet (Oxford 85/310). The coil former consisted of 11 squares of 3/8" AB plywood 15.9 cm on a side. The square coil former just fit into the 22.5 cm clear bore. A hole saw was used to bore a 3" diameter hole for the sample. Grooves were made with a 1/8" router bit to accommodate the wire in 10 of the squares. The winding consists of 27 AWG enameled magnet wire.

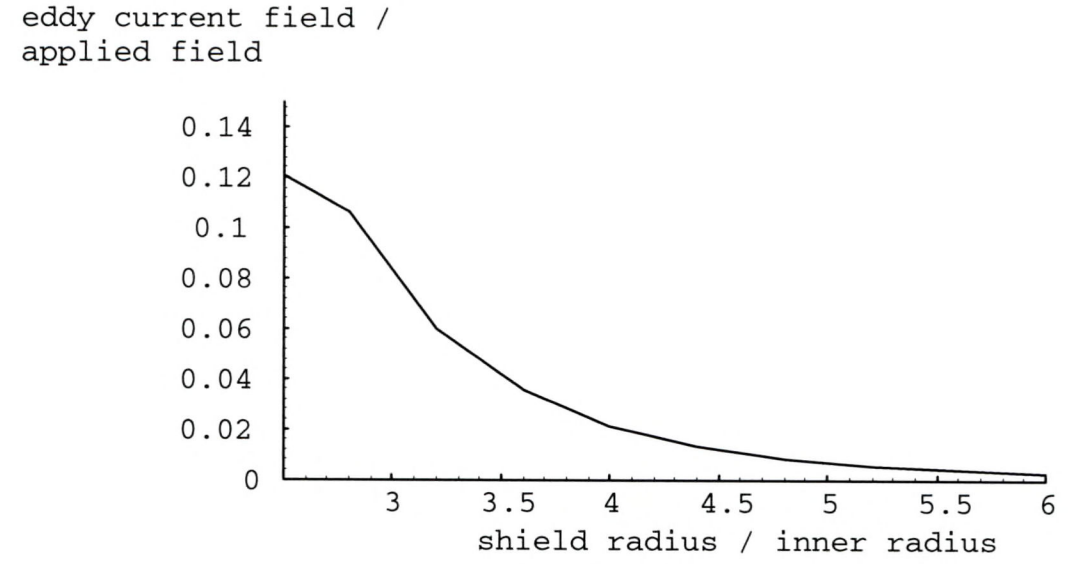

Figure 37. Eddy current field of the 10-element CRPC, expressed as a fraction of the applied gradient.

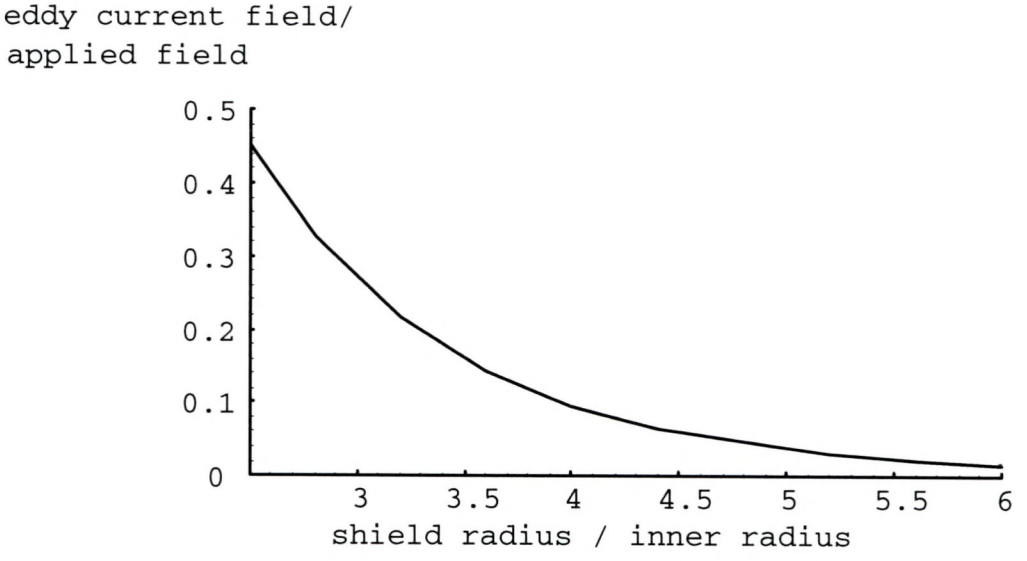

Figure 38. Eddy current field of the 30-element CRPC, expressed as a fraction of the applied gradient.

The coil was connected to a Techron 7540 power supply amplifier. All the windings were placed in series, so that only one of the two channels was used.

The phantom was integrated into the RF coil assembly. It consisted of a five by nine cell section of 1/2" deep

white plastic eggcrate diffuser intended for fluorescent lighting fixtures (Area Lighting Products A4524). The cells are nominally 1/2" on a side, separated by 1/16" walls. Acrylic sheets (K-S-H, Inc., MS CLR ACY 30 x 36) 1/8" thick sealed the top and bottom of the grid. The acrylic was welded into place with methylene chloride, then the joints were coated with epoxy to seal against leaks. The assembly was filled with de-ionized water during the assembly process. The RF coil consisted of a single turn of 1/2" copper tape around the outer edge of the plane defined by the diffuser. Variable capacitors (Johanson Manufacturing Corp., Boonton, NJ) and chip capacitors (American Technical Ceramics Corp., Huntington Station, NY) were used to tune and match the coil to 85.4 MHz. The circuit is shown in Figure 39. The coil had a measured Q of 214. The phantom just fit into the 3" aperture of the CRP coil, as shown in Figure 40. Inside the gradient coil, the measured Q was

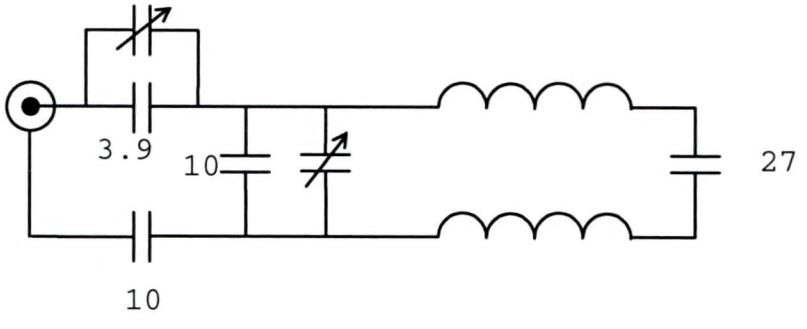

Figure 39. The RF coil. All capacitances are in pF.

169. The tuning shift when the RF coil was centered in the gradient coil was 125 KHz, although the shift was much larger when the coil was not centered.

An image of the eggcrate phantom was acquired with the CRP coil, and can be compared to a reference image and a simulated image. In a perfect image, the square grid of the

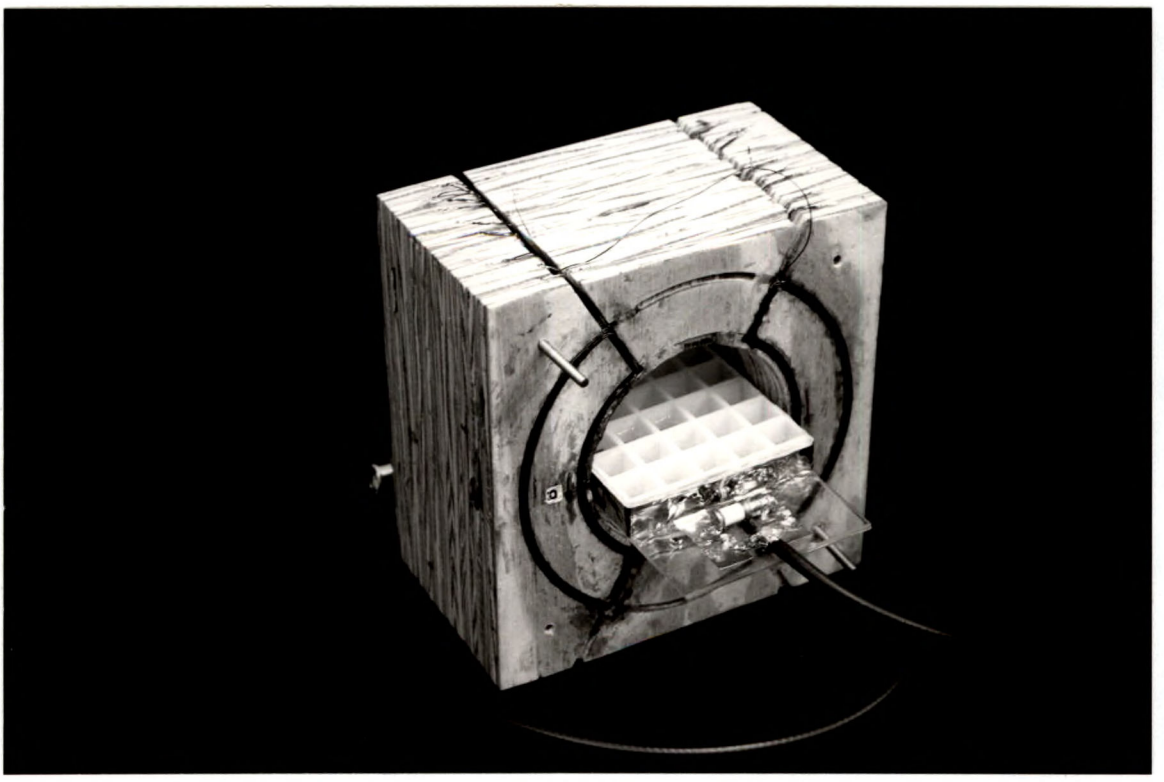

Figure 40. Photograph of the prototype CRP coil with the eggcrate phantom inserted.

eggcrate will be reproduced without distortion. A calculated "image" of the intersections of a grid with approximately the same spacing and position as the eggcrate phantom shown in Figure 41(a) illustrates the large size of the linear region of the CRP coil, and the character of the distortions that are observed at the edges of the field. A Biot-Savart calculation of the field of the CRP coil was used to produce the horizontal spacing, and the vertical

spacing is simply that of the undistorted grid. It can be seen that the field is a little larger at the ends of the coil, causing the phantom to appear to bulge. Just beyond the end of the coil the field changes sign. The points in the simulation are not connected, but the sign change would be visible if they were.

The only difference between the phantom images is the difference in the X gradient coil. The standard SISCO spin-echo sequence "image" was used as the pulse sequence for both images. The slice thickness was 2.3 mm. Two averages were collected. The gain of the amplifiers was adjusted so the size of the inner cells is the same; that is, the calibration factor is the same for the Oxford and the CRP coils. The RF coil is so close to the sample that the periphery of the sample is liable to be much brighter than the center. To compensate, the RF power was adjusted beyond the power needed for maximum signal so that the intensity is as homogeneous as possible.

A CRP coil image of the eggcrate phantom acquired in the XZ plane is shown in Figure 41(b). The Oxford gradients were used for the Y and Z localization, and the CRP coil used only for X. X was chosen to be the phase-encode direction so that there would be no position errors due to shimming. The sign reversal of the field beyond the end of the coil is clearly visible here. The grid distortion generally matches that in the simulated image. The bulge in the upper left corner is probably due to the poor machining

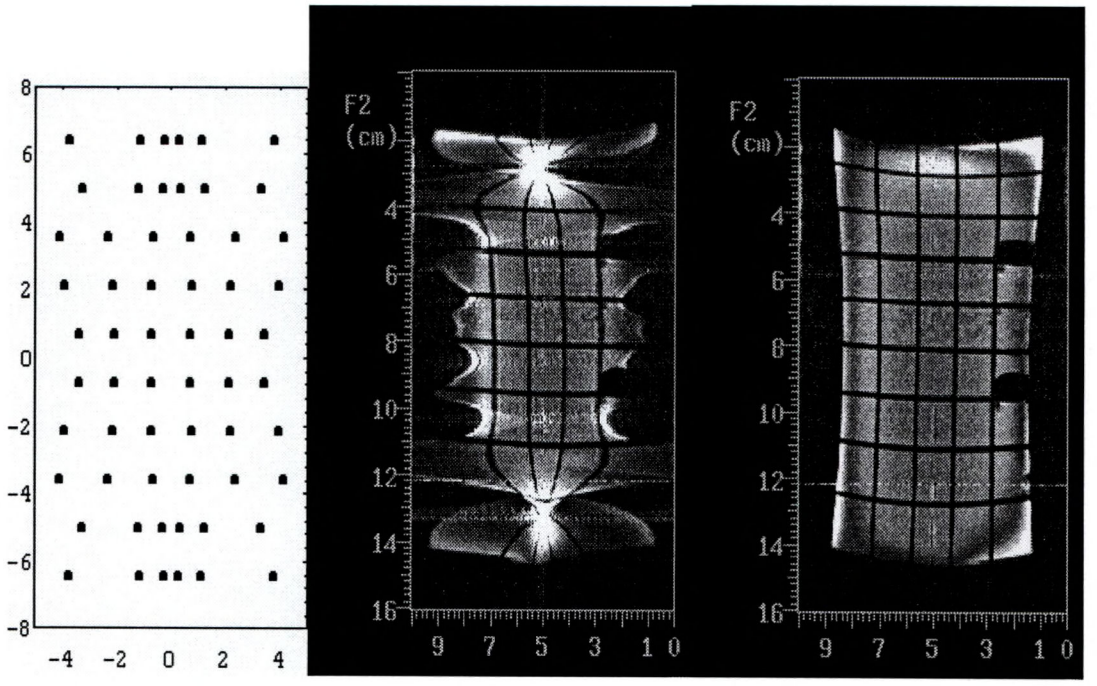

(a) (b) (c)

Figure 41. Simulated and real CRP coil images. The real and simulated phantom have the same width. a) The image is simulated from the Biot-Savart law; b) Image of egg crate phantom obtained with CRP coil; c) Image obtained with Oxford coil.

tolerance of the plywood. The length of the useful region is about 7 cm. Since the distance between the outermost planar units is 9.5 cm, the useful region extends to 74% of the coil length.

An image obtained with the Oxford gradients used in all three directions was made for comparison and shown in Figure 41(c). The Oxford gradients have a much larger linear region due to their larger size. There is some distortion visible in the Y direction at the ends of the phantom.

The CRP approach has yielded a radial gradient coil design that has a useful volume that can be made to extend

nearly to each end of the coil. The coil is inherently torque-free, a practical advantage that is particularly important for safety in clinical applications. While the coil is not self-shielded, the eddy current field has the sign opposite to that of a coil on a single cylinder, which reduces the dynamic range required of the amplifier. Insignificant tuning shift or reduction of Q was observed when an RF coil was placed inside, even in the absence of a Faraday shield. Any RF field used for NMR would be in the plane of the planar units, and so flux through the planes should be minimized. This may make it possible to use an RF coil that is an especially large fraction of the inner radius of the CRP coil.

Many refinements of the design are possible. A more efficient coil might be designed by including power efficiency in the error function. It would be possible to locate the useful volume off-center, which would improve the usefulness of the coil for head imaging, since more of the neck could be visualized. Dr. Raymond Andrew and Dr. Eugene Sczezniak are refining the design for use on the human head.

SYSTEM DEVELOPMENT FOR NMR MICROSCOPY

Introduction

NMR imaging has the capability to reveal the structure and hydration state of soft tissue in biological systems. The technique has been successfully applied to routine diagnostic procedures on human subjects with a typical in-plane resolution of 1 mm and slice thickness of 5 mm. Imaging of embryos or pathological specimens requires higher resolution, resulting in fewer spins per voxel and so less signal. The NMR sensitivity scales as roughly the 3/2 power of the polarizing field, so increasing the magnetic field can in part make up for the loss of signal.

It is desirable to use as small a bore as possible to image a given system. NMR microscope systems are typically built around wide bore magnets, but narrow bore magnets are much less expensive and more popular, and so it would be desirable to use them instead.

The purpose of the NMR microscope project was to develop an NMR imaging spectrometer for the study of microscopic biological specimens in a narrow-bore superconducting magnet. Technical issues included the pulsed field gradients, the RF homogeneity, and the sample positioning. Problems of using pulsed field gradients in a narrow bore magnet include eddy current fields, gradient

linearity over the field of view, and interaction between the gradient coils and the RF coil. Specimens consisted of amphibian oocytes and excised tissue samples because of the ease of handling these samples. The biological studies guided the hardware and software design. The goal was to begin to consider whether NMR can detect changes in quality or maturation stage of oocytes in vivo. High-field systems also show promise for pathology, since excised tissue tends to be somewhat smaller than what is effectively imaged on the 2 T system. Also, there is no other route to studying very high-field imaging, since large-bore high-field magnets do not exist.

Accordingly, a 7.1 T Nicolet NT-300 multinuclear pulsed NMR spectrometer was modified to perform NMR microscopy and other experiments requiring pulsed field gradients. Previous work by faculty, graduate students and staff was extended to produce a practical imaging system. Both hardware and software enhancements to the instrument were required. The additional capability included the production and control of magnetic field gradients for imaging and localized spectroscopy, the production of amplitude-modulated RF pulses for slice selection, the ability to display and store images, and improved sensitivity. Also, a user interface was designed to facilitate the control of imaging experiments. The spectrometer was used for preliminary imaging experiments on phantoms, excised rodent spinal cords, and follicles from *Tarichula Granulosa*.

Single slice gradient and spin echo images as well as preliminary chemical shift images were obtained.

Literature Review

NMR microscopes have been created or adapted from instruments designed for spectroscopy by a number of research groups. Typically, these instruments are based on 89 mm bore magnets. Field strengths vary from 4.7 to 11.75 T.

L. D. Hall added imaging capability to a home-built high-resolution spectrometer based on an Oxford Instruments 6.2 T magnet with a 54 mm bore.[85] Early images of capillary tubes containing water, benzene, acetone and methylene chloride were made using the first-order shim coils to produce field gradients for a projection-reconstruction experiment. The shim coils provided a gradient of about 0.11 G/cm which yielded about 0.5 mm resolution for the axially invariant capillary samples. Systematic characterization of the shim coils as imaging gradient coils was performed for the radial gradients using glass capillary tubes filled with water and placed in a teflon plug and, for the axial gradients, by a teflon plug into which was cut a series of holes.[86] It is much easier to use these phantoms to characterize small bore systems than to make point-by-point measurements. To overcome the effects of magnetic

[85]L. D. Hall and S. Sukumar, J. Magn. Reson. 50, 161, 1982.
[86]L. D. Hall et al., J. Magn. Reson. 60, 199, 1984.

field inhomogeneity and to observe resonances with larger line widths, a high-resolution probe was subsequently adapted to produce larger gradient fields.[87] The glass variable-temperature dewar was replaced with an acrylic tube of 37 mm O. D. and 5 mm thickness. Grooves 3 mm deep were cut into the former, and 27 AWG copper wire was placed into the grooves. For the radial gradients, the radius of the coil was 14.5 mm and 8 turns were used. The axial gradient consisted of a Maxwell pair, also with 8 turns. Using an Amcron model M-600 audio amplifier to supply a 1 A pulse, they obtained the fields shown in Table 6. Melting point

Table 6. Gradient field and inductance of Hall's microscopy coils.

Direction	Inductance (μH)	Field (G/cm)
X	35	3.71
Y	35	3.95
Z	12	2.5

capillaries were imaged without slice selection to obtain images with 100 μm resolution. A 10 ms delay between the gradient pulse and the data acquisition period was required to produce an undistorted spectrum.

An 8.5 T, 89 mm bore magnet at the Francis Bitter National Magnet Laboratory served as the heart of a home-built spectrometer imaging system.[88] The Maxwell and Golay

[87]L. D. Hall et al., J. Magn. Reson. 66, 349, 1986.
[88]E. W. McFarland et al., Magn. Reson. Imag. 6, 507, 1988.

gradient coils were wound on a 4.5 cm diameter cylinder. Sixteen AWG wire was used. The coils produced fields of 0.8 for x, 1.0 for y and 0.6 G/cm-A for z. A 100 A, 5V power supply was used to drive the coils, with the current switched on and off by a transistor switch controlled by the pulse sequencer. Only a single level of gradient field was possible with this arrangement. The gradient switching rate was 0.4 G/cm-ms. Solenoidal RF coils were used, with 10 and 2 mm diameter versions for the ^{1}H coil. A sample in the 2 mm proton coil could be shimmed to 10 Hz. Images of *Rana pipiens* egg cells were acquired with 15 μm resolution and 200 μm slice thickness.

Cho et al. predict and measure the SNR obtainable at 7.1 T.[89] They derive a diffusion-limited resolution of $\Delta r = \sqrt{\frac{2}{3} DT_{acq}}$, which yields 1 μm for D = 10^{-5} cm^2/s at T_{acq} = 1.5 ms. They selected a 5-turn solenoid with a diameter of 1 mm, length of 0.8 mm, and wire diameter of 0.14 mm, as an RF coil. The loaded *Q* was 83; unloaded *Q* was 86. Other solenoid designs were tried and rejected as being less sensitive. They built unshielded double-saddle gradient coils that provided 800 G/cm with a rise time of 100 μs. Images of human hair in glycerin with 4 μm resolution in-plane and 300 μm slice thickness were acquired in one hour. They use a gradient echo pulse sequence in which the half-

[89]Z. H. Cho et al., Med. Phys. 15, 815, 1988.

echo is sampled in order to reduce echo time. Evidently they reconstruct the images using a phase map to determine the real part and avoid taking the magnitude.

An NMR microscope was created for an 11.74 T, 89 mm bore magnet at the University of Nottingham.[90] The transverse gradient coils are of the primary/screen type, with the spacing of the primary coils adjusted to correct for the effect of the screen. The axial gradient coil was designed with the target field method. The coils are wound on cylinders of 30 mm and 65 mm inner diameter. Grooves for the screens were cut into the formers with a computer-controlled cutting machine. The gradient coils have the characteristics given in Table 7.

Table 7. Gradient field and inductance of Nottingham microscopy coils.

Direction	Efficiency (G/cm-A)	Inductance (μH)
X	2.33	30
Y	2.04	40
Z	1.41	20

The instrument has been used to study stems of the geranium (*Peargonium graveoleus*). The RF coil used is a 6-turn solenoid with an inner diameter of 1.5 mm. The resolution is as little as 4.5 μm in-plane with a slice thickness of 100 μm. Use of a half-Fourier imaging sequence

[90] R. Bowtell et al., Phil. Trans. R. Soc. Lond. A 333, 457, 1990.

reduces attenuation due to diffusion. Long, cylindrical air spaces result in local B_0 gradients that dominate the appearance of the images. First, the local inhomogeneity results in distortion in the readout direction, as spins at (y, z) are mapped to $(y, z + \Delta B_0(y,z)/G)$. More importantly, the gradient due to the air spaces is as much as 2000 G/cm, which greatly increases attenuation associated with diffusion. One simple solution to the problem might be to turn the sample so the long dimension of the air spaces is parallel to B_0 and the susceptibility effect is minimized. Another solution would be to use two phase-encode directions.

However, a sequence of 180° pulses in the readout period was used to reduce the effects of susceptibility and diffusion.[91] The magnetization is sampled once at the peak of each of a train of echoes. This CPMG (Carr-Purcell-Meiboom-Gill) approach removes the effect of the B_0 inhomogeneity and reduces the attenuation loss due to diffusion.

The first images of a single cell were obtained by Aguayo et al. in a 9.5 T, 89 mm bore spectrometer modified for NMR microscopy.[92] The gradient coil system was capable of developing gradients of 20 G/cm. Using a 5 mm solenoid RF coil, an image of a *Xenopus Laevis* ovum was obtained with spatial resolution of 10 by 13 μm and a slice thickness of

---

[91]J. C. Sharp et al., SMRM 1992, 688.
[92]J. B. Aguayo et al., Nature 322, 190, 1986.

250 μm. The cell nucleus was easily visible in the dark background of the cytoplasm.

Magnetization transfer was used to show that the shortened T_2 in cell cytoplasm comes from a broad component with restricted mobility, not from "microsusceptibility" broadening at surfaces.[93] The T_2 weighted images suggested the presence of bound water.

Images of blood flowing through a beating, perfused rat heart were obtained using a modified Nicolet NT 360 (8.45 T) spectrometer by Delayre et al.[94] ^{23}Na was imaged, and contrast depended on the fact that there is more Na in the blood than in the heart tissue. Imaging gradients were produced by the x, y, and z shim coils that were controlled from the computer through digital-to-analog converters. An oscillating z gradient defined the 1.5 mm thick slice. Projection-reconstruction was used to reconstruct the image matrix of 64 by 64 pixels. The heart was placed in a 20 mm diameter tube. The NMR signal was detected with a saddle coil. The NMR imaging experiment was gated to the cardiac cycle to obtain images at systole and diastole.

Instrument Development

To enable an existing, commercially available NMR spectrometer to perform NMR imaging, capability was added to produce and control pulsed field gradients and amplitude-

---

[93]E. W. Hsu et al., SMRM 1992, 974.
[94]J. L. Delayre et al., Science 212, 935, 1981.

modulated RF pulses. An imaging display and storage workstation was added, along with enhancements to the

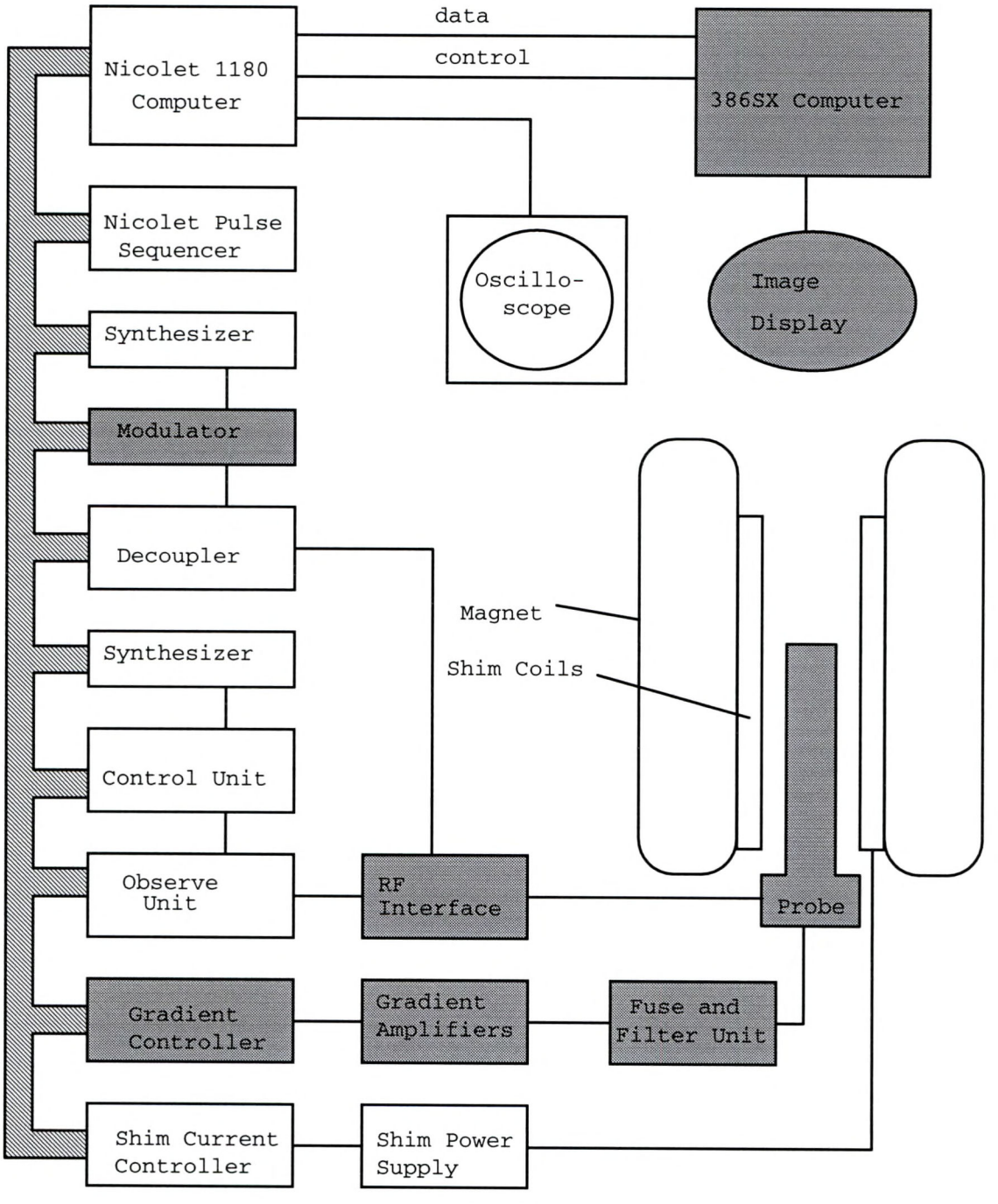

Figure 42. Block diagram of Nicolet NT-300 Spectrometer as modified for NMR microscopy. Modified or added sections are shaded.

control and processing capability of the system. The original Nicolet NT-300 spectrometer and the modifications are outlined in Figure 42.

The system is based on a 7.1 T vertical bore superconducting magnet manufactured by Nicolet Nalorac Corporation, Concord, CA. (now Nalorac Cryogenics Corporation, Martinez, CA.) The room temperature bore of the magnet has a diameter of 51 mm. The bore inside the shim coil and spinner stack has a diameter of 37 mm. In order to facilitate adjustment of the field homogeneity the factory shim coils were left in place, at the cost of considerable bore space. Since the gradient coil is much smaller than the shim coils, coupling between the gradient and shim amplifiers did not become a problem. Basic and essential gradient control hardware and software originally developed by Mareci, Cockman, and Thomas for another project was adapted for the NMR microscope.

A pulsed field gradient (PFG) control unit designed and constructed by Ray Thomas allowed programmed analog levels produced by digital-to-analog converters (DACs) intended to control the shim power supply to be switched to the gradient amplifiers. Spare control lines from the experiment controller were used to operate the PFG control unit. The gradient demand could be switched between two gradient levels and off during experiment execution for each of the three channels. For the NMR microscope, buffer amplifiers were added to lower the output impedance in the off state,

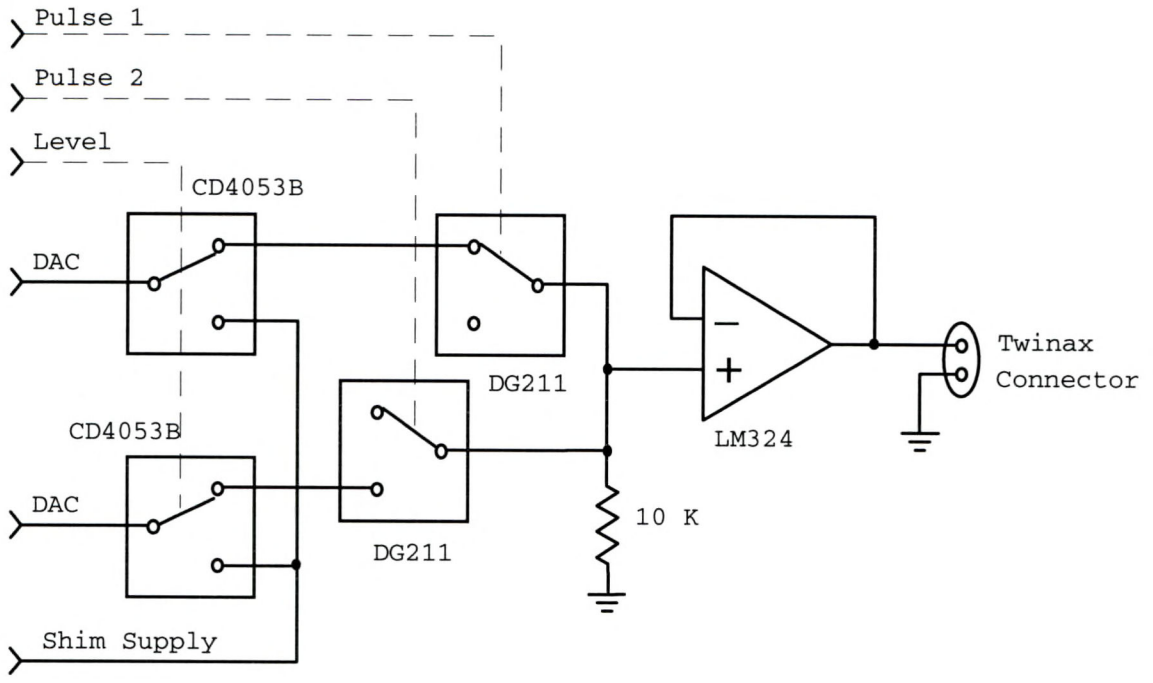

Figure 43. One of the 3 channels of the pulsed field-gradient controller.

as shown in Figure 43. Also, twinaxial cables were used to couple the gradient demand to the gradient power amplifiers. Care was taken to place the PFG control unit as close as possible to the source of the analog DAC levels to minimize noise pickup. On the high-power side, the gradient coils were not designed to dissipate the output of the amplifier at a high duty cycle, so a fuse and filter unit as shown in Figure 44 was incorporated between the power amplifiers and

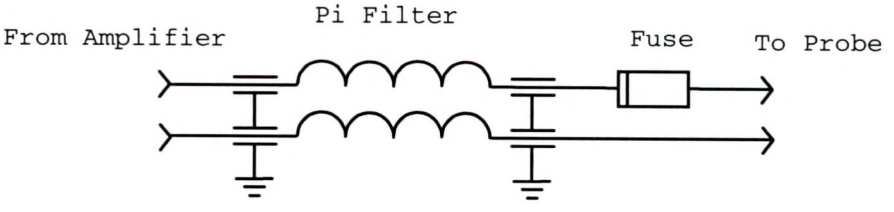

Figure 44. One channel of the gradient filter unit. The Pi filter is a Murata-Erie 1212-502.

the gradient coils in order to protect the gradient coils. Slow-blow fuses, typically 1 A, protected the gradient coils. A set of power low-pass filters in the same chassis ensured that RF pickup from the probe or cables to the probe would not be coupled back into the gradient amplifier and that the cable from the gradient amplifier would not serve as an antenna coupling RF noise into the probe. Software modifications by Mareci and Cockman[95] enabled the amplitude of the gradient pulse to be varied in a two dimensional experiment, making possible experiments based on the spin-warp modification[96] to 2D Fourier imaging.[97]

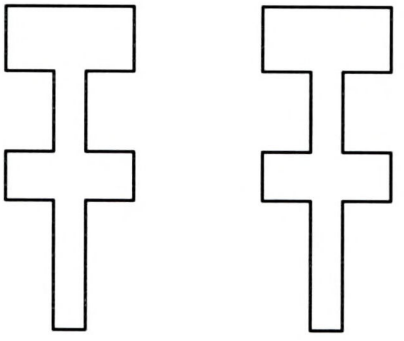

Figure 45. Foil sheets for RF probe.

The RF probe is a slotted resonator of conventional design. Copper foil sheets cut as shown in Figure 45 are wrapped around a tube so that the tabs overlap to form capacitors. Figure 46 is the equivalent circuit. The foil

[95]M. D. Cockman, Dissertation, 1988.
[96]W. A. Edelstein et al., Phys. Med. Biol. 25, 751, 1980.
[97]A. Kumar et al., J. Magn. Reson. 18, 69, 1975.

sheets of 2 mil thickness are separated by 1 mil mylar film. The capacitance density is about 115 pF/cm^2. The angular width of the foil strips is about 60°. The foil and mylar sheets are wrapped on a 6.5-PP quartz tube with 6.5 mm O. D. (Wilmad Assoc., Buena, NJ). Balanced matching reduces losses in conductive samples.[98] The Q of the RF coil inside the gradient set is about 100. To avoid eddy currents, no Faraday shield was used between the RF coil and the gradient coil. To reduce the effect of coupling between the RF and

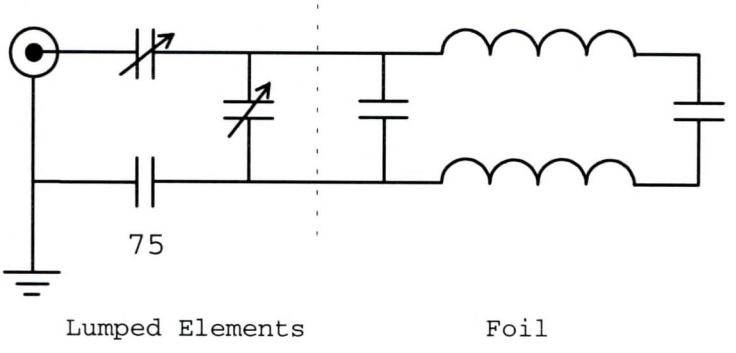

Figure 46. Equivalent circuit for RF probe. Components on the left are lumped; those on the right are formed from foil sheets.

gradient coil leads, feed-through capacitors were placed at the base of the probe. The standard commercial probe design includes a glass dewar surrounding the RF coil to facilitate variable temperature operation. An otherwise standard design can be converted for PFG operation by replacing this dewar with a cylindrical PFG coil set. The range of variable-temperature (VT) operation would be restricted, but

[98]J. Murphy-Boesch and A. P. Koretsky, J. Magn. Reson. 54, 526, 1983.

some VT capability would remain. The details of the gradient coils are set forth in the previous chapter. In the prototype probe, no VT capability was provided. The probe is shown in Figure 47.

Figure 47. Probe assembly with RF coil and PFG coils visible.

The RF front end supplied with the NT-300 consisted of a rack into which filters, Transmit/Receive switches, filters and preamplifiers are plugged. The plug-in modules select the frequency band and type of experiment. It was possible to use the factory front end for NMR microscopy experiments; however, the noise figure of the NT-300 was measured to be 6.5 dB. Replacing the Avantek UTO-511

preamplifiers with a new preamp decreased the noise figure to 5.5 dB.

The new preamp is a low-nose bipolar type model AU-1054-1103 (Miteq, Inc., Hauppauge, NY). The gain as measured at the factory is 30.7 +/- 0.25 dB. The noise figure was measured by the factory to be 1.28 dB at 250 MHz, 1.46 dB at 500 MHz. The -1 dB gain compression point is +9 dBm.

Better results were obtained by replacing the entire transcoupler circuit, which switches the probe between the RF power amplifier for transmit and the preamplifier for receive. The circuit and photographs of the home-built 300

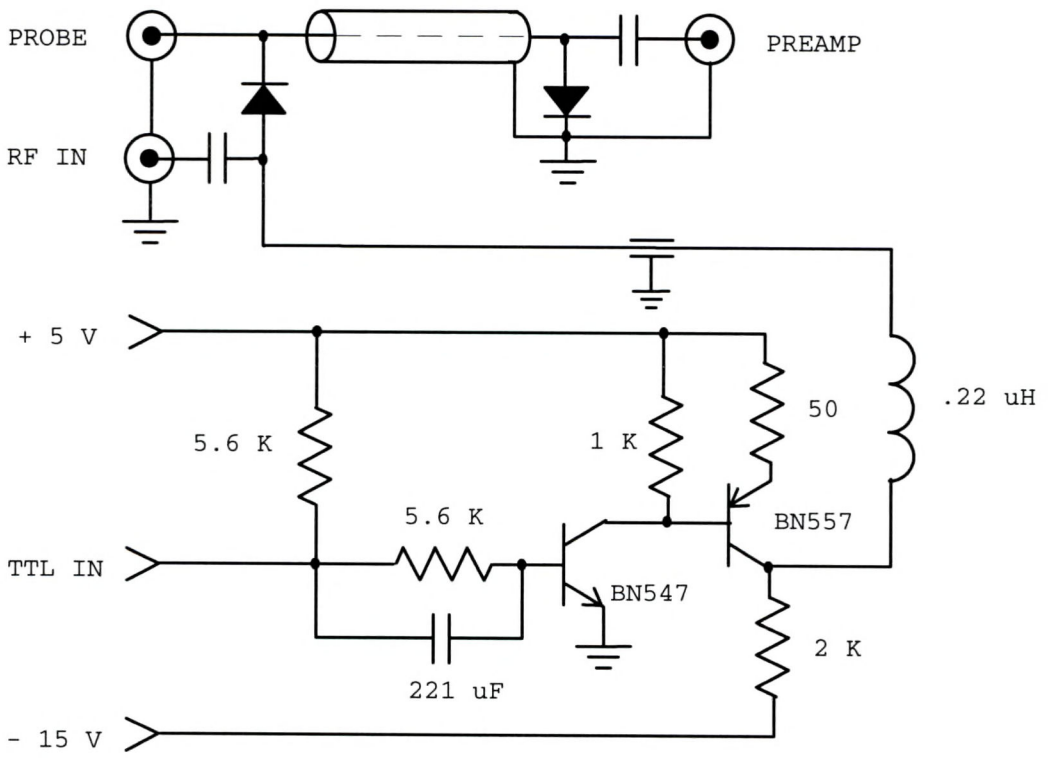

Figure 48. The transcoupler circuit.

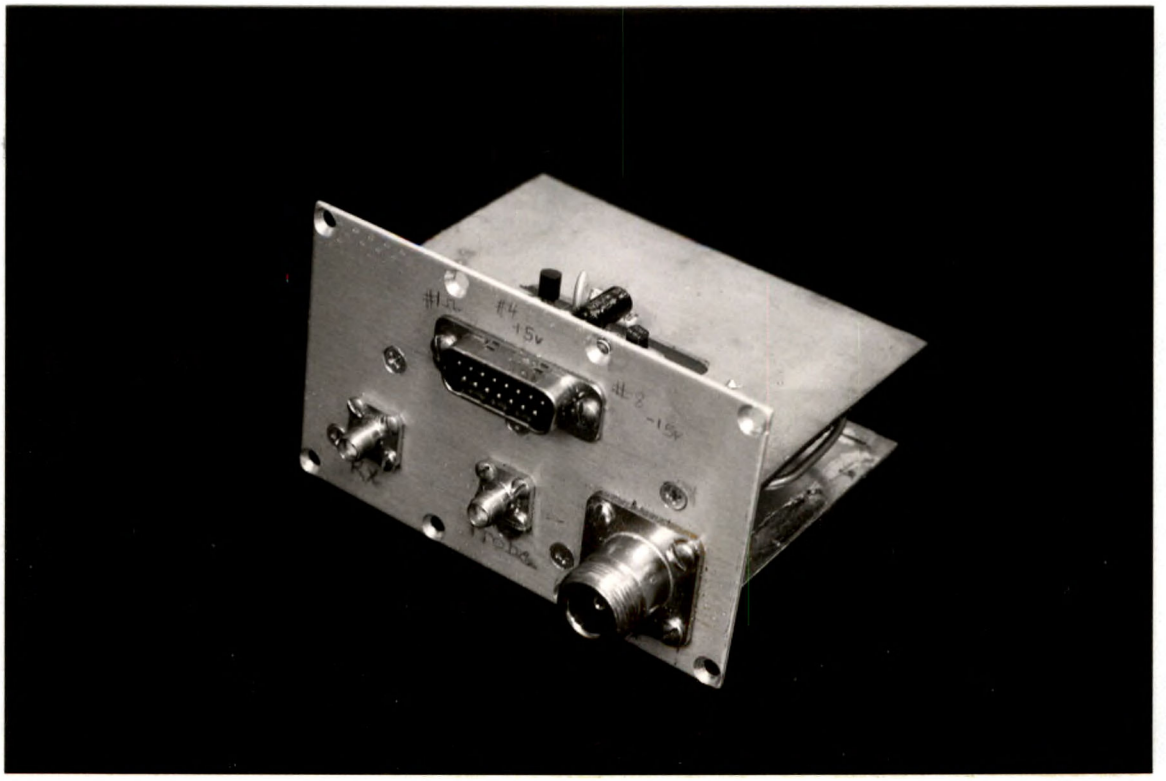

(a)

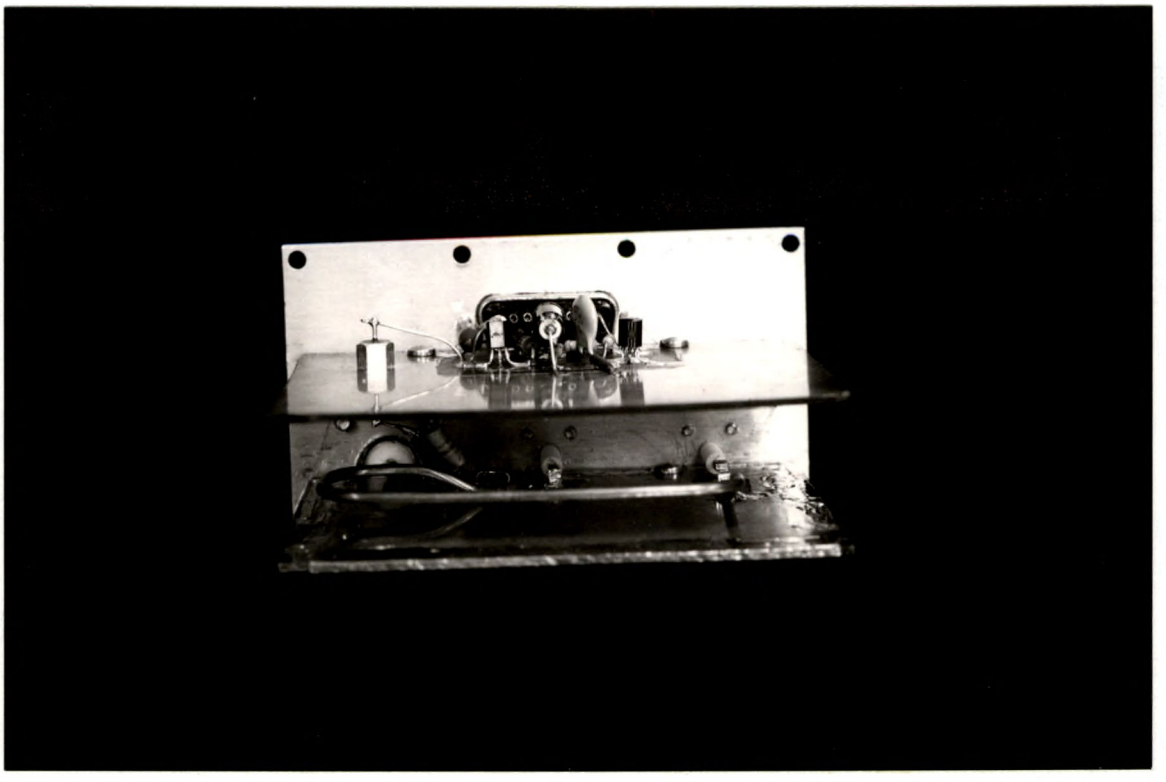

(b)

Figure 49. The transcoupler. a) Front view; b) Rear view.

MHz transcoupler are shown in Figures 48 and 49, respectively. Bench tests with a network analyzer showed the isolation between the RF IN and PREAMP ports to be 30.0 dB at 300 MHz. The loss between the PROBE and PREAMP ports was 0.87 dB, and the loss between the RF IN and PROBE ports was 1.3 dB. The Miteq preamp was used in conjunction with the new transcoupler.

NMR spectrometers often possess a second RF transmitter system known as a decoupler. In the Nicolet NT-300, the decoupler is a single-frequency transmitter tuned to 300 MHz. Its control is more flexible than for the first, or observe, transmitter system. The decoupler level can be changed by means of a PIN diode switch between two power levels set by rotary attenuators. The phase is under quadrature control. The amplifier, although lower in power at 20 W, is suited to RF pulses of longer duration.

Because of its flexibility, the decoupler was chosen to replace the observe channel for experiments that require modulated RF pulses. Dual attenuator control of the RF level facilitated separate power adjustment of $\pi/2$ and π pulses. An additional advantage over the observe channel that we did not exploit is that the decoupler frequency can be moved independently of the receiver, so that off-center slices can be excited.

In order to operate the selective pulse capability of the spectrometer, the operator loads a pulse shape into the pattern generator board described below using a program

written by David Brown. The internal RF trigger of the spectrometer starts the free-running pattern generator. An inverter/driver shown in Figure 50 converts the spectrometer

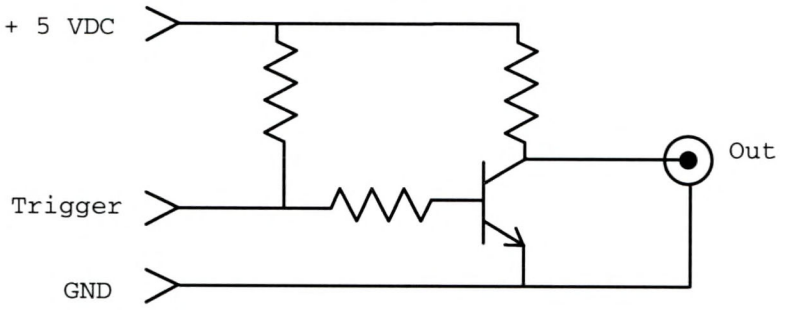

Figure 50. Inverter/Driver circuit for Pattern Generator trigger. All resistors are 2 KΩ. The transistor is type 2N3053.

trigger to the correct polarity and impedance. The pattern generator output controls a four-quadrant double-balanced diode mixer type SRA-1 (Mini-Circuits, Brooklyn, NY) as shown in Figure 51. The mixer can be placed at almost any low-power point in the transmitter chain, but the best results were achieved with the mixer modulating the 160 MHz

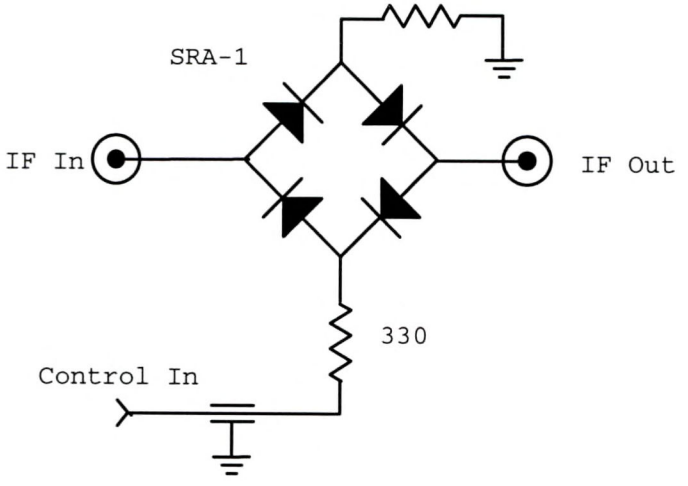

Figure 51. Simple ring modulator to control the sign and amplitude of the RF pulse.

reference to the decoupler. The intermediate frequency allowed for better isolation between the mixer input and output than the 300 MHz observe frequency. The complete system configuration is illustrated in Figure 52.

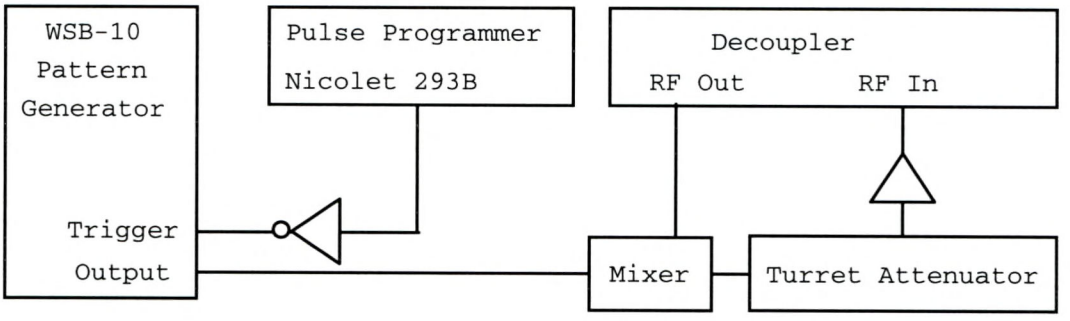

Figure 52. Block diagram of RF transmitter chain. Amplifier is a Minicircuits ZFL 500, with 20 dB of gain.

The pattern generator consisted of a WSB-10 (Quatech, Inc., Akron, OH) arbitrary analog waveform synthesizer card in a Gateway 386SX 25 MHz microcomputer. The WSB-10 allows analog signals to be generated independent of the host computer. The operator is then free to use the computer for data analysis and display while the experiment executes. The onboard clock allows data rates up to 200 ns/point. The DAC has 12 bits of resolution.

The simple ring modulator mixer shown in Figure 51 suffers from nonlinearity. The distortion can be partly alleviated by using a lookup table to filter the desired pulse shape. The lookup table is simply the response curve of the modulator to a full-scale ramp. For these measurements, the spectrometer was used as a digital oscilloscope to measure the output voltage of the decoupler.

A pulse sequence turns on both the decoupler, triggering a full-scale linear ramp in the pattern generator, and the ADC. The output of the decoupler is routed through 70 dB

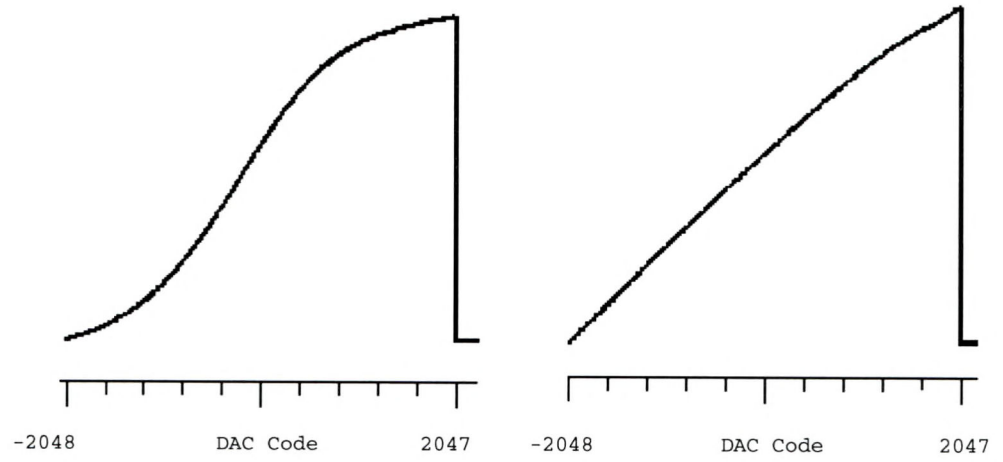

Figure 53. Response curve of modulator. a) Uncorrected; b) corrected with lookup table.

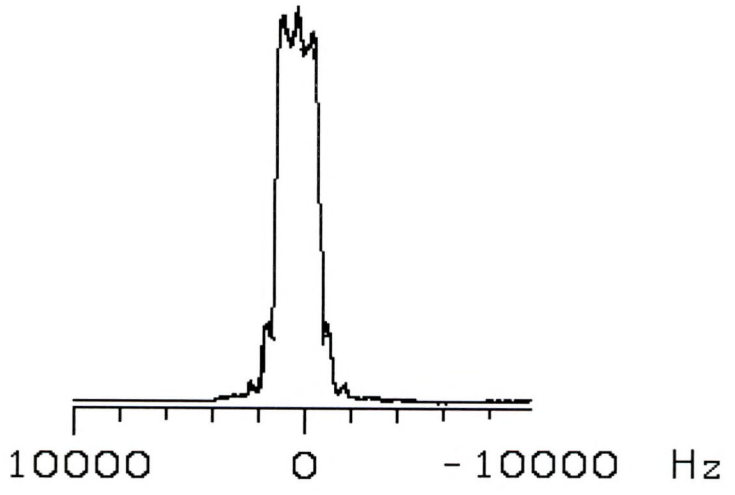

Figure 54. Slice profile of selective RF pulse.

of attenuation and back into the receiver. The magnitude of the detected signal is proportional to the voltage produced by the decoupler and can be used to construct a lookup table. The transfer function of the modulator before and after compensation is reproduced in Figure 53. A slice profile of a frequency-selective pulse shaped in the time domain is shown in Figure 54. Spin echo and gradient echo imaging sequences were developed for use on the NMR microscope. A timing diagram of a gradient echo experiment is shown in Figure 55.

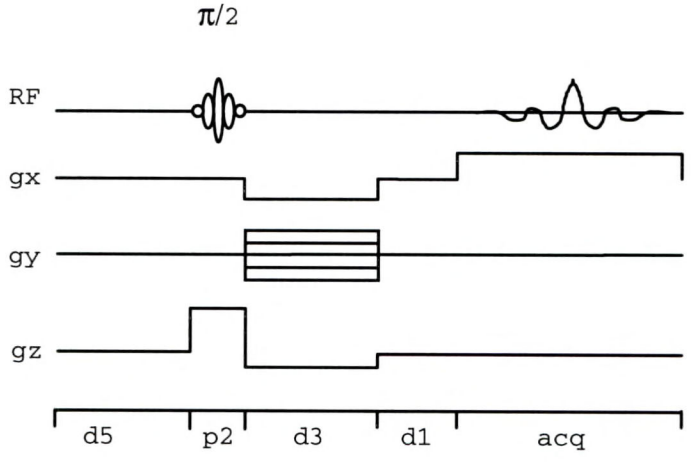

Figure 55. Timing diagram for single slice gradient echo imaging pulse sequence GESXYZ.

The code for this experiment is reproduced below.

```
GESXYZ
GRADIENT ECHO, TRANSVERSE V1.1
D5
P2/0,N,C@A+0,G
D3,F,U,W
D1
A@A,E
D2,E  J1
PHASE A = (2*S)+(2*#)
```

The suffixes E, F, G, U, W, V turn on a field gradient pulse in the interval. The suffix A defines the transmitter and receiver RF phase. The suffix N enables the decoupler, and C sets the output to continuous wave.

The instrument could be controlled directly from a virtual terminal on the PC, which replaced the usual

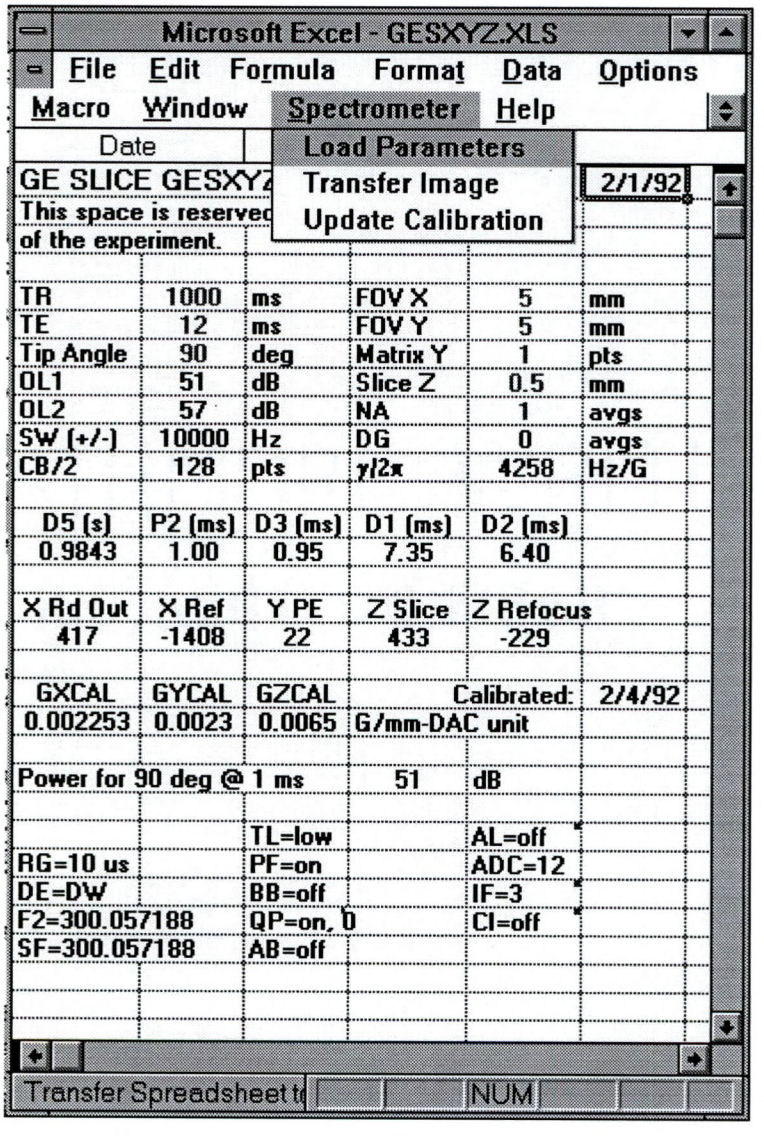

Figure 56. Excel spreadsheet calculates dependent parameters in spin-echo imaging experiment. The spectrometer can be controlled from the pull down menu.

electromechanical input device. A second virtual terminal is used to control the data transfer. Two 9600 baud serial RS-232 lines connect the PC and the Nicolet 1180E computer, one for control and one for data.

It is desirable to control an imaging experiment by setting parameters such as the echo time, *TE*, that must be translated into hardware delays. An Excel (Microsoft Corp.)

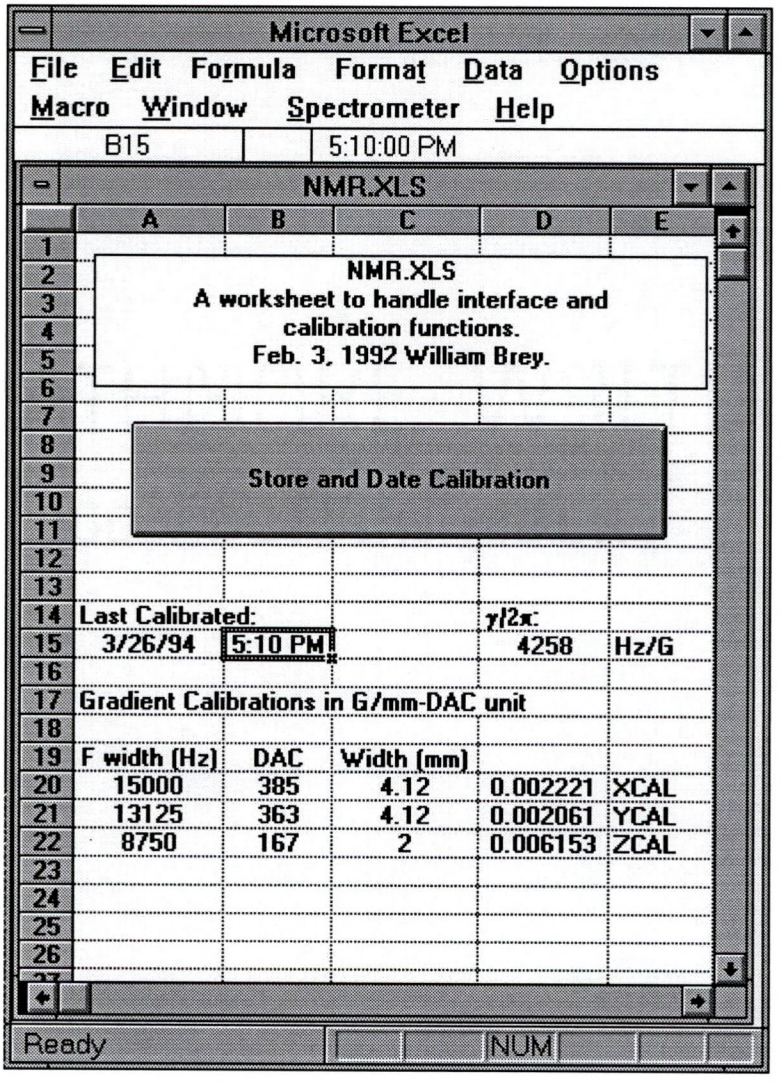

Figure 57. Spreadsheet to update gradient calibration parameters.

spreadsheet as shown in Figure 56 provided a convenient way to make the necessary calculations. Command macros were created to set up the spectrometer automatically for an experiment, then to transfer the image to the PC for storage and display. The macros were executed from a pull-down menu. The parameters in the spreadsheet can be divided into dependent and independent. The independent parameters are those that would be set by the operator and are color-coded red or blue. The dependent parameters are color-coded black. Front-panel control of the gain of each of the channels of the Techron amplifier facilitated manual adjustment of the magnetic center of the gradient coils. However, adjusting the gain resulted in small changes in gradient calibration. In order to account for the changing calibration factors in a convenient way, NMR.XLS shown in Figure 57 provided a worksheet for calculating the current calibration and storing it in the relevant worksheets.

Results

Phantoms consisting of melting-point capillary tubes in a 5 mm NMR tube of water are used to test the NMR microscope; an example is shown in Figure 58. The capillary tubes are 5, 10, 25, and 50 μL. The 5 μL tubes have the smallest I. D. of 270 μm. The *TE* is 10 ms; the repetition time *TR* is 1 s. The slice is 0.5 mm thick. Two averages were used. A spin-echo sequence is employed. The field of view is 5 mm by 5 mm, and the image matrix is 128 by 128.

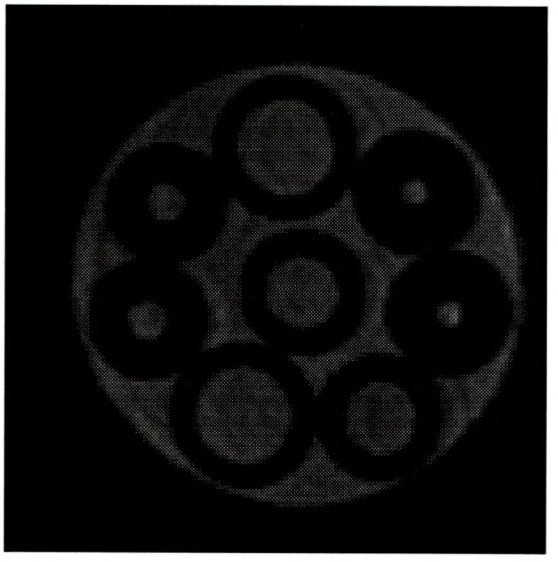

Figure 58. Spin-echo image of capillary phantom. Tap water fills the open melting point capillary tubes and the spaces between them.

Note the absence of phase- encode artifacts that would be due to inadequate filtering of alternate coherence pathways.[99]

When using long capillary tubes, slice selection is not essential if the shims are adjusted carefully and the tubes are straight. With a known phantom, the RF power can be adjusted to get even intensity in the image, compensating for the inhomogeneity of the coil. It is possible to center the image by adjusting the gain of the gradient amplifiers. Then the height and width of the image are used to calibrate the gradients.

A series of images of follicles of the salamander *Taricha granulosa* illustrates the contrast effects possible

[99]G. J. Barker and T. H. Mareci, J. Magn. Reson. 83, 11, 1989.

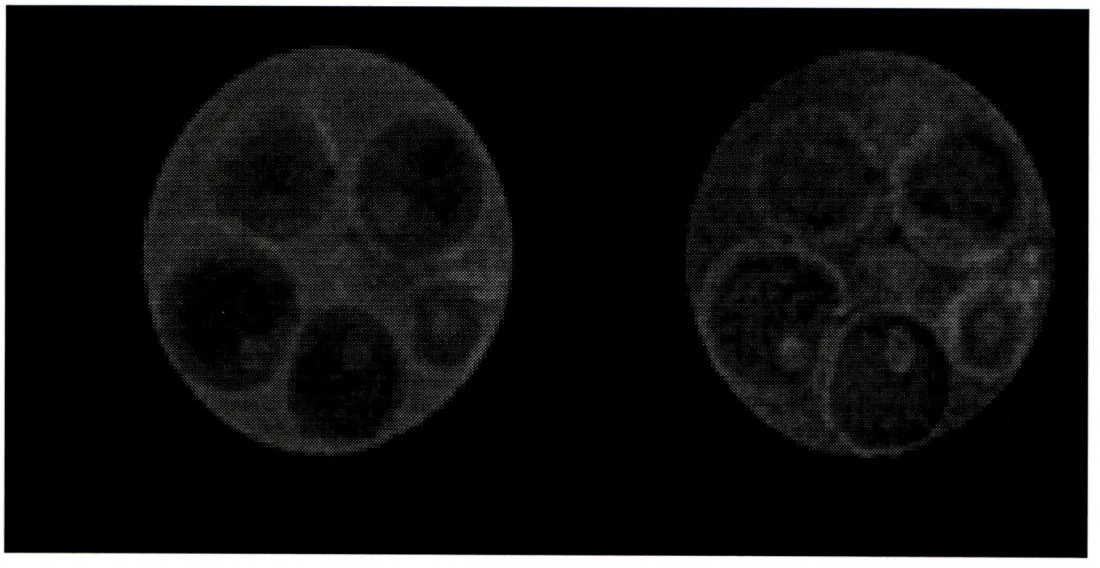

(a) (b)

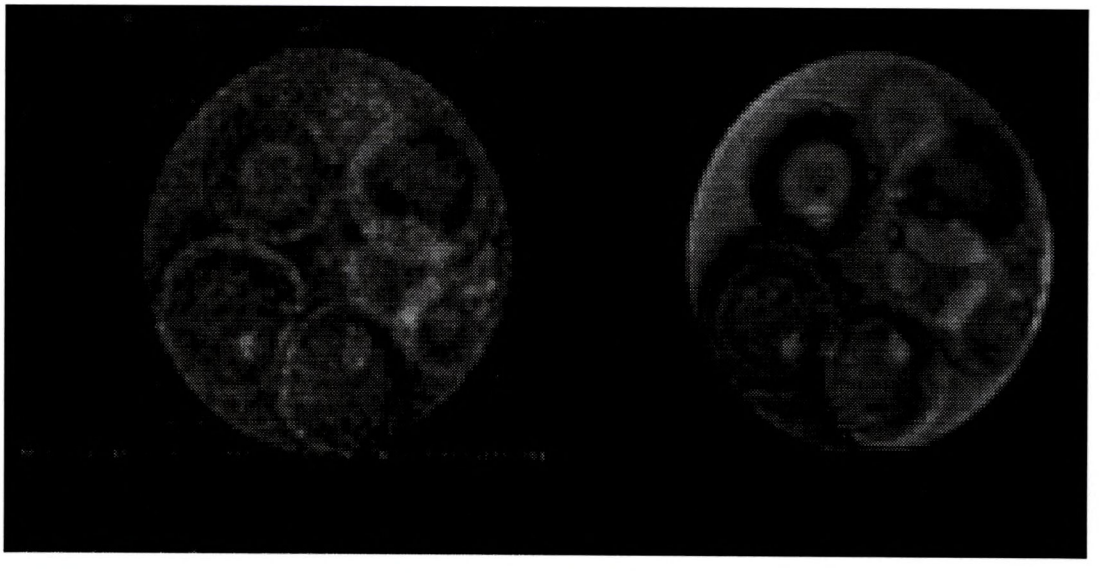

(c) (d)

Figure 59. Salamander (*Taricha granulosa*) follicles in 5 mm NMR tube. Image series with various *TR* shows T_1 variation. In the gradient echo images, *TE* = 5.45 ms, FOV = 4 by 4 mm, slice thickness = 0.5 mm. a) *TR* = 500, NA = 2; b) *TR* = 200 ms, NA = 20; c) *TR* = 100 ms, NA = 40 ms; d) *TR* = 50 ms, NA = 1000.

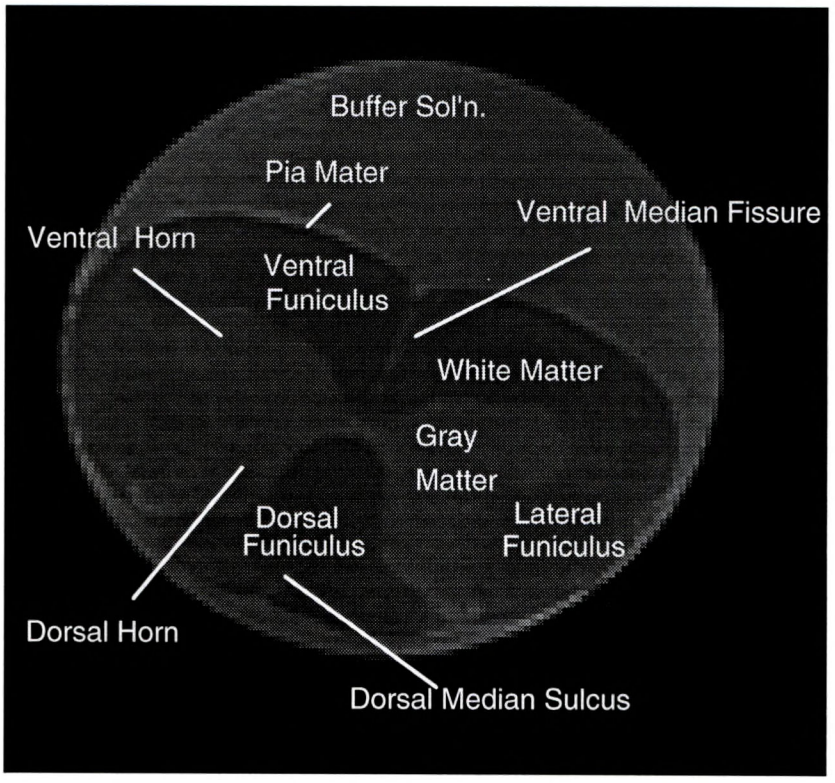

Figure 60. Spin-echo NMR image at 7.1 T of excised rat spine in buffer solution. The parameters are: *TE*/*TR*: 13/2000 ms, FOV = 5 mm by 5 mm, slice thickness = 1.0 mm, matrix = 128 by 128.

by varying the *TR* to provide T_1 contrast. In these gradient echo images, *TE* = 5.45 ms, the field-of-view (FOV) is 4 by 4 mm, and the slice thickness is 0.5 mm. The repetition times *TR* range from 50 to 500 ms. The number of acquisitions is varied along with *TR* to keep the intensity approximately constant. The bright rings in (b) and (c) of Figure 59 appear to indicate the medullary cytoplasm. The bright central spot is the germinal vesicle. The dark area is the cortical cytoplasm.

The image of Figure 60 illustrates the contrast still present in fixed tissues. The transverse section through

the excised spinal cord of an adult female Sprague-Dawley rat shows a clear distinction between white and gray matter. A spin-echo image sequence was used. The parameters are: *TE/TR*: 13/2000 ms, FOV = 5 mm by 5 mm, slice thickness = 1.0 mm, matrix = 128 by 128. It is evident from the characteristic butterfly shape of the gray matter that the slice is at the level of the cervical enlargement, approximately C5. The bright signal present around the cord is the Sorenson's phosphate-buffered solution. The slight hyperintensity in the dorsal horns indicates the substantia gelatinosa, a myelin-free region that is involved in transmission of pain signals.

Conclusion

An NMR spectrometer has been adapted to perform NMR microscopy. A resolution of 40 by 40 by 500 μm has been obtained. Although a 7.1 T magnet with 51 mm bore was used, the images compare favorably with those obtained on 9 T, 89 mm bore magnets. A fixed tissue sample and living amphibian follicles were studied. Meaningful contrast was obtained in both cases.

The high noise figure of the spectrometer and the limited performance of the RF coil did not provide especially high sensitivity. A ^{1}H transcoupler and preamplifier improved the noise figure and eliminated RF interference. The RF coil Q was about half, and 90° pulse length about twice, that obtained by spectrometer

manufacturers. Reducing the stray inductance by routing both leads from the same side of the coil should improve the sensitivity. Some loss in Q was due to loading of the gradient coil.

The vertical orientation of the coil and sample helped to eliminate problems with susceptibility that have been observed with horizontal samples. It also facilitated changing the sample. The lack of control over the rotational position provided by the pneumatic sample insertion system was not a problem for the samples studied.

The unshielded three-axis gradient set provided enough gradient strength and switching time to use for diffusion or other more demanding experiments. There is adequate gradient strength for higher-resolution imaging if the sensitivity of the RF coil were improved. Some spatial distortion in the images can be attributed to inaccuracy in the wire position. Nothing observed in the images was attributed to eddy currents. The eddy current measurement technique described above should be applied to evaluate the system experimentally.

CONCLUSION

These developments in pulse field gradient technology may find application in research areas ranging from functional imaging to NMR microscopy. Stimulated echo techniques allow measurement of the eddy current field over a wide dynamic range without any special hardware and can be used to adjust the eddy current compensation and assess the effectiveness of reduced-size gradient coils. This technique is now being used to adjust the compensation for new gradient coils for a 4.7 T small-animal spectrometer. Reduced-size gradient coils produce reduced eddy currents and short switching times and can be applied to small-animal imaging and NMR microscopy. The CRP coil is a good candidate for application to clinical imaging. Moving the region of sensitivity to one end, for example, will allow better coverage of the human neck.

REFERENCES

Abduljalil, A. M., A. H. Aletras, J. C. Pruski, A. Ahmad, B. S. Palmer, and P-M. L. Robitaille. "Torque Compensated Asymmetric Gradient Coils for EPI." Book of Abstracts, SMRM, 12th Annual Meeting, 1993, p. 1306.

Aguayo, J. B., S. J. Blackband, J. Schoeniger, M. A. Mattingly, and M. Hinterman. "Nuclear Magnetic Resonance Imaging of a Single Cell." Nature 322: 190 (1986).

Anderson, W. A. "Electrical Current Shims for Correcting Magnetic Fields." Rev. Sci. Inst. 32: 241 (1961).

Bangert, V., and P. Mansfield. "Magnetic Field Gradient Coils for NMR Imaging." J. Phys. E.: Sci. Instrum. 15: 235 (1982).

Barker, G. J., and T. H. Mareci. "Suppression of Artifacts in Multiple-Echo Magnetic Resonance." J. Magn. Reson. 83: 11 (1989).

Boesch, Ch., R. Gruetter, and E. Martin. "Temporal and Spatial Analysis of Fields Generated by Eddy Currents in Superconducting Magnets: Optimization of Corrections and Quantitative Characterization of Magnet/Gradient Systems." Magn. Reson. Med. 20: 268 (1991).

Boesch, Ch., R. Gruetter, and E. Martin. "Temporal and Spatial Characterization of Eddy Current Fields in High Field Superconducting Magnets." Book of Abstracts, SMRM, 8th Annual Meeting, 1989, p. 965.

Bowtell, R., G. D. Brown, P. M. Glover, M. McJury, and P. Mansfield. "Resolution of Cellular Structures by NMR Microscopy at 11.7 T." Phil. Trans. R. Soc. Lond. A 333: 457 (1990).

Bowtell, R., and P. Mansfield. "Screened Coil Designs for NMR Imaging in Magnets with Transverse Field Geometry." Meas. Sci. Technol. 1: 431 (1990).

Brooker, H. R., T. H. Mareci, and J. Mao. "Selective Fourier Transform Localization." Magn. Reson. Med. 5: 417 (1987).

Brühwiler, D., and G. Wagner. "Selective Excitation of ^{1}H Resonances Coupled to ^{13}C. Hetero COSY and RELAY Experiments with ^{1}H Detection for a Protein." J. Magn. Reson. 69: 546 (1986).

Cho, Z. H., C. B. Ahn, S. C. Juh, H. K. Lee, R. E. Jacobs, S. Lee, J. H. Yi, and J. M. Jo. "Nuclear Magnetic Resonance Microscopy with 4-μm Resolution: Theoretical Study and Experimental Results." Med. Phys. 15: 815 (1988).

Cockman, M. D. "Novel Pulse Methods for Multidimensional NMR Imaging and Spectroscopy." Dissertation. University of Florida, 1988.

Cory, D. G., and A. N. Garroway. "Measurement of Translational Displacement Probabilities by NMR: An Indicator of Compartmentation." Magn. Reson. Med. 14: 435 (1990).

Crown International. Techron 7540. Elkhorn, Illinois.

Delayre, J. L., J. S. Ingwall, C. Malloy, and E. T. Fossel. "Gated Sodium-23 Nuclear Magnetic Resonance Images of an Isolated Perfused Working Rat Heart." Science 212: 935 (1981).

Edelstein, W. A., J. M. S. Hutchison, G. Johnson, and T. Redpath. "Spin Warp NMR Imaging and Applications to Human Whole Body Imaging." Phys. Med. Biol. 25: 751 (1980).

Egloff, H. "Elimination of Base Field Shifts Due to Pulsed Magnetic Field Gradients." Book of Abstracts, SMRM, 8th Annual Meeting, 1989, p. 969.

Engelsberg, M., R. E. de Souza, and C. M. Dias Pazos. "The Limitations of a Target Field Approach to Coil Design." J. Phys. D.: Appl. Phys. 21: 1062 (1988).

Frahm, J., K. Merbolt, W., Hänicke. "Functional MRI of Human Brain Activation at High Spatial Resolution." Magn. Reson. Med. 29: 139 (1993).

Frese, G., and E. Stetter. "Tesseral Gradient Coil for a Nuclear Nagnetic Resonance Tomography Apparatus." U. S. Patent 5,198,769 (1993).

Gideon, P., C. Thomsen, and O. Henriksen. "Increased Self-Diffusion of Brain Water in Normal Aging." J. Magn. Reson. Imag. 4: 185 (1994).

Golay, M. J. E. "Field Homogenizing Coils for Nuclear Spin Resonance Instrumentation." Rev. Sci. Inst. 29: 313 (1958).

Hall, L. D., S. Luck, and V. Rajanayagam. "Construction of a High-Resolution NMR Probe for Imaging with Submillimeter Spatial Resolution" J. Magn. Reson. 66: 349 (1986).

Hall, L. D., V. Rajanayagam, and S. Sukumar. "Adaptation of High-Resolution NMR Spectrometers for Chemical Microscopy. Evaluation of Gradient Magnitudes and B_1 Homogeneity." J. Magn. Reson. 60: 199 (1984).

Hall, L. D., and S. Sukumar. "Chemical Microscopy Using a High-Resolution NMR Spectrometer. A Combination of Tomography/Spectroscopy Using Either ^{1}H or ^{13}C." J. Magn. Reson. 50: 161 (1982).

Hsu, E. W., N. R. Aiken, J. S. Schoeniger, and S. J. Blackband. "Magnetization Transfer Microimaging of Single Neurons." Book of Abstracts, SMRM, 11th Annual Meeting, 1992, p. 974.

Hughes, D. G., Q. Liu, and P. S. Allen. "Spatial Dependence of the Eddy Current Fields in a 40 cm Bore Magnet." Book of Abstracts, SMRM, 11th Annual Meeting, 1992, p. 362.

Jackson, J. D. Classical Electrodynamics. John Wiley and Sons: New York, 1975.

Jehenson, P., M. Westphal, and N. Schuff. "Analytical Method for the Compensation of Eddy-Current Effects Induced by Pulsed Magnetic Field Gradients in NMR Systems." J. Magn. Reson. 90: 264 (1990).

Jensen, D. J., W. W. Brey, J. L. Delayre, and P. A. Narayana. "Reduction of Pulsed Gradient Settling Time in the Superconducting Magnet of a Magnetic Resonance Instrument." Med. Phys. 14: 859 (1987).

Keen, M., M. Novak, R. Judson, R. E. Ellis, W. Vennart and I. R. Summers. "Characterization of Eddy Current Compensation over a Large Volume." Book of Abstracts, SMRM, 11th Annual Meeting, 1992, p. 4029.

Kumar, A., D. Welti, and R. R. Ernst. "NMR Fourier Zeugmatography." J. Magn. Reson. 18: 69 (1975).

Kwong, K. K., J. W. Belliveau, D. A. Chesler, I. E. Goldberg, R. M. Weisskoff, B. P. Poncelet, D. N. Kennedy, B. E. Hoppel, M. S. Cohen, R. Turner, H. M. Cheng, T. J. Brady, and B. R. Rosen. "Dynamic Magnetic Resonance Imaging of Human Brain Activity During Primary Sensory Stimulation." Proc. Natl. Acad. Sci. 89: 5675 (1992).

Lide, D. R. (Ed.) CRC Handbook of Chemistry and Physics, 51st Edition. CRC Press: Boca Raton, 1970.

Lide, D. R. (Ed.) CRC Handbook of Chemistry and Physics, 72nd Edition. CRC Press: Boca Raton, 1991.

Mansfield, P., and B. Chapman. "Active Magnetic Screening of Gradient Coils in NMR Imaging." J. Magn. Reson. 66: 573 (1986).

Mansfield, P., and I. L. Pykett. "Biological and Medical Imaging by NMR." J. Magn. Reson. 29: 355 (1978).

Mareci, T. H., and H. R. Brooker. "High-Resolution Magnetic Resonance Spectra from a Sensitive Region Defined with Pulsed Field Gradients." J. Magn. Reson. 57: 157 (1984).

McFarland, E. W., L. J. Neuringer, and M. J. Kushmerik, "Chemical Exchange Magnetic Resonance Imaging (CHEMI)." Magn. Reson. Imag. 6: 507 (1988).

Morich, M. A., D. A. Lampman, W. R. Dannels, and F. T. Goldie. "Exact Temporal Eddy Current Compensation in Magnetic Resonance Imaging Systems." IEEE Trans. Med. Imag. 7: 247 (1988).

Murphy-Boesch, J., and A. P. Koretsky. "An in Vivo NMR Probe Circuit for Improved Sensitivity." J. Magn. Reson. 54: 526 (1983).

Myers, C. C., and P. B. Roemer. "Highly Linear Asymmetric Transverse Gradient Coil Design for Head Imaging." Book of Abstracts, SMRM, 10th Annual Meeting, 1991," p. 711.

Petropoulos, L. S., J. L. Patrick, M. A. Morich, M. R. Thompson, and R. W. Brown. "Torque-Free Asymmetric Transverse Gradient Coil." Book of Abstracts, SMRM, 12th Annual Meeting, 1993, p. 1305.

Petropoulos, L. S., M. A. Morich, J. L. Patrick, D. A. Lampman, Haiying Liu, and R. W. Brown. "Insertable Asymmetric Cylindrical Gradient Coils." Book of Abstracts, SMRM, 11th Annual Meeting, 1992, p. 4032.

Riddle, W. R., M. R. Wilcott, S. J. Gibbs, and R. R. Price. "Using the Phase of the Quadrature Signal in Magnetic Resonance Spectroscopy to Evaluate Magnetic Field Homogeneity and Temporal Stability." Book of Abstracts, SMRM, 10th Annual Meeting, 1991, p. 453.

Romeo, F., and D. I. Hoult. "Magnet Field Profiling: Analysis and Correcting Coil Design." Magn. Reson. Med. 1: 44 (1984).

Sharp, J. C., R. W. Bowtell, and P. Mansfield. "Elimination of Susceptibility Distortions and Reduction of Diffusion Attenuation in Microscopic NMR Imaging by Line Narrowed 2DFT." Book of Abstracts, SMRM, 11th Annual Meeting, 1992, p. 688.

Suits, B. H., and D. E. Wilken. "Improving Magnetic Field Gradient Coils for NMR Imaging." J. Phys. E: Sci. Instrum. 23: 565 (1989).

Teodorescu, M. R., A. E. Badea, R. C. Herrick, and F. R. Huson. "Experimental Analysis and Finite Element Solution of Eddy Current Effects in Superconductive Magnets." Book of Abstracts, SMRM, 11th Annual Meeting, 1992, p. 364.

Terman, F. E. Radio Engineers' Handbook. McGraw-Hill: New York, 1943.

Trick, T. N. Introduction to Circuit Analysis. John Wiley and Sons: New York, 1977.

Turner, R. "Gradient Coil Design: A Review of Methods." Magn. Reson. Imag. 11: 903 (1993).

Turner, R. "A Target Field Approach to Optimal Coil Design." J. Phys. D: Appl. Phys. 19: L147 (1986).

Turner, R., and R. M. Bowley. "Passive Screening of Switched Magnetic Field Gradients." J. Phys E: Sci. Instrum. 19: 876 (1986).

van Vaals, J. J., and A. H. Bergman. "Optimization of Eddy Current Compensation." J. Magn. Reson. 90: 52 (1990).

van Vaals, J. J., A. H. Bergman, and R. P. van Stapele. "Optimization of Eddy Current Compensation: Competition for Shielded Gradients." Book of Abstracts, SMRM, 8th Annual Meeting, 1989, p. 183.

Wong, E. C., P. A. Bandettini, and J. S. Hyde. "Echo-Planar Imaging of the Human Brain Using a Three Axis Local Gradient Coil." Book of Abstracts, SMRM, 11th Annual Meeting, 1992, p. 105.

Wong, E. C., and J. S. Hyde. "Short Cylindrical Transverse Gradient Coils Using Remote Current Return." Book of Abstracts, SMRM, 11th Annual Meeting, 1992, p. 583.

Wong, E. C., A. Jesmanowicz, and J. S. Hyde. "Coil Optimization for MRI by Conjugate Gradient Descent." Magn. Reson. Med. 21: 39 (1991).

Wysong, R. E., and I. J. Lowe. "A Simple Method of Measuring Gradient Induced Eddy Currents to Set Compensation Networks." Book of Abstracts, SMRM, 10th Annual Meeting, 1991, p. 712.

Zur, Y., S. Stoker, and R. Morad. "An Automated Algorithm for Eddy Current Compensation." Book of Abstracts, SMRM, 11th Annual Meeting, 1992, p. 363.

BIOGRAPHICAL SKETCH

William W. Brey was born in Gainesville, Florida, in 1961. He attended Rice University and graduated in 1983 with a B.A. in physics and a concentration in space physics. After working for four years as a senior research assistant in the labs of Jean Delayre and Ponnada Naryana at the University of Texas Medical School in the University of Texas Health Science Center in Houston, Mr. Brey returned to Gainesville to pursue graduate studies with Raymond Andrew and Tom Mareci. He has enjoyed the cooperative nature and diverse interests of the NMR group at the University of Florida.

Following completion of his degree, Mr. Brey will join Conductus, Inc., in Sunnyvale, California, to develop superconducting electronics technology for NMR applications.

I certify that I have read this study and that in my opinion it conforms to acceptable standards of scholarly presentation and is fully adequate, in scope and quality, as a dissertation for the degree of Doctor of Philosophy.

E. Raymond Andrew, Chairman
Graduate Research Professor
of Physics

I certify that I have read this study and that in my opinion it conforms to acceptable standards of scholarly presentation and is fully adequate, in scope and quality, as a dissertation for the degree of Doctor of Philosophy.

Thomas H. Mareci
Associate Professor of Physics

I certify that I have read this study and that in my opinion it conforms to acceptable standards of scholarly presentation and is fully adequate, in scope and quality, as a dissertation for the degree of Doctor of Philosophy.

Neil S. Sullivan
Professor of Physics

I certify that I have read this study and that in my opinion it conforms to acceptable standards of scholarly presentation and is fully adequate, in scope and quality, as a dissertation for the degree of Doctor of Philosophy.

Richard W. Briggs
Associate Professor of
Biochemistry and Molecular
Biology

I certify that I have read this study and that in my opinion it conforms to acceptable standards of scholarly presentation and is fully adequate, in scope and quality, as a dissertation for the degree of Doctor of Philosophy.

K N Scott

Katherine N. Scott
Professor of Nuclear Engineering Sciences

This dissertation was submitted to the Graduate Faculty of the Department of Physics in the College of Liberal Arts and Sciences and to the Graduate School and was accepted as partial fulfillment of the requirements for the degree of Doctor of Philosophy.

December, 1994

Dean, Graduate School